TU Delft
Delft University of Technology

Department of Precision and Microsystems Engineering

Young's Modulus Decrease After Cold Forming
(An Investigation Into the Mechanism using Bake Hardenable Steel)

Submitted for the Fulfilment Of the Requirement of
Master of Science Thesis

Student Name:	**Abdul Haleem**
Study ID:	WB1337327
Report no:	PT 09.001
University Coach:	**Dr. Ir. Jilt Sietsma**
	Department of Material Science
	3me, TU Delf
	Ir. Jan Neve
	Department of Mechanical Engineering, PME
	3me- TU Delft
Industry Coaches:	**Dr. Ir. Eisso Atzema**
	Product Application Centre (PAC)
	Corus, Ijmuiden
	Ir. Pascal Kömmelt
	Product Application Centre (PAC)
	Corus, Ijmuiden
Professor:	**Dr. Ir. Urs Staufer**
	Department of Mechanical Engineering, PME
	3me- TU Delft
Specialisation:	Production Technology (PT)
Type of report:	Master Thesis (35 ECTS)
Date of Defense:	13th Feb 2009

Dedication

This work is dedicated to my mother Mariam, father Moeen Khan, and my wife Tahira whose support and encouragement in the difficult times proved a candle in the dark night. Also, I would like to dedicate the work to my eldest uncle, Abdul Qayyum Khan, who died in Pakistan during my thesis work and I could not attend his funeral.

Contents **Page**

Executive Summary

The start of 21st century saw an increasing level of competition among automotives. Automotive company needs to cope with the challenges of production of high quality, cheap and environment friendly cars. This becomes possible by the use of High Strength Steel (HSS), Advance High Strength Steel (AHSS) and Ultra High Strength Steel (UHSS) with thinner gauges for automotive bodies. Besides this, automotive has also to face the issue of the reduction in "Design to Market time" which plays an important role for the company to remain competitive. This issue can be best met by the production of a "first time right" product and process and becomes possible by the use of Computer Aided Engineering (CAE).

In most sheet metal forming operations, springback, which is undesirable, takes place at the end of operation which results in the deviation of final geometry from the design geometry. Springback is found higher for the metal with higher strength and for the thinner gauges and this is the reason of the higher amount of springback when HSS, AHSS and UHSS with thinner gauges are used for automotive bodies. The need of prediction of springback before an actual operation is therefore emphasized so that it can be compensated in the manufacture of expensive dies and tooling. The current practise of the manufacture of these dies is trial and error process which is time consuming, labour extensive and very expensive. An advance approach, which eliminates these problems, is the use of Finite Element (FE) analysis for the prediction of springback. In most cases, the springback with FE analysis is under predicted. There are many factors which contribute to the inaccurate springback prediction.

One factor responsible for the inaccurate springback prediction is the assumption of constant Young's modulus in FE analysis. Young's modulus, however, is found to decrease during plastic deformation. Therefore, an accurate model is needed to be implemented in FE analysis which can predict the decrease in Young's modulus. With passage of time, Young's modulus is found to restore to its initial value. The present study focuses on this aspect of springback prediction.

Bake Hardenable (BH) steel has been selected to investigate the degradation and recovery in Young's modulus. Two models are presented from literature in this report which are responsible for degradation when sheet metal is subjected to plastic deformation. The recovery in BH steel is considered to be due to strain ageing phenomenon in BH steel. The degradation in E modulus is found to be a function of dislocation density and average dislocation loop length between pinning points. In order to estimate the Young's modulus as a function of prestrain, these two parameters need to be known.

The decrease in Young's modulus and its recovery has been measured experimentally by two methods i.e. the dynamic method (Impulse Excitation Technique) and a static method (Tensile Test). The results are thoroughly discussed and some conclusions are drawn from it. At the end of the report, some recommendations are suggested for the future work. The report also compares the two methods of measurement and helpful tips are given for future work using these methods of measurement.

Acknowledgments

I am much grateful to the God, the first and foremost, who gave me this beautiful life and existence and provided the humans with a powerful brain to make our lives from better to best. I am thankful from the core of my heart to the following people who directly or indirectly helped me in my thesis work.

- To the nice administration of Corus for providing me the opportunity to work my master thesis in a world class multinational environment.
- To my industrial supervisors, Dr. Ir. Eisso Atzema and Ir. Pascal Kömmelt for their support and guidance during the thesis work including report writing and presentation.
- To my university supervisor, Dr. Ir. Jilt Sietsma for his nice and kind way of teaching/guidance and feedback on report.
- To my university initiators, Prof. Dr. Ir. Urs Staufer and Ir. Jan Neve for their nice feedback and participation in my examination committee.
- To Dr. Ir. Daniel Rixon, for cooperation and facilitating in dynamic testing of the experiments
- To Muamer Ozbek (Ph.D guy in Dynamics Group, TU Delft) for his cooperation and support in dynamic testing of the experiments.
- To Pieter Van Der Wolk, Jan Brussel and their team for support and cooperation in static testing of experiments.
- To library services in Corus and TU Delft who facilitated me with availability of right research material.

I would like to take this opportunity to forgive me if I have hurt someone unintentionally during this work.

Abdul Haleem
Delft, 8th Feb 2009

List of abbreviations

a. [CAE]	Computer Aided Engineering
b. [CAD]	Computer Aided Design
c. [CAM]	Computer Aided Manufacturing
d. [FE]	Finite Element
e. [HSS]	High Strength Steel
f. [AHSS]	Advanced High Strength Steel
g. [UHSS]	Ultra High Strength Steel
h. [HSLA]	High Strength Low Alloy
i. [SS]	Stainless Steel
j. [CQ]	Commercial Quality
k. [DQ]	Drawing Quality
l. [DDQ]	Deep Drawing Quality
m. [BH]	Bake Hardenable
n. [BHI]	Bake Hardening Index
o. [HSLA]	High Strength Low Alloy
p. [IF]	Interstitial Free
q. [DP]	Dual Phase
r. [TRIP]	Transmission Induced Plasticity
s. [LC]	Low Carbon
t. [ULC]	Ultra Low Carbon
u. [UHS]	Ultra High Strength
v. [BIW}	Body in White
w. [YPE]	Yield Point Elongation
x. [FD	Frequency Dependent
y. [Amplitude Dependent]	AD
z. [BCC]	Body Centered Cube
aa. [RD]	Rolling Direction
bb. [Laser Doppler Vibrometer]	LDV
cc. [Frequency Modulated]	FM
dd. [Forming Limit Diagram]	FLD
ee. [RT]	Room Temperature

List of Chemical Symbols

I.	*C*	Carbon
II.	*Mn*	Manganese
III.	*Si*	Silicon
IV.	Al_{tot}	Aluminium (total solubility in solid solution)
V.	Al_{zo}	Aluminium (Solubility of Aluminium in salt)
VI.	*N*	Nitrogen
VII.	*P*	Phosphorous
VIII.	*S*	Sulphur
IX.	*Nb*	Niobium
X.	*B*	Boron
XI.	*Sn*	Tin
XII.	*V*	Vanadium
XIII.	*Ti*	Titanium
XIV.	*Cu*	Copper
XV.	*Cr*	Chromium
XVI.	*Ni*	Nickel
XVII.	*Mo*	Molybdenum

List of Mechanical Symbols

I.	R_m	Tensile Strength
II.	$R_{p0.2}$	Proof Strength
III.	L_0	Original Gauge Length
IV.	A_g	Uniform Elongation
V.	A_{80}	Total Elongation(L_0=80mm*)*
VI.	*r*	Plastic Strain Ratio/Lankford Coefficient
VII.	*n*	Strain Hardening Exponent
VIII.	BH_0	Bake Hardening at 0 prestrain
IX.	BH_2	Bake Hardening at 2% prestrain

1. Introduction

1.1 Introduction

The aim of this thesis is to know more about the underprediction of springback in numerical simulation of sheet metal forming. There are a lot of factors which influence the accuracy of springback with numerical simulation. Some of them are discussed in this chapter and ultimately one factor (Young's Modulus) responsible for underprediction of springback is selected in this thesis to investigate further. The contents of this chapter are organized as follows

- "Design to Market Time" in Automotive Industries
- Goals for Automotive Industries
- Geometrical Defects with HSS, AHSS and UHSS
- Springback
- Prediction of Springback with FE
- Influential Factors for FE Analysis

1.2 "Design to Market Time" in Automotive industries

In recent years, the competition level between automotives has substantially increased. The increased level of competition has compelled these industries to produce high quality, cheap and environment friendly cars. Moreover, these industries have to face challenges like coping with diverse individualised customer demands, production of increasingly complex products and shorter innovation cycles. The situation of competition has become tougher due to the current financial crisis in the world which ultimately results in reduction of customers. Therefore, the design to market time needs to be reduced for new vehicles for the company to remain competitive in automotive market. Since 1980s, the time required for design and development process has roughly halved [1]. This has become possible due to two major innovations; concurrent engineering and Computer Aided Engineering (CAE) [2].
In concurrent engineering approach, the platform strategy is adopted for saving development time and production cost. In this approach, the manufacturing of a car is divided into separate modules, each module is assigned with a unique system or part of the car like sub frames, engines, suspension systems, body in white etc. These modules can be used for different types and models of the car. This is useful for large companies which build different models under various brand names. In this way, different development teams can work on the same project at the same time.
The 2nd approach adopted is that of Computer Aided Engineering (CAE). Fig 1.1 shows different stages of development process in CAE [2]. Stage 1 of the process, called Computer Aided Design (CAD), enables engineer to create complex product designs and shapes, store and archive them, review, modify and update them. All car parts are digitally coupled so that modification in one geometry can be readily updated in the entire assembly smoothly without any problem. When this data is used in production processes for manufacturing, this is called, Computer Aided Manufacturing (CAM). An example of this can be Numerically Controlled (NC) machining. This is the 2nd stage of the CAE development process. The 3rd stage of the CAE is a combination of CAD, CAM and Finite Element (FE). FE analysis is being used to analyze the stiffness, strength, dynamic properties in a great detail before the production of prototype. Today it is possible to model production processes like polymer injection moulding and forging of gears. The conclusion of such an analysis is transferred to CAD system to optimize the product. In the final stage of virtual product process, CAD and FE are fully integrated so that the production of a "first time right" product and production process become possible.

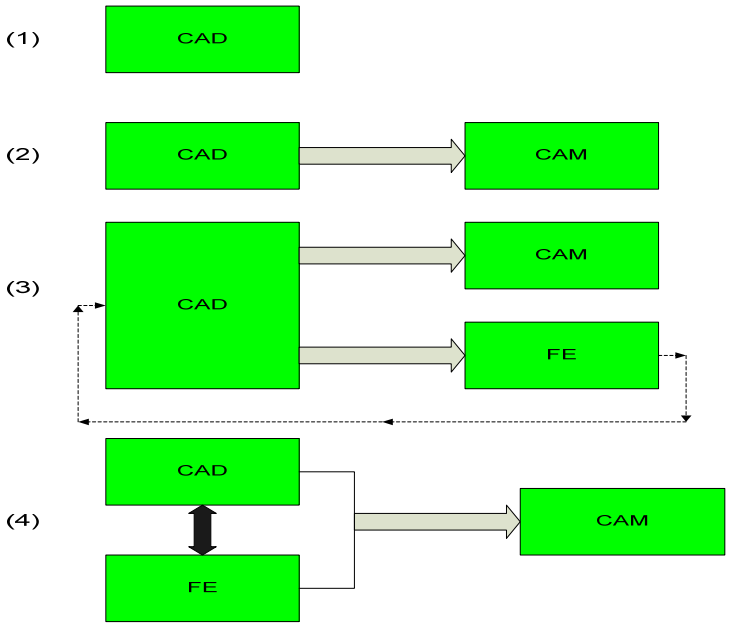

Fig 1.1: Four stages in virtual product development [2]

1.3 Goals for Automotive Industries

The increasing levels of emission of CO_2 pose severe threat to a clean environment. The fluctuation in fuel prices, which is mostly a hike in fuel prices, is another problem. Therefore, the goal of high quality, cheap and fuel efficient cars can be achieved by the reduction in car weight and improvement in safety. The reduction of weight directly contributes to the fuel economy of cars. This is illustrated in figure 1.2.

The objective of reduction in weight can be achieved mainly through the use of light weight and high strength design for body in white (BIW). The realization of this concept is manifested by the use of Aluminium alloys and High Strength Steel (HSS), Advanced High Strength Steel (AHSS) and Ultra High Strength Steel (UHSS) for body parts. Figure 1.3 shows variety of steel grades and their strength in a modern car.

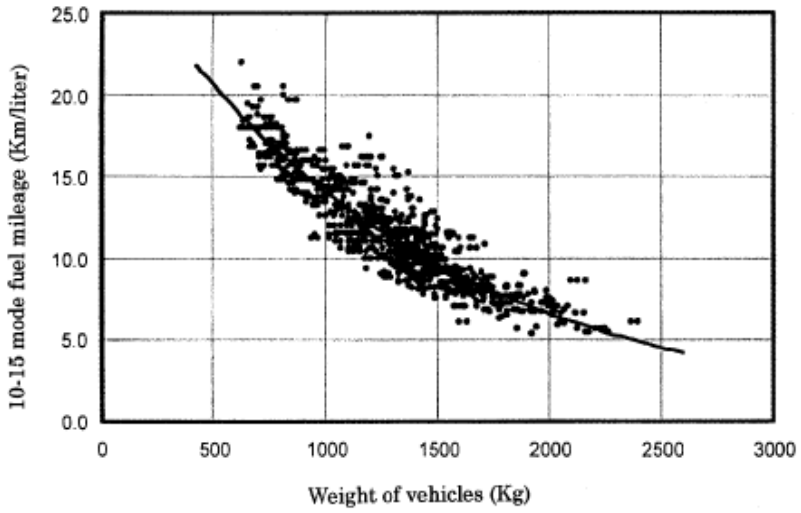

Fig 1.2: Relationship between fuel mileage and automotive weight [3]

1.4 Geometrical Defects with HSS, AHSS and UHSS

A large variety of steel components for automobiles are produced by deformation processing. Some well known examples include forging, rolling, drawing, extrusion, sheet metal forming and hydroforming. For body in white (BIW), a large variety of automotive parts are made from steel by sheet metal forming. For example, Fig 1.3 shows the percent use of different grades of steel and their strength in auto body.

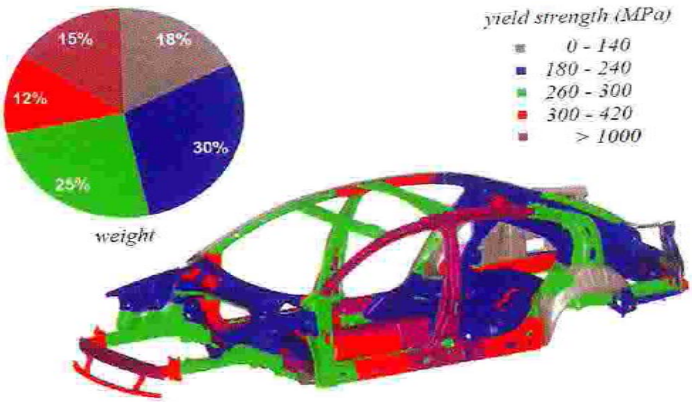

Fig 1.3: Steel Grades in a Modern Car (Volkswagen AG), [2]

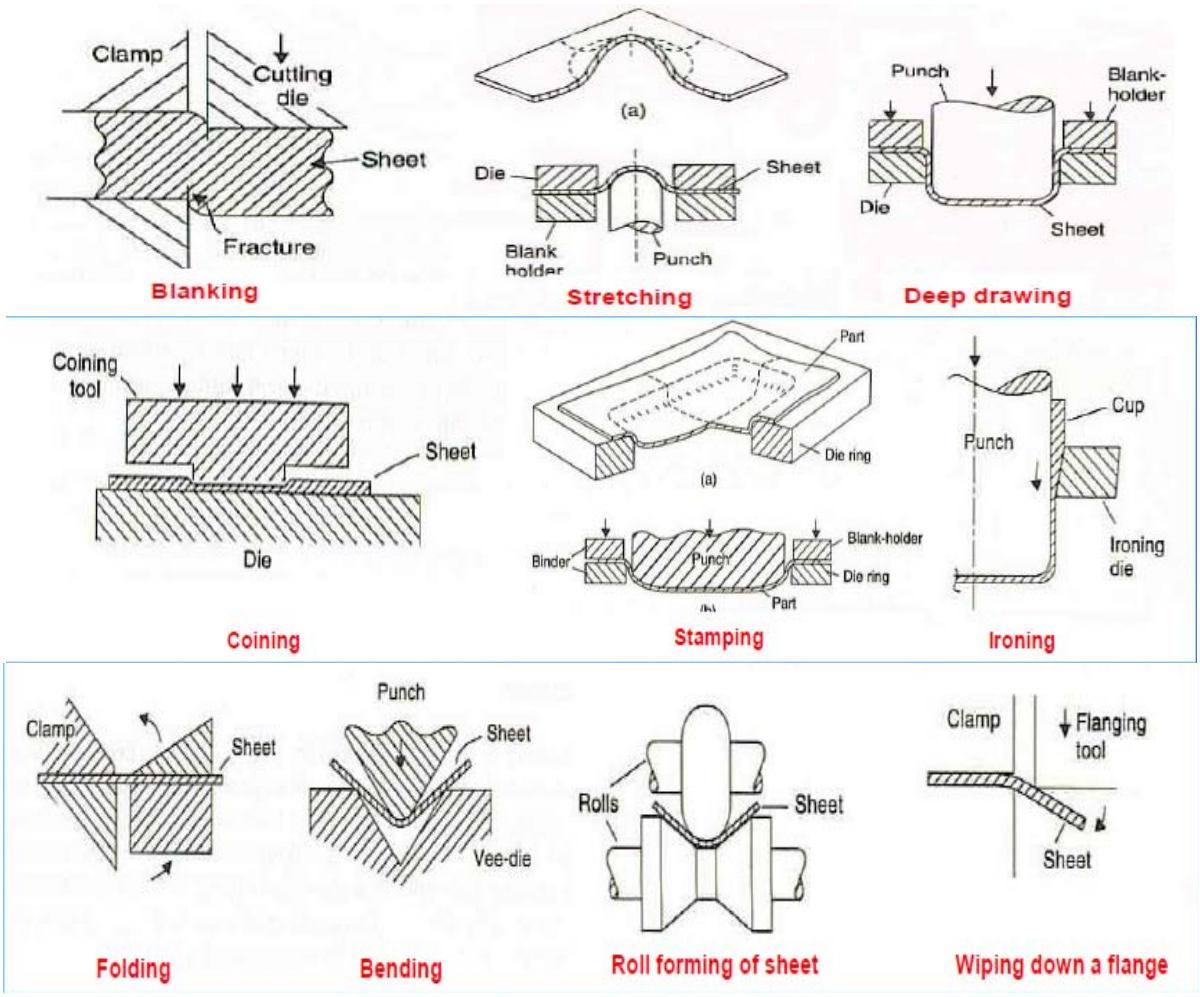

Fig 1.4: Some of sheet metal forming operations

An advantage of the use of HSS is due to its favourable properties of forming with conventional technology. Conventional technologies of sheet metal forming like bending, deep drawing, stretching, rolling, and rubber forming can be used without the need of further investment. Some of conventional sheet metal forming operations are shown in fig 1.4. Among these processes, deep drawing process is one of the most used operations in automotive manufacturing. Deep drawing allows production of large quantities of sheet metal parts of various complexities. An exploded view of a typical set up for deep drawing is shown in fig 1.5 (a) [4]. An initially flat or pre-shaped sheet material, the blank, is clamped between a die and a blankholder. The blankholder is loaded by a blankholder force, which is necessary to prevent wrinkling and to control the material flow into the die cavity. Then the punch is pushed into the die cavity, simultaneously transferring the specific shape of the punch and the die to the blank. An automotive product produced with this process is shown in fig 1.5(b).

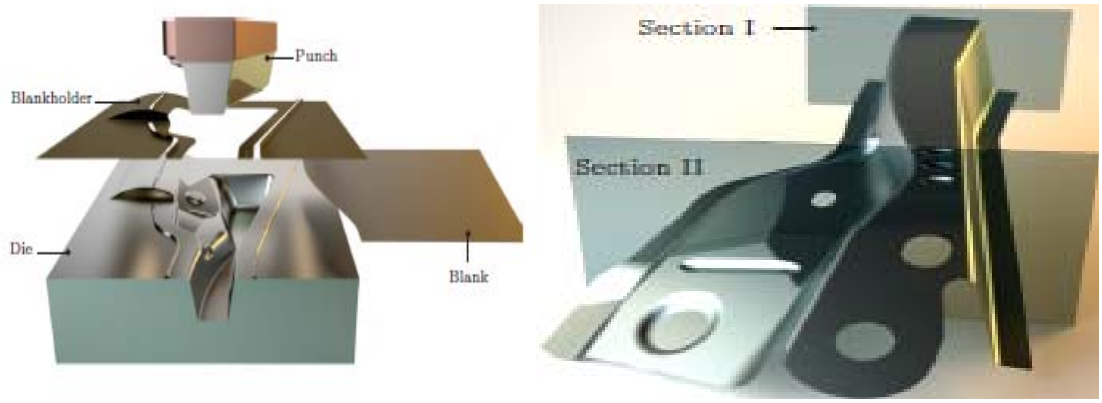

Fig 1.5: (a) Exploded view of Deep Drawing Set for an automotive part (b) An automotive product produced by the deep drawing process [4]

The quality of the final product with deep drawing depends on process parameters (such as blank holder force, lubrication, blank shape and the right amount of clearance between punch and die), tool design and choice of material. Some typical deep drawing defects are wrinkling, necking, scratching, drawing grooves and orange peel. Wrinkling may occur in areas with high compressive strains, necking may occur in areas with high tensile strains, scratching is caused by defects of the tool surface and orange peel may occur after excessive deformation, depending on the grain size of the material. For a successful product, these parameters need to be considered before production starts.

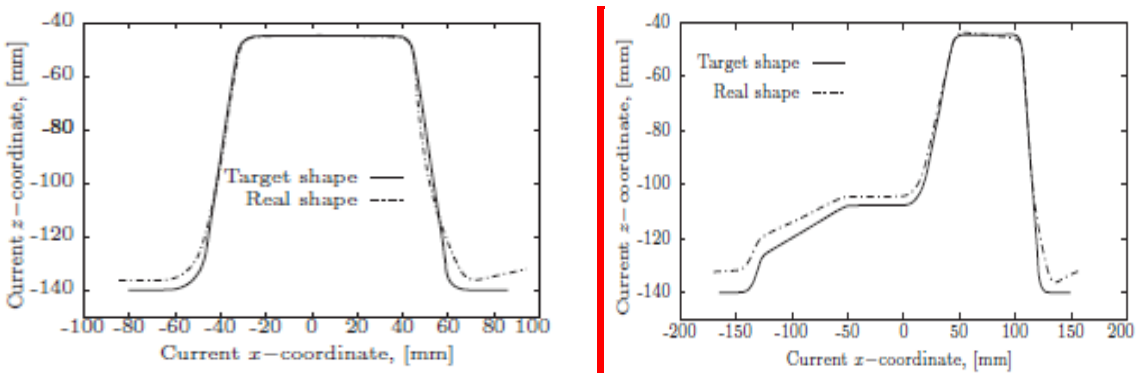

(a)Section I (b) Section II

Fig 1.6: Shape deviation due to springback (a) section I from fig 1.5(b) Section II from fig 1.5(b) [4]

An important defect, which is always present, is geometrical distortion caused by elastic springback. Right after forming, the shape of the deformed product closely conforms to the geometry of the tools. However, as soon as the tools are retracted, an elastically driven change of shape occurs. The significance and magnitude of springback is illustrated by the fig 1.6 where the geometry of the part is shown two-dimensionally. It is clear from this figure that springback causes considerable deviation from design specification. The deviated geometry causes major assembly problems.

1.5 Springback

Springback can be defined as an elastically driven change of shape that takes place during removal of the external load. It is a complex physical phenomenon which is mainly governed by the stress state obtained at the end of a deformation. During plastic deformation in sheet metal forming, the contact forces with the internal stresses form force equilibrium. At the end of operation, when the tool is retracted, these contact forces are removed, the force equilibrium is disturbed and a new equilibrium must be achieved. Since a change of internal stress can only be accomplished by a change of strain, a shape change takes place which is referred to as springback. Springback can be in plane and out of plane. In in-plane springback, for example, in a tensile test, final stress state is zero while in most out of plane springback; the component is left with residual stresses. A simple example of this is pure bending (for example with a brake press) which is useful for understanding this phenomenon.

Suppose that a moment is applied to a strip of sheet with thickness *t* to a bend radius *R* and a bend angle *θ*. During bending, the stresses at both the inner and outer fibres of the material exceed the yield stress, producing a plastic deformation which holds the shape. In this case, radial (ρ) and circumferential (θ) directions are principal strain directions and for isotropic materials, these are also the principal stress direction (see fig 1.7(a)). The mid surface is not necessarily the neutral surface and in presence of a tensile force during bending, the neutral line shifts towards the centre of curvature, say by a distance *a*. Fig 1.7(b) shows stress and strain profiles in a cross section of the material after bending to a radius under tension.

It is clear from this figure that at outer surface of the bend, there is a tensile stress and strain while the inner fibre is under compressive stress and strain. Both of the outer most regions have crossed the elastic limit and are in plastic zone. However, the stresses near the neutral axis have still not crossed the yield limit and therefore are in an elastically deformed region, so at the end of operation after bending the sheet to the radius R, a moment M remains due to elastic region. After load removal, the sheet will springback to a different shape to reach a new equilibrium. The magnitude of the stresses will decrease and the amount of shape change can be related to the applied bending moment or the elastic deformation around neutral axis.

This situation is illustrated in fig 1.8(a) considering material that has the same stress strain relationship under both tension and compression and that neutral axis is at the centre of the bend. The plastic deformation is distinguished by a light hatching while the elastic deformed region is distinguished by heavy crosshatch pattern. For plane strain bending situation, Burchitz [4] gives a mathematical relation for the change of angle (springback) after bending as

$$\Delta\theta = -\frac{12M}{Et^3}\rho\theta \text{ ----------[1.1]}$$

where M is the applied bending moment, E the Young's modulus, ρ the circumferential radius and θ is the circumferential direction.

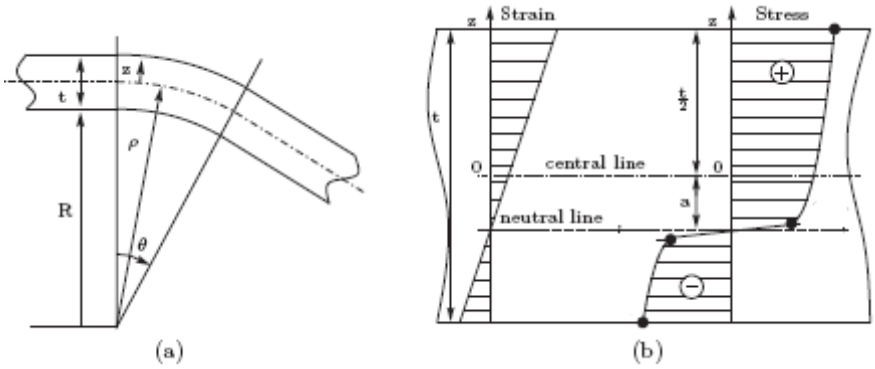

Fig 1.7: Strain and Stress Profile during plane strain bending [4]

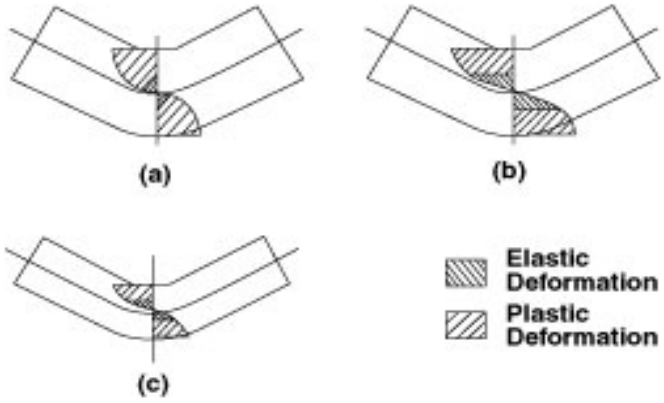

Fig 1.8: Elastic and Plastic deformation zones for a general strength material (b) More Springback with higher Yield stress and hence a large elastic deformation zone around neutral axis (c) More Springback with the same material as in (a) but with a thinner gauge with effect of relatively same elastic deformed zone as with a thicker gauge

The above equation defines some basic relations between material and process parameters and the amount of springback. Some inferences can be concluded from the above relations such as

I. Since bending moment, M, is a function of initial yield stress; therefore, the amount of springback increases with yield stress of the material. This means with the use of HSS and AHSS with higher yield stress, the amount of springback will be higher. The effect of higher yield stress increase the area of elastically deformed region and causes a larger springback as can be seen in fig 1.8(b). The effect of higher yield stress but same Young's modulus of two materials can be seen on a stress strain diagram in fig 1.9 with higher springback for high strength material.
II. Springback is inversely proportional to Young's modulus. This means, for example, the use of Aluminium Alloys with lower Young's modulus will result in a higher amount of springback. The effect of lower Young's modulus on the amount of springback can be seen on a stress strain curve in fig 1.9(b).
III. Springback is inversely proportional to the thickness of the material. This means with use of HSS and AHSS with the thinner gauges for mass reduction will cause a significant higher springback in automotive bodies. The effect of thinner gauge can be seen in fig 1.8(c). Here the same material as in 1.8(a) is used but with a thinner gauge. The area of elastic region is the same so for a thinner gauge, the amount of springback becomes higher.

IV. Springback is higher for a higher bend radius (ρ) and bend angle (θ).

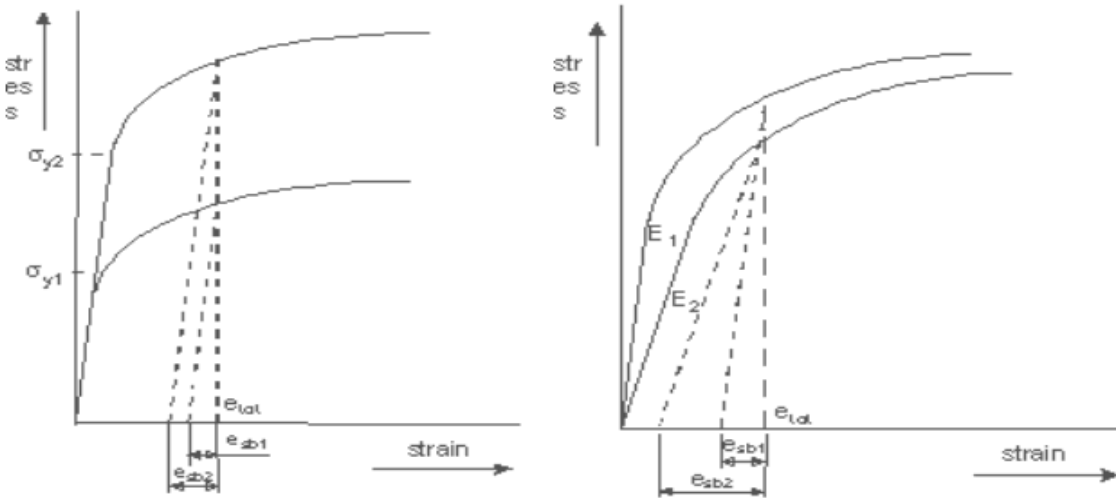

Fig 1.9: Springback is higher when (a) Higher Yield Stress but same Young modulus (b) Lower Young's modulus but same Yield Stress

It can be anticipated from these points that the amount of springback is multiplied in modern steel car manufacturing due to employment of higher strength and thinner gauge materials. For Aluminium alloys, the higher springback is due to lower Young's modulus.
There are many undesirable consequences of higher springback. For example,

I. During assembly the part does not fit. This may affect the aesthetic appeal of the product.
II. In welding tool assembly, the gap between mating part may be large due to springback in one or both parts and thus higher forces will be need by the welding tool to overcome the gap.
III. Product may not fulfil its desired function e.g. crash performance becomes lower with shape aberrations.

1.6 Prediction of Springback with FE

The consequences of higher springback have been described briefly in the previous section. Due to the springback, often the product has to be reworked which causes a loss of productive time and may cause degraded quality. An alternative is to modify the die geometry equal to negative of springback magnitude so that at the end of springback, the product achieves its design specification. This methodology is currently used in automotive sector. But the main obstacle of this method is the lack of knowledge of springback magnitude. For a particular product shape, geometry and material, probably a large number of press strokes are required, before knowing the exact amount of springback. This trial and error process causes loss of productive time. In an automotive body, probably there are hundreds of stamped and press worked components. So, for example, when a new design of car has to be introduced, then the trial and error process of each component may result in considerable lost time and can cause a big delay in design to market time of the final product i.e. the car.
The significance of CAE has been described in sec 5.1. The last stage of CAE in fig 1.1 is the integration of CAD and FE analysis in order to fulfil the dream of "first time right" product and production process. FE analysis is a powerful tool that gives the possibility to observe effects of changing any process parameters prior to the actual tool manufacturing. It is possible to predict springback with FE analysis to define the actual tool geometry. Despite

significant development in the field of FE simulation, the accuracy of springback prediction, unfortunately, does not yet satisfy the industrial needs [37]. The use of expensive and time consuming experimental try outs to determine the proper tool geometry is still needed to produce a product with the desired shape. The low accuracy of springback prediction is attributed to the lack of understanding of this phenomenon and the use of oversimplified models describing, for example, material behaviour or contact conditions during deformation [4]. Accurate prediction of springback will enable the die designers to numerically evaluate the possibility of obtaining the specified product shape and to perform the necessary modification before the actual production starts. The possibility of accurate numerical prediction will minimize the experimental try outs and will result in reduction of lead time and manufacturing costs. An ideal design process employing FE process is shown in fig 1.10.

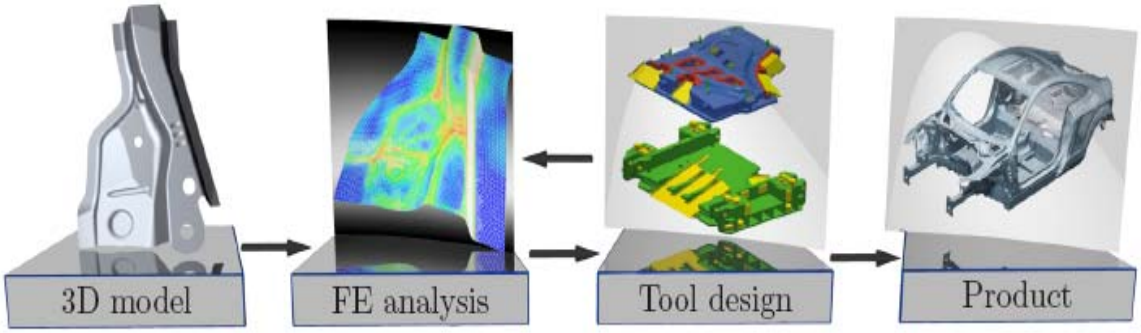

Fig 1.10; Design Process of a Product incorporating FE analysis [4]

Accurate prediction of springback with FE needs an accurate model of springback. For a successful model construction, the phenomenon of springback needs to be understood well. Some experimental procedure could be helpful for getting acquaintance with the sensitivity of springback to various process and material parameters such as Livatyali studied springback in straight flanging [6] and Yang's study of unconstrained bending [7].

1.7 Influential Factors for FE Analysis

The success of a model depends on many numerical, process and material parameters. Burchitz [4] has extensively studied various factors affecting the accuracy of springback prediction with FE analysis. In the following some of the factors will be discussed briefly.

1.7.1 Numerical Parameters

Three numerical parameters will be discussed here i.e. element type, time integration scheme and iterative solver.

1.7.1.1 Element Type

The selection of an appropriate element type is a crucial step for accurate modelling with FE. Different types of elements are in use depending on the problem and geometry of the blank for example, 2D plane strain, and shell, solid or solid shell. Shell type of element is mostly used in sheet metal forming due to computational efficiency. In some cases, to speed up the analysis time, a full 3D problem is represented by a model which uses 2D plane strain elements. The accuracy obtained with these modes can be questionable.

1.7.1.2 Time Integration Scheme

There are two time integration schemes used in simulations of the springback phenomenon in sheet metal forming i.e. static implicit and dynamic explicit schemes. In static implicit schemes, the inertia effects are neglected and the state variables are found iteratively. The drawback of static implicit method is difficulties in finding the convergence within a time increment and an increase in computational time when a direct solver is used [4]. In dynamic explicit method, the inertia effects are considered dominant and state variables are updated at every time increment without solving system of equations. Therefore, dynamic methods are not plagued by convergence problems and memory requirements are minimized so that final solution is usually obtained faster with this method. A disadvantage of this method is the use of a small time step during solution process. There are some algorithms proposed which combine the merits of both methods. Another approach is to have both methods available in the same FE code and be able to switch automatically between them within one simulation.

1.7.1.3 Solver Type

The results of FE simulations can be affected by the method to solve the global system of equations especially for the method of static implicit FE simulation as dynamic explicit method do not require solution of system of equations. Two groups of methods are used to solve linear systems of equations in static implicit method i.e. direct solvers and iterative solvers. Direct solvers are based on Gaussian elimination and are useful for accurate solution of a linear system of equations. But the disadvantage of direct solver is high memory requirement in large scale FE simulations [4]. For large problem, iterative solvers are generally preferred as they solve global system of equations with less memory than a direct solver. Burchitz [4] compared simulated springback with direct and iterative solver for a draw bended test. It can be seen in fig 1.11(a) that springback prediction obtained with iterative solver is not realistic while the direct solver data closely matches with experiment. However, when the number of iteration is increased, the accuracy of the springback prediction improves. This is shown in fig 1.11(b). Therefore, for accurate result of springback, direct solver is preferable. Iterative solver can be used for accurate prediction only when allowed sufficiently high number of local iterations to reach the specified accuracy.

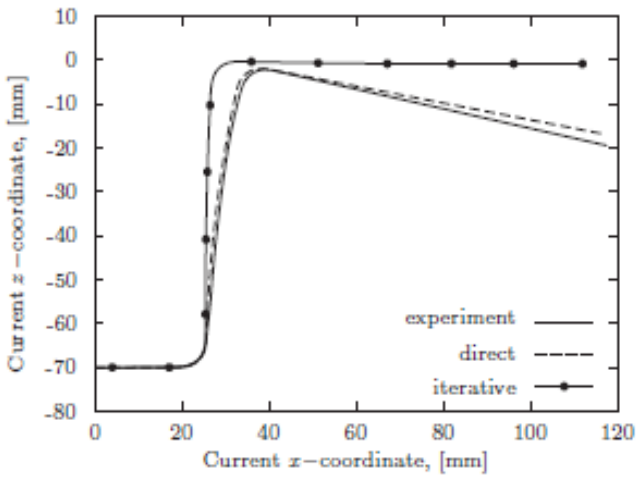

(a)

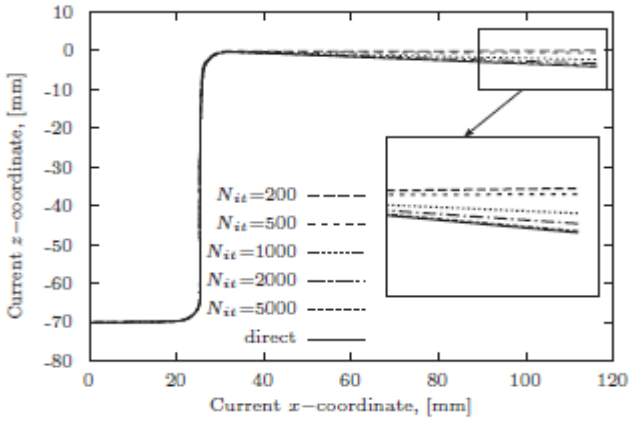

(b)

Fig 1.11: (a) Influence of solver type on springback, (b) Effect of number of iterations on springback in iterative solver [4]

1.7.2 Process Parameters

Some process parameters that will be discussed are as follows, contact description, unloading method, equivalent drawbead and press and tool deformation.

1.7.2.1 Contact Description

The contact description of tool and blank in numerical simulation is an important factor which influences the result of springback simulations. Contact conditions in simulation analysis in sheet metal forming are usually that material cannot penetrate the tool and in case of no contact, there are no contact forces between tool and blank. For accurate prediction of springback through FE analysis, it is important to incorporate the accurate stress state at the end of forming by avoiding false penetration or incorrect contact forces during simulations. There are two methods available for this purpose, Lagrange multiplier method and penalty method. The benefit of Lagrange method is the implementation of exact non-contact condition at the cost of extra degrees of freedom while in penalty method, there is always some penetration and non-contact description can only be implemented with an infinite contact stiffness [4] which causes a numerical singularity and the simulation terminates prematurely. But the advantage of penalty method is that no extra degrees of freedom are required.

Accurate description of friction in FE analysis is also important for accurate prediction of the final stress state at the end of forming. The commonly used Coulomb model assumes a constant friction coefficient which is not realistic. Coefficient of friction depends on the local contact conditions which differ for each blank-tool contact. For accurate springback prediction, an advance model like Stribeck model [4] is more appropriate. In this model, coefficient of friction depends on parameters like pressure and viscosity of a lubricant between the contacting surfaces, the tool's velocity and the surface roughness.

1.7.2.2 Unloading Method

Generally, simulation of springback involves two process steps i.e. loading or forming and unloading or springback. There are two methods employed for unloading, namely, instantaneous method and gradual release method. Instantaneous method is used mostly in FE analysis due to its computation efficiency. In this method, all contact forces are suddenly removed, transformed into residual stresses which are then reduced to zero. While in

gradual release method, the contact forces are reversed and tools is retracted gradually. Gradual method of unloading is more realistic but is computationally costly. Burchitz [4] compared the two methods of unloading for two components with and without friction coefficient in FE analysis. It is found for both components that gradual method of release is superior in predicting the springback when compared with experimental results especially when it is employed with coefficient of friction.

1.7.2.3 Equivalent Drawbead

In sheet metal forming, when shallow or arched parts are formed, drawbeads (shown in fig 1.12) are usually incorporated into the tools to introduce additional stretching and a more uniform flow of the material. The incorporation of drawbeads in FE analysis, however, requires a large number of elements due to the small radii of the drawbead. Therefore, it is generally replaced by an equivalent drawbead and thus helps to avoid a drastic increase in computation time. An equivalent draw bead is represented by a line on tool surface and thus FE experiences an additional drawbead restraining force and a plastic strain and a lift force is subtracted from the total blank holder force. It has been shown by some researcher [4,9] that an equivalent drawbead results in an inaccurate springback prediction. For example, Burchitz compared the experimental true thickness strain in section I-I of automotive under body cross member (shown in fig 1.13(a)) with a real and equivalent drawbead. This comparison is shown in fig 1.13(b). It can be seen in fig 1.13(b) that equivalent drawbead is predicting thickening in the region from -100 to -200 mm while the real drawbead and experimental results shows a thinning in this region. Further to this, one has to also keep in mind that the complex stress state occurring during bending-unbending inside a drawbead is lost when using equivalent drawbead.

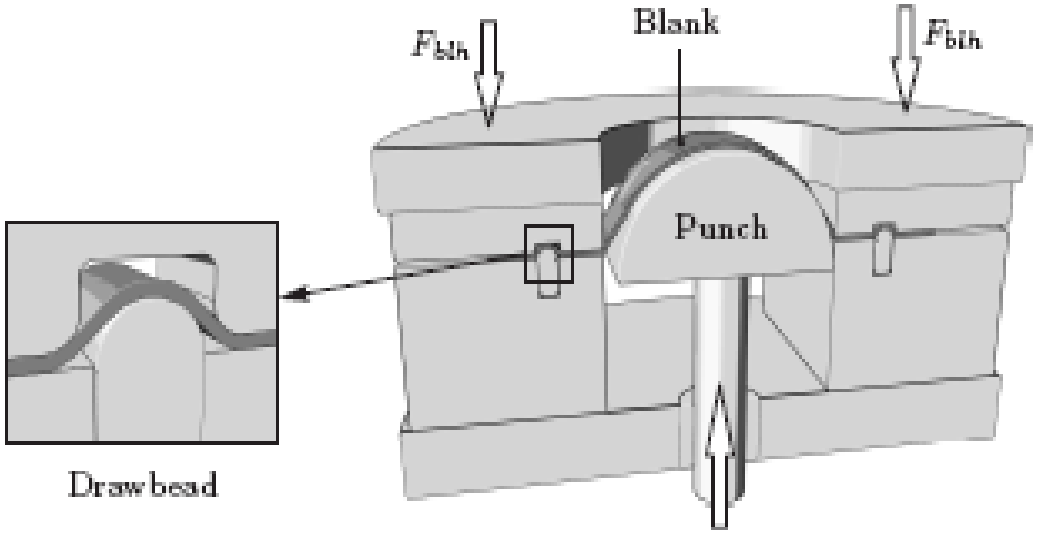

Fig 1.12: Drawbead in a stretch bending test [8]

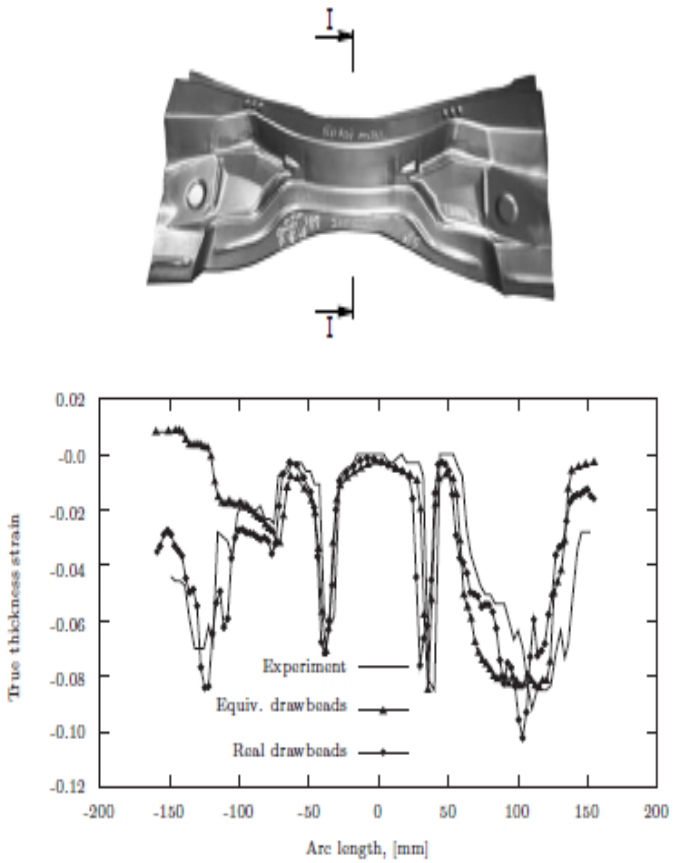

Fig 1.13: (a)(top) Automotive underbody cross member [4], (b) (bottom) True thickness strain distribution after forming in sec I-I for DP965 [4]

1.7.2.4 Press and Tool deformation

Deep drawing process is an incredibly sensitive process and even small phenomena, generally considered negligible and hard to measure, may influence the blank flow and therefore the quality of the final product [2]. Four different categories are shown in fig 1.14. In 5.14(1) deformation of press frame is shown which is very heavy structure and its deformation is therefore not significant. Unlike press frame deformation, press deformation, shown in fig 1.14(2), includes deformation of the bed plate and slide and these can deform substantially, the deformation being in the order of magnitude of several millimetres. In addition to slide deflection, there is also slide tilting affecting the drawing process. Heavy loads on punch, blankholder and die results in tool deformation. This is shown in fig 1.14[3]. Another problem is that the separation of tool deformation from the press deformation is impossible, as the bed plate and slide support the tools. The deformations in fig 1.14, from 1 to 3, are referred to as macro or global deformations. Tool surface deformation, shown in fig 1.14(4), is referred to as micro or local deformation and is caused by high contact pressure between blank and tool such as at the die shoulder and in the blankholder area. The order of magnitudes of these deformations is considerably lower at around 0.1 mm maximum. Since friction depend strongly on small changes in the pressure field between the blank and the tool, small changes in the tool geometry have a large influence on the simulation results, blank draw and springback.

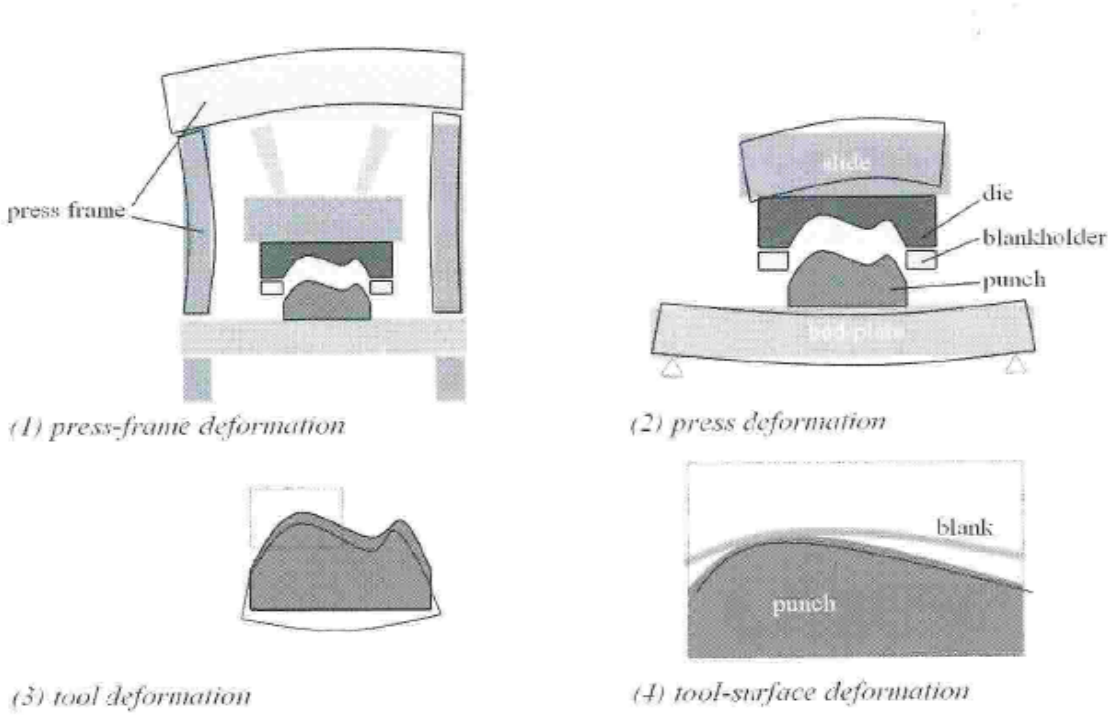

Fig 1.14: Types of tool and press deformation [2, 10]

For accurate springback prediction, tool deformation needs to be included in FE forming simulations. However, especially in the case of complex and large car body parts, the size of the required tool meshes increases the cost of simulation immensely. Due to complex tool design, tool meshes with several millions of degrees of freedom are no exception. The cost of these simulation increases so high that it becomes unaffordable in an industrial context, despite the fact of rapid increase in computer performance. Therefore more efficient ways of tool modelling are required. Due to small deformations, tool and press deformations can be considered as a linear elastic problem. There are two strategies to increase the efficiency of such problems i.e. static reduction and Deformable Rigid Bodies (DRB). Lingbeek [2, 10] has extensively studied these strategies. Local deformation modelling remains unfeasible. Due to approximations in contact algorithms and limited size of tool meshes, the results are not reliable [10]. Tool surface deformation is the focus of almost all present publications on elastic deformations in tools, for example [51] and [12]

1.7.3 Material Parameters

The choice of an appropriate material model is one of the crucial steps in preparing a numerical set up for analysis of sheet metal forming. The most important factors are yield function and hardening law.

1.7.3.1 Yield Function

Yield function used in numerical analysis is one of the factors which have a significant influence on the internal stress state at the end of a deformation. The importance of choosing an appropriate yield function is therefore necessary for accurate springback prediction. A number of researchers have mentioned the significance of the appropriate yield function such as [13-16].

A yield function is the surface that encloses the elastic region in a multi axial stress space. Usually in sheet metal forming, all out of plane stresses are assumed to be zero and a yield

criterion is formulated in plane stress space. Simple yielding theories like Von Mises and Tresca are limited in applicability as their parameters are defined only for isotropic materials. Generally, sheet metal is anisotropic in nature and its mechanical properties depend on the chosen direction. The planar anisotropy within sheet metal develops during rolling process in production.

For accurate calculation of internal stresses at the end of deformation, the yield function should be able to cater for the anisotropic nature of the sheet metal. A simple and most widely used yield function is that of Hill's 1948 function. However, the major drawback of this function is its poor predictability in equi-biaxial tension for material with low r value when compared with experiments. This is shown in fig 1.15 for aluminium alloy AA5182 when plotted in the normalized principal stress space when compared with Vegter's experimental results. The Vegter's yield locus is an interpolation through measured multi-axial stress states. Values in fig 1.15 are normalized to σ_y which is the average of uniaxial yields stresses measured in 0°, 45° and 90° to the rolling direction. As can be seen, the Hill's 48 criterion predicts a much lower equi-biaxial yield stress

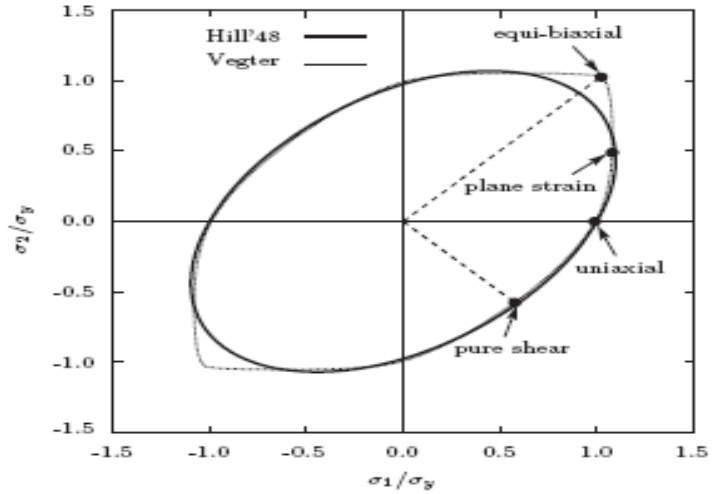

Fig 1.15: Comparison of Hill'48 Yield function with Vegter's experimental Yield locus for AA5182 alloy [4]

This means, if Hill'48 criterion is used in FE analysis, an inaccurate stress state will be obtained and therefore an inaccurate prediction of springback. To overcome the problem, advanced yield functions are presented such as Hill 90 [17], Hosford [18], Barlat [19] and Vegter [20]. Although, some extra parameters are introduced in these advanced functions and hence there is a drawback while implementing in FE simulation but ultimately the results obtained with these advance models will be more realistic.

1.7.3.2 Hardening Model

The accuracy of springback prediction depends on the accurate hardening models to be used in numerical simulations. The hardening law describes the evolution of initial yield surfaces that may change its shape, size, position due to plastic deformation. There are two simple hardening models i.e. isotropic and kinematics hardening. In isotropic hardening model, the centre of the yield locus is fixed and shape remains the same, while in kinematics hardening model, yield surface with no change in shape and size translates only.

It is described in sec 1.7.3.1 that sheet metal is anisotropic in behaviour due to production process. In addition to this, there is also deformation induced anisotropy for which some models have been developed. Those models are unfortunately time consuming and

computationally expensive. Therefore, simple models are mostly used with the assumption of changes of anisotropic properties during forming to be negligibly small. These simple hardening models cannot accurately describe the behaviour of the material under strain path changes.

For example, a blank strip clamped between die and blank holder is formed by the punch into a U-shaped profile as shown in fig 1.16. In fig 1.17, the evolution of stresses is shown when the sheet enters (a) the die radius and (b) the draw bead. When the blank is entering the draw radius, tensile stresses develop in the outer layer of the sheet and compressive stresses in the inner layer (Fig 1.17(a)). The subsequent straightening of the sheet inverts the stress distribution. Another stress reversal may occur in the sheet after it has passed the draw radius. Cyclic plastic deformation may also occur when a sheet passes a draw bead (Fig 1.17(b)). The stress distributions and springback prediction with Isotropic and kinematic models are illustrated in fig 1.18. There is a clear difference of predictions with both hardening models.

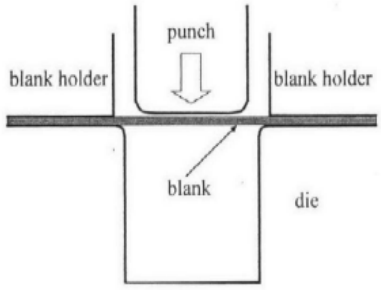

Fig 1.16: Draw Bending Test [21]

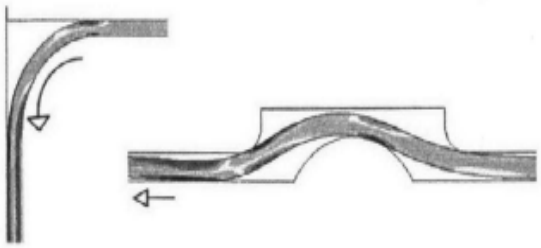

Fig 1.17: Stress distribution in a sheet passing through (a, left) draw radius (b, right) draw bead [21]

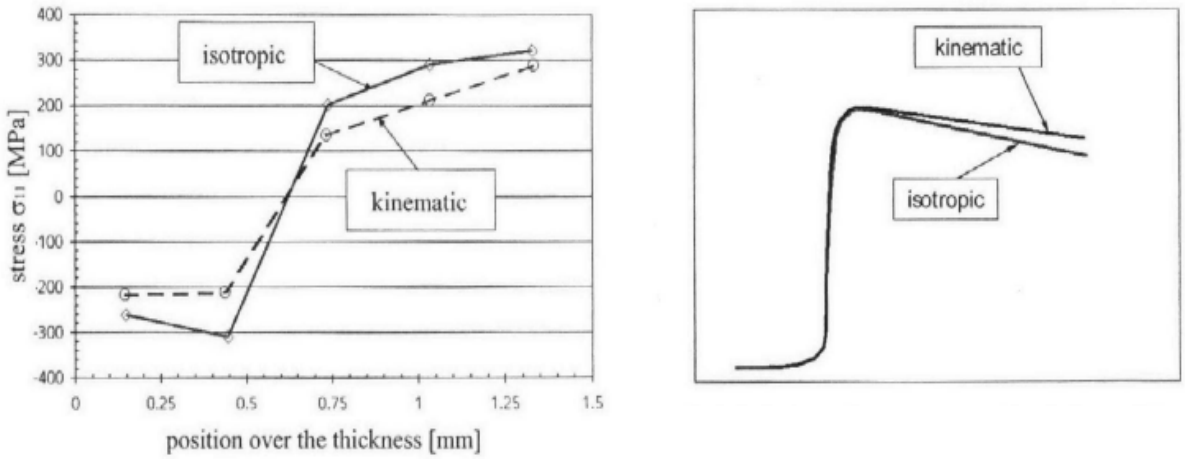

Fig 1.18: Comparison of hardening models for (a, left) stress distributions over sheet thickness at the end of drawing (b, right) springback predicted [21]

The most important aspect during cyclic plastic stresses is the Bauschinger effect which is characterized by early re-yielding, smooth elastic plastic transition and work hardening stagnation when the load is reversed. This effect is also shown by Riel and Boogard [31] in reverse loading when interstitial free steel DC06 is subjected to a simple shear deformation of opposite sign. This can be seen in fig 1.19 where the material exhibits the above stated stages of Bauschinger effect. Therefore, use of an accurate model in numerical simulation which is able to describe the effect of strain path changes is needed.

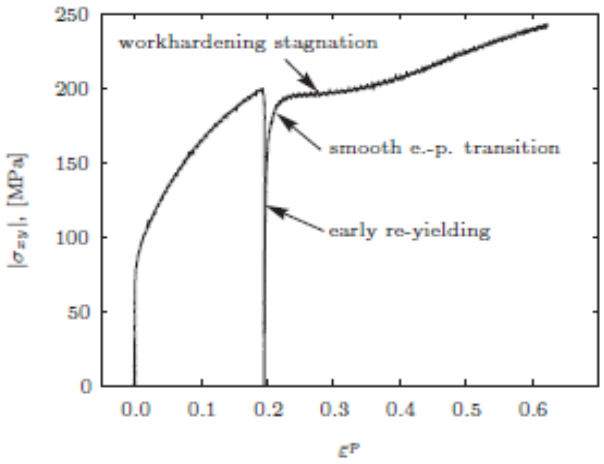

Fig 1.19: Absolute Stress and Strain diagram for DC06 during reverse loading [4]

1.7.3.3 Young's Modulus

The amount of springback during unloading depends on the Young's modulus. This has been shown mathematically for pure bending in sec 1.5. The amount of springback is in inversely proportional to the Young's modulus. So the springback is more for smaller Young's modulus like for Aluminium alloys. In numerical simulation analysis, the Young's modulus is assumed to constant. However experimental observation has shown that Young's modulus degrades during plastic deformation. This is shown in [23, 24]. An example is shown in fig 1.20 for Mild steel by Yang [25]. The springback is, therefore, not accurately predicted in numerical simulation with assumption of constant Young's modulus and underprediction of springback takes place. Therefore, the need to incorporate an accurate material model in numerical analysis is important.

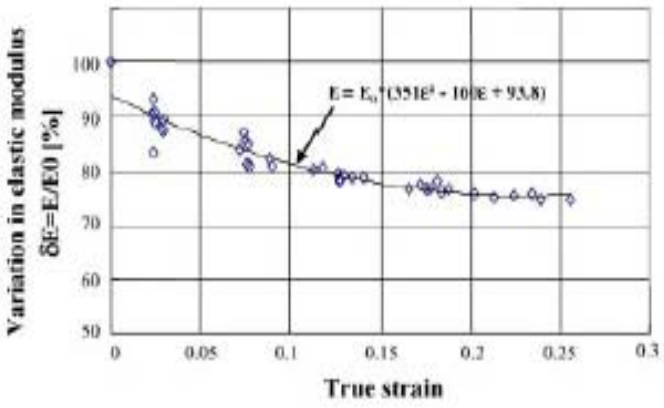

Fig 1.20: Degradation in E modulus for Mild Steel [25]

The model given in fig 1.20 behaves erratically outside the fitting range and is therefore not of much use. For example, it has been extracted purely experimentally so it means may be it will of help for the material investigated but may not be applicable to other materials. Therefore, this model is not a generalized one. Another problem is that the function is a quadratic and so with further increase in strain (which is not shown in the fig), the curve will again slope up and there will be an increase in Young's modulus. While, from experiments it is clear that it is not the case. This is, therefore, another indication that the model may only be useful for the strain range described and outside this range of measurement, the accuracy of the model can become at stake. Still another problem is that the models described do not give any hint of the microstructural phenomena occurring inside the material e.g. strain in one direction may or may not have the same effect on E modulus in that or other directions.

The aim of the present study is, therefore, to investigate the phenomena metallurgically and to come up with a material model that is general for each material and hence a better springback prediction with the new model. In following chapters, the Young's modulus will be referred as E modulus.

2. Degradation and Recovery of E Modulus

2.1 Introduction

In the previous chapter, it has been described that during plastic deformation, the E modulus does not remain constant and decreases with increase of plastic straining. It has also been known by some researchers that E modulus restores to its original value with time [24, 26]. The contents of this chapter are described in the following way.

- Theory of Degradation
- Theory of Recovery
- What is needed of steel to verify the theory?

2.2 Theory of Degradation

Following plastic deformation, the decrease in E modulus is presumably due to the increase of dislocation caused by deformation. Among different theories of degradation [27-30,23, 24], the pinning theory is most popular and successful in explaining the possible mechanism of degradation There are two types of degradation in pinning theory according to literature [29,30,31].i.e. frequency dependent and strain amplitude dependent. These will be discussed briefly here.

2.2.1 Frequency Dependent Degradation

The Frequency Dependent (FD) but strain amplitude independent model was originally proposed by Koehler [29] and later developed further by Granato and Lücke [30]. In this model, a dislocation line is supposed to be fixed at two ends by unspecified barriers which may be dislocation intersections or nodes, composite jogs, precipitates or impurities etc. An analogy of this dislocation line pinned at two ends is made with forced damped vibration of a string. Suppose that a rapidly oscillating external shearing stress is applied to a crystal. The portion of the dislocation line between the nodes oscillates back and forth on its slip plane like a stretched string (see fig 2.1). The motion/vibration forced by external stress is opposed by some damping mechanism and there is a phase lag for the oscillating stress and hence a change of modulus occurs. This type of loss is frequency dependent, since it has a resonance type character. It is largest near the resonant frequency determined by the loop length and goes to zero for very low and very high frequencies.

Fig 2.1: The oscillations of anchored dislocation

2.2.2 Strain Amplitude Dependent Modulus Defect

The strain amplitude (SA) dependent and FD mechanism of degradation is also explained by Koehler [29] and further developed by Granato and Lücke [30]. When an external stress is applied, there is in addition to elastic strain, an additional strain due to dislocation called dislocation strain. The idea can be explained best with reference to fig 2.2. For zero applied

stress, the length L_N is pinned by the impurity particle (A). For a very small stress, the loops Lc bow out as in (B) and continue to bow until the breakaway stress is reached. The effective modulus of the stress strain curve is determined by Lc in this range. At the breakaway stress, a large increase in the dislocation strain occurs for no increase in the stress (C-D). A further increase in the stress, the new loop length L_N bows out (D-E) until the stress required to activate the Frank Read is achieved. In this region, the effective modulus is determined by L_N. A further increase in the stress leads to creation and expansion of new closed dislocation loops as in stages F-G. The dislocation strain due to this process is irreversible and is called plastic strain. In this theory, it is assumed that the network pinning (major pins) is so strong that no breakaway occurs. The corresponding stress strain curve is shown in fig 2.3. In fig 2.3, the elastic strain has been subtracted and only dislocation strain is shown. The path ABCDEF is followed for increasing stress while the path FA is followed for decreasing stress. Solid line in fig 2.3 shows stress strain curve for the model in fig 2.2 and dashed line curve is the curve if not all the of the loops have the same length but there is a distribution of lengths Lc.

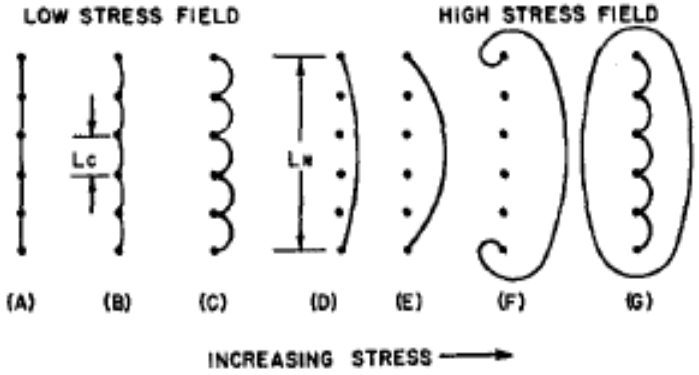

Fig 2.2: The successive stages while straining until the breakaway and then the activation of Frank-Read mechanism [30]

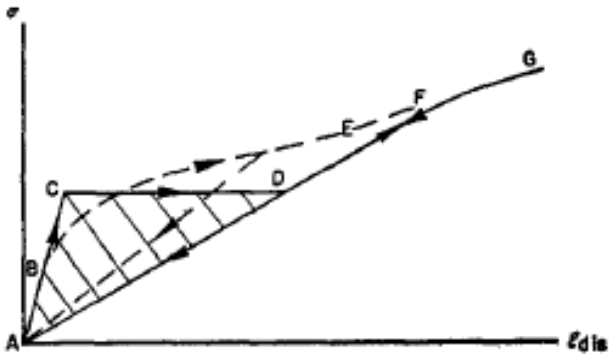

Fig 2.3: The corresponding stress strain curve. The lettered points match the sequence A-G in fig 2.2 [30]

In the elastic straining region i.e. before start of plastic deformation and Frank Read mechanism, when the load is decreased, the stress cycle will go from D to A in fig 2.2 and 2.3. In this unloading part, the long loop will collapse again and they will be pinned by the impurity particle again and the same type of paths is followed in other half cycle. This loss in modulus is proportional to the area enclosed by stress dislocation strain loop and therefore for loop L_N the modulus is small. For small enough stresses, the modulus decrease is

negligibly small as in fig 2.2(b) and therefore it is strain amplitude dependent and independent of frequency.
The theory outlined above is actually applicable at room temperature (RT). It is not expected that dislocation lines will be pinned by impurity particles at high temperature (Well above room temperature [32]. The problem of modulus defect at high temperature is beyond the scope of this report and will not be discussed here. Interested readers are referred to Blair [33] and Kosugi [34] for further reading.

2.2.3 Distinction between FD and SA Loss

The limit of strain amplitude between FD and SA dependent E modulus degradation is of the order of 10^{-7} -10^{-6} [27, 28, 35]. These two losses and their dependence on strain amplitude can be made clear by inspection of fig 2.4. This figure shows internal friction (decrement) of a Copper single crystal as a function of strain amplitude and temperature. Below strain amplitude equal to 10^{-7}, the FD internal friction is active and above it the SA dependent internal friction. It is expected that E modulus has also the same limit for FD and SA dependent loss.

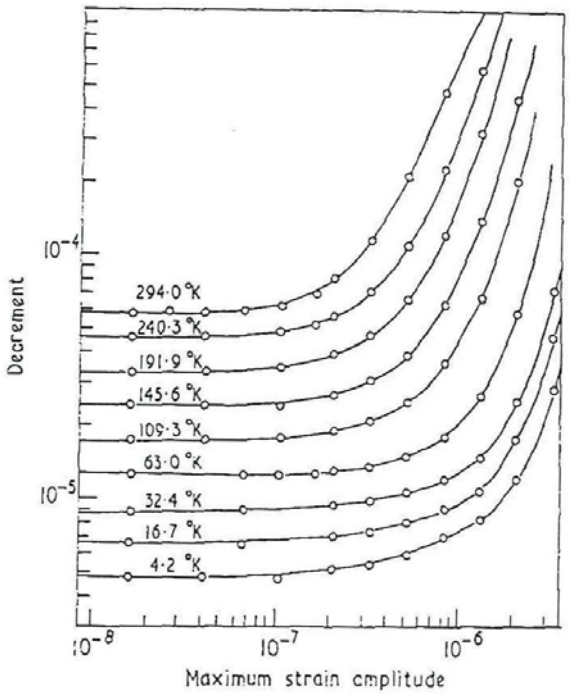

Fig 2.4: The internal friction of a Copper single crystal as a function of strain amplitude and temperature measured at 40 kHz [35]

2.3 Theory of Recovery

Following plastic deformation, E modulus recovers to its original value with time [24, 28, and 36]. For example, Krempaszky [36] observed partly restoration of E modulus after 5 days and full restoration after baking treatment at 170°C for 20 minutes (see fig 2.5). The degradation of E modulus below the recrystallization temperature is known to be due to oscillation of dislocations under the influence of applied stress. The degradation is considered to be due to an increase in dislocation density caused by the deformation. Therefore, the recovery must be then due to disappearance (annihilation theory) or immobilization of these dislocations [31]. Immobilization of dislocations is considered to be

due to the interaction of dislocations with other dislocations (rearrangement) or with point defects. The interaction of dislocations with point defects is generally referred to as pinning.

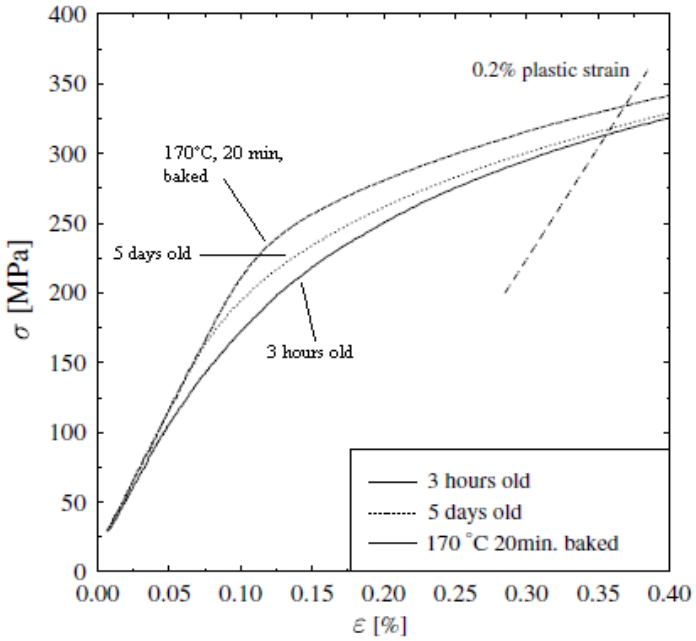

Fig 2.5: Stress-Strain Diagram for specimen aged for 3 hours, 5 days at room temperature and baked 20 minutes at 170°C [36]

The pinning mechanism of point defects or interstitials to dislocations is generally called strain ageing. There are several stages of strain ageing like Snoek relaxation, Cottrell atmosphere formation and Carbide precipitation. However, the most important among them is the locking of dislocations by point defects or interstitials which is called Cottrell atmosphere formation.

The mechanism of bake hardening is usually considered as a kind of strain ageing caused by segregation of carbon and/or nitrogen atoms (point defects or interstitials) to the dislocations generated by prior forming. During bake hardening (as the name suggests) the yield strength of the component increase and is discussed by many authors [37,38, 39, 40, 41, 42].

The restoration of E modulus is believed to be [31, 43] due to a decrease in the free dislocation loop length as the point defect and solute impurity atoms migrate to the dislocations and reduce their length. This is because E modulus is a function of [24] free dislocation length, besides dislocation density as shown in fig 2.2.

As discussed above, the strain ageing process (or the bake hardening process) can be called a recovery process. Normally, the bake hardening process can be broadly categorized in three stages. The first stage is called Snoek relaxation which is a stress induced local ordering of the impurities. This stage is followed by Cottrell atmosphere formation during which dislocations are anchored by clouds of carbon atoms followed by the final stage of bake hardening, called precipitation hardening. The three stages of bake hardening are shown for increase of yield stress versus the ageing time in fig 2.6.

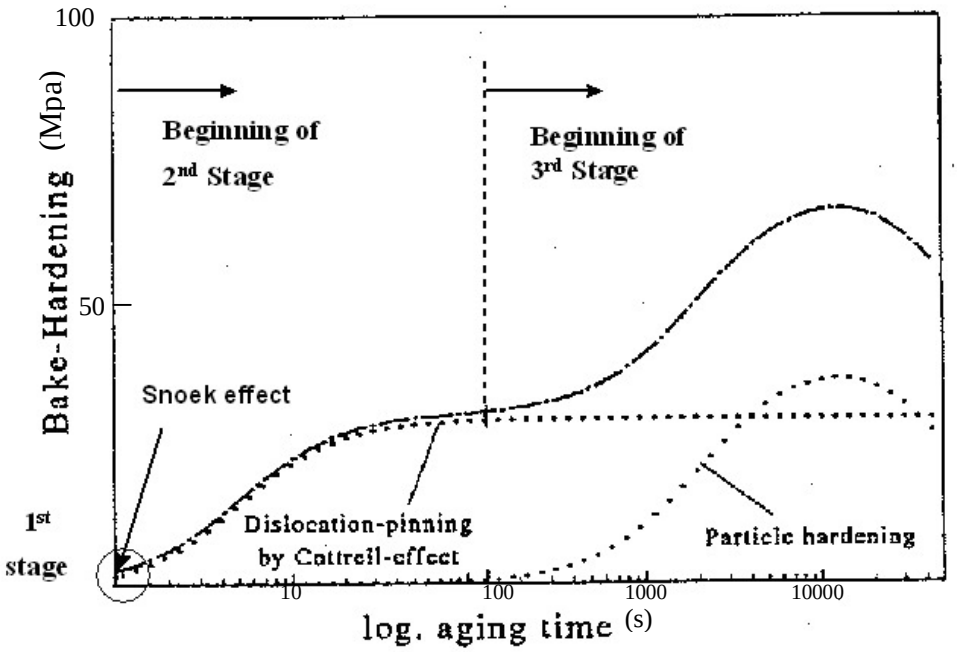

Fig 2.6: The three stages of the Recovery [37]

2.3.1 Snoek Relaxation

The Snoek ordering is a local ordering of the impurities when present in the stress field of the dislocation [44]. An interstitial atom such as carbon can occupy any one of three possible equivalent positions in the body-centred cubic iron lattice. If the crystal is strained, however, certain sites lead to a greater reduction in free energy than others, and a state of order correlated to the strain distribution may arise. This happens in the vicinity of the dislocations. This ordering involves only single atomic jumps and therefore does not lead to any migration to the dislocations.

Fig 2.7 shows an atomic model of Snoek relaxation. The interstitial solute atoms are positioned on interstitial sites in the bcc lattice. There are two types of sites which may be occupied by the solute atoms, octahedral (a) and tetrahedral (b). An inspection of the defect symmetry for the site 1 with respect to the surrounding atoms shows that both sides, octahedral and tetrahedral, exhibit tetragonal symmetry [51]. There exists three group of sites, indicated with 1, 2 and 3, with equal distribution of the interstitial atoms. Applications of stress lead to a redistribution of the interstitials. The stress induces reorientation of the interstitial atoms at temperatures where the interstitials can diffuse. This results a redistribution of the population of the sites with lower energy to increase, whereas that of the sites with higher energy will decrease. A similar redistribution of interstitials on different lattice sites will take place in the stress field of dislocation. By this process, the energy of system is lowered, the dislocation is locked which causes a rise to a mechanical loss peak, called Snoek peak.

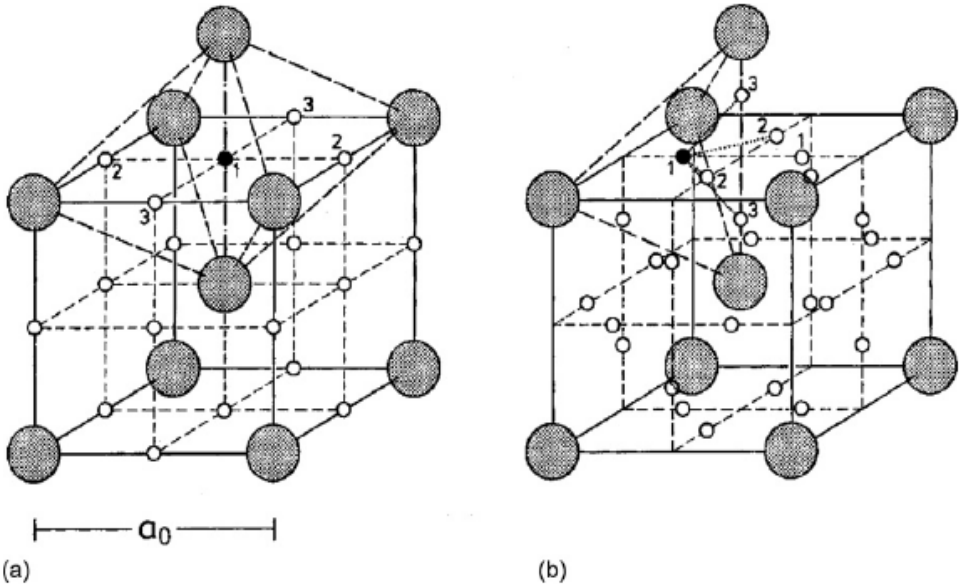

Fig 2.7: Atomic model of the Snoek relaxation in bcc metals (a) Octahedral and (b) tetrahedral interstitial sites [45], a_o is the lattice parameter

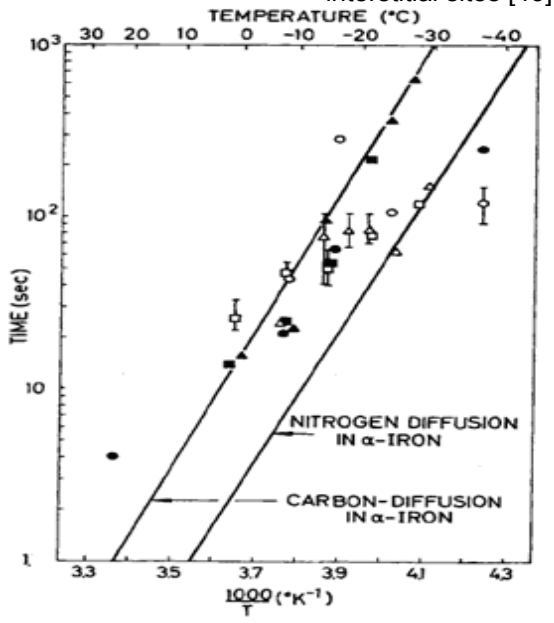

Legends	Description
○	Single Crystal iron annealed at 870°C, aged at stress
●	Single Crystal iron annealed at 870°C and aged at zero stress
□	Polycrystalline iron annealed at 870°C, Aged at Stress
■	Polycrystalline iron annealed at 870°C, Aged at Zero Stress
△	Polycrystalline iron quenched from 700°C, Aged at stress
▲	Polycrystalline iron quenched from 700°C, Aged at zero stress
+	Yield Point Return Data of [80] on polycrystalline iron annealed at 870°C

Fig 2.8: Inflexion time between first and second stage of strain ageing versus reciprocal of absolute temperature [43]

Since, essentially only a single jump of a carbon atom is necessary for the Snoek rearrangement stage, the time involved is much shorter than the time required to form a Cottrell atmosphere (Sec 6.3.2). The time required to complete Snoek relaxation, called inflexion time, is shown in fig 2.8 against the reciprocal of the absolute temperate. It can be seen from the figure that increasing the ageing temperature decreases the time required for the completion of the first stage of strain ageing. The initial stage has an activation energy corresponding to the short range motion of interstitials in dislocation stress field of 58.576 ± 9.6 kJ/mol, while that of 2nd stage with longer range diffusion has an activation energy of 92 ± 8.3 kJ/mol [43].

2.3.2 Cottrell Atmosphere

If a dislocation (Fig 2.9) is present in the material, the application of externally applied shearing stresses causes the breaking of atomic bonds in the deformed plane, which is replaced by slip of the dislocation-containing plane and hence the dislocation moves from one end to other causing plastic deformation. A dislocation also introduces local volume change. Below the line of a positively oriented edge dislocation, local tensile stresses exist while above the defect line, local compression stresses are present. Changes in the stress field of the dislocation are the driving force for the migration of impurity atoms to the dislocations. The characteristics of the segregation depend on the chemical nature of solute atoms. If the atoms are substitutional, those smaller than the matrix species choose the compressed regions; while large substitutional atoms and interstitial solute atoms migrate to the dilated parts of the crystal around the dislocation. This latter phenomenon is known as Cottrell atmosphere which is medium range diffusion of carbon and nitrogen atoms to the stress field of the dislocations and the 2^{nd} stage of bake hardening mechanism (See fig 2.10). During this process, nano sized rod shaped clouds forms by the segregation of impurity (carbon and/or Nitrogen) atoms along the dislocation line.

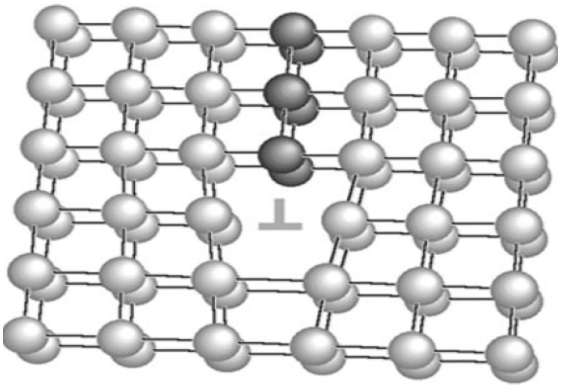

Fig 2.9: Schematic representation of an edge dislocation in a cubic crystal

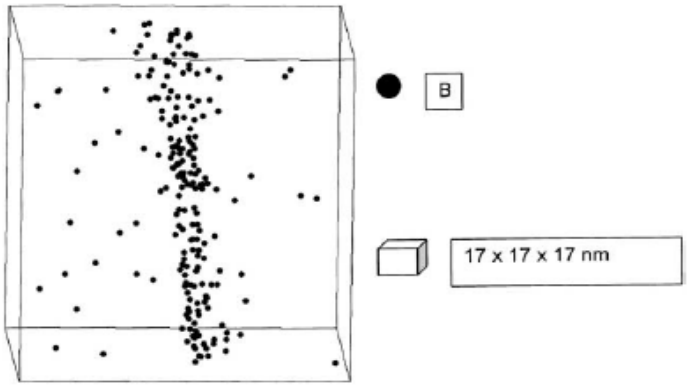

Fig 2.10: Atomic scale image of Boron rich Cottrell atmosphere in FeAl. The area under analysis is a square of 17 nm^2 .Boron rich atmosphere appears as a 5 nm-diameter rod [46]

The force with which the carbon atoms are pulled towards dislocation core is called drift force. The drift force arises from the decrease in dilatational energy of a carbon atom in sites near the tensions side of an edge dislocation. It is also suggested that a drift force of similar magnitude should also exist near a screw dislocation

The concept of Cottrell atmosphere was introduced by Cottrell and Bilby in 1949 [47]. They suggested that the mobility of dislocations is strongly affected by Cottrell atmosphere so that an additional stress is necessary to make the dislocation leave the impurity cloud to start plastic flow. Cottrell's model of atmosphere formation describes only the kinetics of the change of carbon content due to diffusion. It is expressed as:

$$\frac{N(t)}{\rho} = \frac{3}{2} n_0 \lambda V_{dis} t^{2/3} \quad \text{----------[2.1]}$$

where $N(t)$ is the number of carbon atoms diffusing to dislocation in a unit volume within time t, ρ is the dislocation density, n_0 is the initial concentration of carbon in solution and λ is the slip distance of dislocations, $V_{dis} = 2(\pi/2)^{1/3}(AD/kT)^{2/3}$ with D being the diffusion coefficient of carbon, k the Boltzmann constant, T the absolute temperature and A is a parameter which defines the magnitude of the interaction between the dislocation and the carbon atom. But this equation is applicable only during early stages of the formation of Cottrell atmosphere before saturation when $N(t)/\rho > 0.3$.

Harper [48] modified the Cottrell's model and took account of the fact that the rate of segregation of interstitial atoms is proportional to the fraction remaining in solution. He described his model as:

$$q = 1 - \exp[-\frac{3}{2} L_0 V_{dis} t^{2/3}] \text{----------[2.2]}$$

Here q is the fraction of the original amount of free carbon which has precipitated during time t, $L_0 = (\lambda/\rho)$ is the dislocation length per unit volume. This equation is often used to describe the change of mechanical properties during ageing. But it is only useful as long as the change of the properties is directly proportional to the change of carbon content. The recovery of modulus should increase with the number of atoms which gather in an atmosphere but the interaction and the pinning effect decrease with the distance between the dislocation and the carbon atom. Cottrell mentioned that the first atoms arriving at dislocation tend to be more effective in anchoring it than those arriving later. Therefore, for later stages of ageing, the direct proportionality between the numbers of carbon atoms around dislocation with E modulus recovery should not be valid.

Zhao [49] has made calculation that a dislocation loses almost all its ability to trap other carbon atoms in further ageing process as soon as a carbon atom has segregated to it. The central part of atmosphere accounts for 98% segregation of carbon atoms to dislocations which are important to pin the dislocation. The instantaneous segregation rate of carbon atoms to dislocations is proportional to the length of effective dislocations which can be approximated as $L(t) = L_0 - \lambda N(t)$, $L_0 = \lambda/\rho$ is the initial length of dislocations. During ageing of bake hardening steels the carbon atoms segregate not only to dislocations but also concurrently to grain boundaries. Keeping in mind the fact that the first carbon atoms arriving at dislocation are more effective in anchoring it and with assumption of segregation of carbon to grain boundaries and to pre-existing cementite negligible [50], Zhao developed the following model for Cottrell atmosphere formation:

$$\frac{N(t)}{\rho} = \frac{1 - \exp[\frac{3}{2}(L_0 - n_0\lambda) V_{dis} t^{2/3}]}{1 - \frac{\rho}{n_0} \exp[\frac{3}{2}(L_0 - n_0\lambda) V_{dis} t^{2/3}]} \text{----------[2.3]}$$

The spatial average saturation level of dislocation, S_{dis} vs. ageing time for Cottrell's formula and Zhao's model for 2% and 5% prestrained specimens aged at 50°C and or 100°C is shown in fig 2.11 which shows that the predictions made with Zhao's model fits the $\Delta\sigma/\Delta\sigma_{max}$

vs. time curve much better than with predictions made with Cottrell's model especially in the later stages of Cottrell formation.

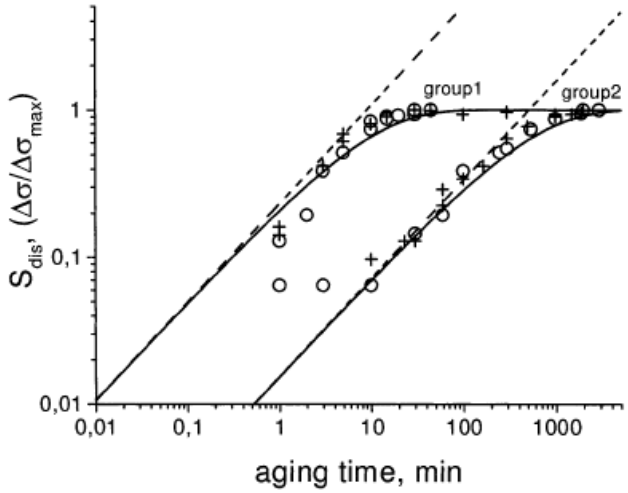

Fig 2.11: Fractional increase in yield stress ($\Delta\sigma/\Delta\sigma_{max}$) (crosses for 2% and circles for 5% prestrained) and the dislocation saturation level predicted for 2% and/or 5% prestrained specimens with Cottrell's formula (dashed line) and the Zhao's model (solid line). Group1: samples aged at 100°C, Group 2: Samples aged at 50°C) [49,50]

Cottrell estimated that for an initial dislocation density of 10^{12} m^{-2}, the amount of Carbon required for saturation has to be about 1 wt-ppm keeping in mind the assumption that 1-2 carbon atoms need to be present per atom plane threaded by the dislocation [47]. De [51] found that for a total dislocation density of $2.8x10^{13}$ to $1.3x10^{14}$ m^{-2} following 10% uniaxial tensile prestraining in an ultra low carbon hardening steel, the required carbon for saturation is 0.25 to 1.2 wt-ppm. Therefore, it can be concluded that extremely small amount of carbon is sufficient to pin all the dislocations in a crystal.

2.3.3 Carbide Precipitation

Carbide precipitation is the last stage of the recovery process. Precipitation of carbides occurs at dislocations during ageing. As the process of ageing continues, more interstitials arrive at dislocations and dense atmosphere form around dislocation which act as nuclei for precipitation. The process results in formation of clusters and finally the precipitation. It is postulated that the carbides in the form of coherent particles are cut by dislocations.
Carbide precipitation exists only in low carbon steel and is absent in ultra low carbon (ULC) steel where carbon content is < 50 wt.% ppm [40,41,42]. This is because almost all carbon content has been used in the 2nd stage for atmosphere formation of Cottrell and therefore no more carbon is available for carbide precipitation.
In case of ULC steel, since there is no carbon available for 3rd stage, the volume fraction of the particles is nearly independent of the number of nuclei per unit volume. The number of favourable precipitation sites and with that the number of particles is raised, if the dislocation density is increased by pre-deformation. In that case, the particle size decreases because of the constant volume fraction of carbides. The stress increment due to cutting coherent precipitates is proportional to the root of the particle size and so it decreases if the particle size decreases. With an increase in prestrain, the particle size decrease and hence $\Delta\sigma_{max\ ppt}$ decreases.

2.4 What is needed of steel to verify the theory?

To verify the degradation theory and recovery phenomena discussed, we need a steel to make experiments on. In automotive industry the following grades are being used [51].

- Commercial Quality (CQ)
- Low Carbon-Drawing Quality(DQ)
- IF stabilized- Deep Drawing Quality(DDQ)
- Dent Resistant
- Bake Hardenable (BH)
- High Strength Low Alloy(HSLA)
- High Strength solution strengthened
- Ultra High Strength(UHS)
  - Dual Phase(DP)
  - Martensitic
- Laminated Steel
- Stainless Steel(SS)

Among these steels, bake hardenable (BH) steel seems the one which can show degrading behaviour on plastic deformation and the possible recovery/increase or strain ageing phenomenon and therefore is being selected for the experiments of this study. The phenomenon of strain ageing at room temperature is a slow process and Corus guarantees 3 month period to its customers for BH steel at room temperature. Since the BH steel is a heat treatable steel, therefore an appropriate heat treatment can be applied to simulate the condition of strain ageing at room temperature and thus time can be saved. The recovery/increase in E modulus for BH steel has been shown by Blaimschein [52] where BH steel ZStE180BH with and without heat treatment is compared with steel types PO_4 and PO_6 (which is probably Phosphorous steel) following plastic deformation up to 5%. The BH grade steel with heat treatment showed an increasing trend unlike other grades of steel following plastic deformation.

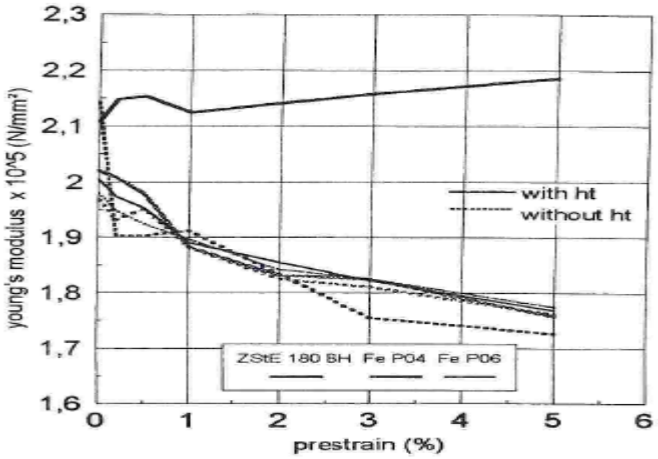

Fig 2.12: Comparison of E modulus values as a function of prestrain with and without heat treatment [52]

3. Bake Hardenable (BH) Steel

3.1 Introduction

From discussion in chapter 1, it is clear that use of high strength steel is important for mass reduction through decrease in sheet metal thickness. Other issues pertaining to forming of steel from the automotive manufacturer point of view are better formability, increased final strength, increased dent resistance, better crash management, increased load bearing capacity, predictable and/or lower springback. Besides the theory of degradation and recovery discussed in chapter 2, the BH steel also shows some of promising features and will be discussed in this chapter. The contents of this chapter are organized as

- Background
- Bake Hardening Effect
- Physical Properties of BH Steel
- Metallurgical and Other Influential Factors
- Dislocation Structure
- Model for Degradation

3.2 Background

The concept of bake hardening of steel was applied unsuccessfully during sixties and seventies. During that time, strain ageing of rimmed steels was mainly caused by nitrogen but its amount could not be controlled in the production process. Strain ageing occurred quite rapidly at room temperature causing changes in mechanical properties like a sharp yield point and loss of ductility before forming operations. This caused problems like stretcher strains [37]. In modern BH steel, all nitrogen is tied as aluminium nitride and only a small amount of carbon in solid solution controls the bake hardenability. Beyond a specific limit, the amount of carbon (that will be discussed in subsequent sections), should not be increased as it may result in an accelerated strain ageing at room temperature which is not desirable.

3.3 Bake Hardening effect

The term BH effect is normally used to denote the increase of yield strength as a result of prestraining and baking treatment. It is defined as the difference between higher yield (R_{bH}) point after prestraining (2%) and ageing (at 170°C for 20 minutes) and proof stress at the prestrain level (R_t). The bake hardening response measured via this procedure is referred as the “bake-hardening index” (BHI). The lower yield point is represented by R_{bL} (See appendix A.2 for definition of these terms)

From the initial literature study [23], we know that dislocations are anchored by the nearby carbon atoms at the end of forming process. The diffusion of carbon to dislocations is slow at room temperature. However, the diffusion process is accelerated by a baking treatment at high temperature like at 170°C. The yield strength increases due to this phenomenon because the anchored or locked dislocation is difficult to move [38] which are necessary for plastic deformation. The process and microstructure is shown schematically in fig 3.1.

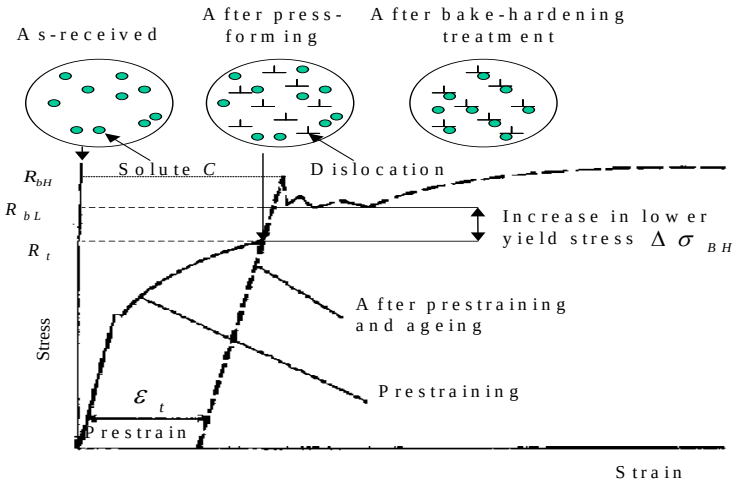

Fig 3.1: Stress-Strain curve showing before and after bake hardening treatment. Bake hardening index with Upper and Lower Yield points are also shown [37, 38]

3.4 Physical Properties of BH steel

Besides recovery phenomenon of BH steel, this grade posses some other desirable physical properties to automotives which will be described in the following

3.4.1 Formability and Strength

One of the most important objectives in the development of automotive steel sheet is the combination of strength and formability. Formability is required when the sheet is shaped into an automobile body panel, and high strength is required after assembly. Bake-hardenable steel sheet was developed by exploiting the fact that these two properties are not needed simultaneously. Bake hardenable steel has excellent initial formability as shown in Elongation – Strength diagram in fig 3.2.

The good formability of the BH steel eliminates the use of heavy duty and high tonnage presses for forming and hence can contribute to the economy of the company. After press forming the component acquires its desired shape. This is followed by paint baking process in automotive companies normally at 170°C for 20 minutes. During this stage, the yield strength of the component increases and hence finally the product is available with higher strength than it was before paint baking.

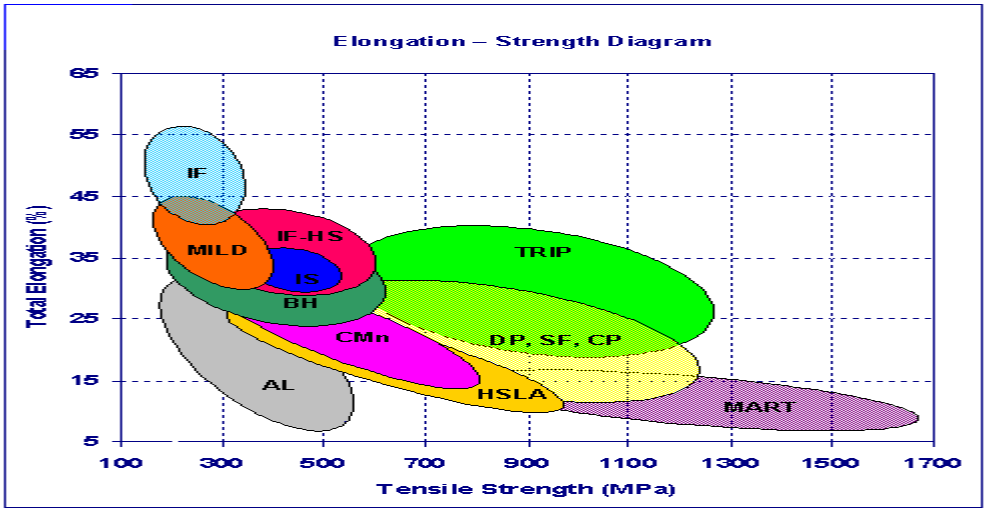

Fig 3.2: Elongation-Strength Diagram for different grades of steel [53]

This process is further explained in fig 3.3. Before press forming of sheet metal, there is initial low dislocation density. After plastic deformation (by press forming) the dislocation density is multiplied and results in work hardening. A further increase in strength is achieved when the interstitial carbon or nitrogen diffuse to them and locks them. This is done by heat treatment in the paint baking process as explained before.

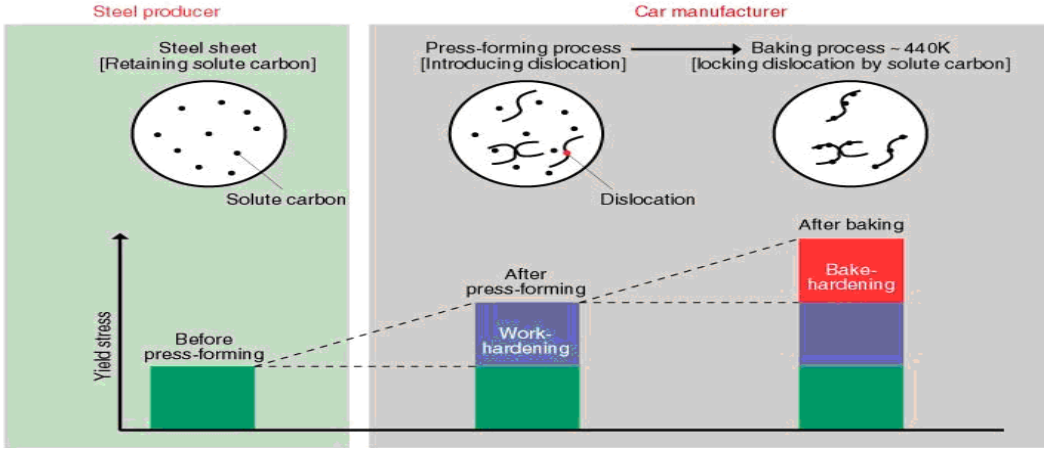

Fig 3.3: Increase of strength after press forming and after baking process

3.4.2 Dent Resistance

The dent resistance of a panel is an important consideration when selecting a type of steel for automotive outer panels. Yield strength, thickness of the formed part, and stiffness (related to curvature) of the panel each contributes to the overall denting behaviour. As discussed previously, to reduce the vehicle weight, steel sheets are down gauged which results in a decrease of dent resistance.

Stiffness is a primary concern when designing outer body panels. There is a minimum stiffness level that must be maintained for the majority of outer body panels. It has been shown that the energy necessary to cause a dent is inversely proportional to the stiffness based on the equation

$$D = K_1 \frac{y^2 t^4}{S} \text{ ----------[3.1]}$$

Here K_1 is a constant, y is the as-formed yield strength, t is the panel thickness and S is the stiffness [8]. Therefore, to increase dent resistance (the energy necessary to cause a dent), the panel stiffness must be decreased. McCormick and Fekete [52] showed increase in dent resistance of more than 50 N for Zste220BH grade as a result of bake hardening. While Blaimschein compared dent resistance of BH grade (ZsTE 180 BH) as a function of sheet thickness with soft grades (PO4 and PO6) in a shell dent resistance test. The comparison can be seen in fig 3.4 which shows that 0.8 mm thick ZsTE 180 BH has the same dent resistance as 0.91 mm FePO4. This results in percent weight reduction of 12%.

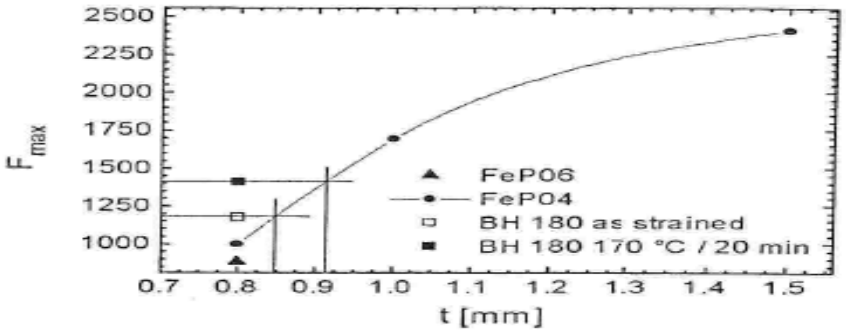

Fig 3.4: Dent resistance of different grades [52]

3.5 Metallurgical and Other Influential Factors

Now some metallurgical and other factors will be discussed which effects bake hardenability. Since, most research on BH steel to this date is being done on yield strength increase after ageing; therefore, in the following sections the effect of different factors will be discussed in terms of its yield strength increase. There is need for further experimental research to see the effect on E modulus with these influencing factors.

3.5.1 Effect of Carbon and Nitrogen content

The amount of carbon obviously controls the possibility of pinning mobile dislocations. Consequently, with more solute carbon, more dislocations can be pinned and a higher recovery of modulus should be obtained. With too little carbon, there will be no more free carbon content available for later stages of ageing (i.e. carbide precipitation) as all of the carbon must have been used for pinning of dislocation by that time. This has been experimentally observed by Vandeputte [40,41,42] where he observed absence of the third stage of recovery (i.e. carbide precipitation) in ULC steel with carbon content equal to 20 wt-ppm while this stage was present in low carbon [LC] steel.

Table 3.1: Activation energy, frequency factor, diffusion and diffusion distance for carbon and nitrogen in bcc metals [55,63

Parameter	*Carbon in Fe*	*Nitrogen in Fe*
Activation energy Q_D (kJ/mol)	80.2 - 84.1	73.2 - 77.8
Frequency factor D_o (cm^2s^{-1})	6.2×10^{-3}	3.0×10^{-3}
Diffusion coefficient D at 25ºC (cm^2s^{-1})	5.9×10^{-17}	1.4×10^{-16}
Diffusion distance $X = \sqrt{2Dt}$ (μm) at 25ºC, for t = 6 months	0.43	0.66
Diffusion distance $X = \sqrt{2Dt}$ (μm) at 170ºC, for t = 20 min	0.74	0.89

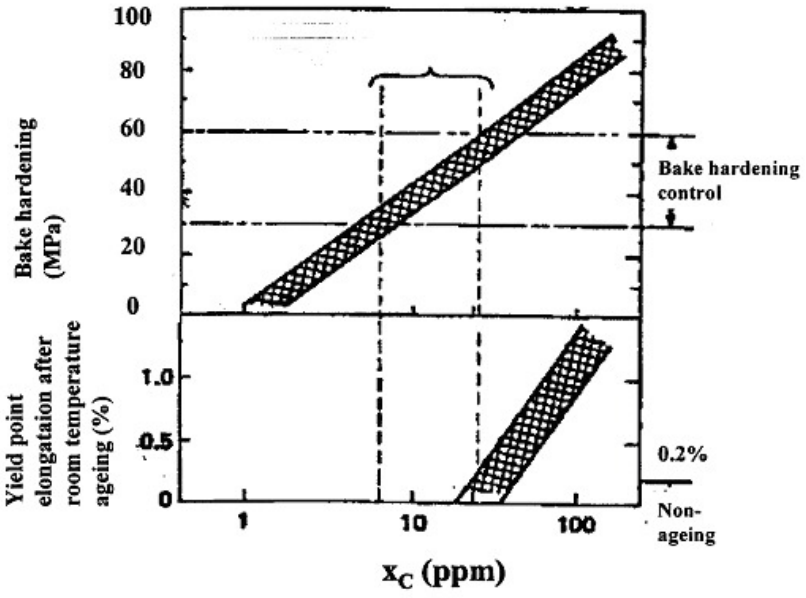

Fig 3.5: Effect of solute carbon on bake-hardenability and room temperature ageing [56]

Like Carbon, nitrogen can also be used as a solute content for bake hardening or recovery but the problem with nitrogen is its ability of very fast diffusion which make BH steel vulnerable for ageing at room temperature. In modern BH steel, therefore, it is tied with Al as AlN [57] and the BH effect is obtained by using carbon instead. A comparison of carbon and nitrogen in BH steel is presented in table 3.1. It can be seen that due to high diffusion coefficient of Nitrogen, the diffusion distance is always higher for one sort of input conditions when compared with carbon.

Some researchers [37] shows that for optimum bake hardenability, the amount of carbon should be in the range of 5 to 15 wt. ppm in solid solution. While others [38] mentions the range between 10 and 25 wt. ppm. From the various researches, it can be said that a very small amount of Carbon is required for Cottrell atmosphere formation even for a highly deformed material. It has been describe by various researchers that to saturate the dislocation at Cottrell atmosphere formation, one carbon atom per atomic plane is required. From this fact, De [42] gave the following mathematical relation between the dislocation density ρ (m^{-2}) in bcc ferrite and the carbon content required for saturation

$$[C]_{ppm} = 8.9x10^{-15}.\rho \text{ ----------[3.2]}$$

Therefore, even for a large density of 10^{14} m^{-2}, only about 1 ppm carbon is required to saturate all dislocations. If the amount of carbon is increased beyond the upper limit, strain ageing occurs at room temperature causing yield point elongation (YPE). Room temperature ageing before forming is not acceptable and poor surface quality of the stamped product due to appearance of stretcher strain marking on the stamped product. The effect of carbon content on YPE and bake hardening is shown in fig 3.5.

3.5.2 Effect of Deformation and Ageing Temperature

There are two types of deformation i.e. temper rolling and tension/compression prestraining. Both of these have different effect on the dislocation structure and behaviour. Temper rolling is a necessary step in the production of BH steel because it eliminates the discontinuous yielding of the as annealed material (see fig 3.6). Usually, a temper rolling of 1% completely eliminates YPE [39]. Strain ageing after temper rolling is more slow process if compared after pre straining. The possible reason is lower magnitude of strain in case of temper rolling than in pre straining.

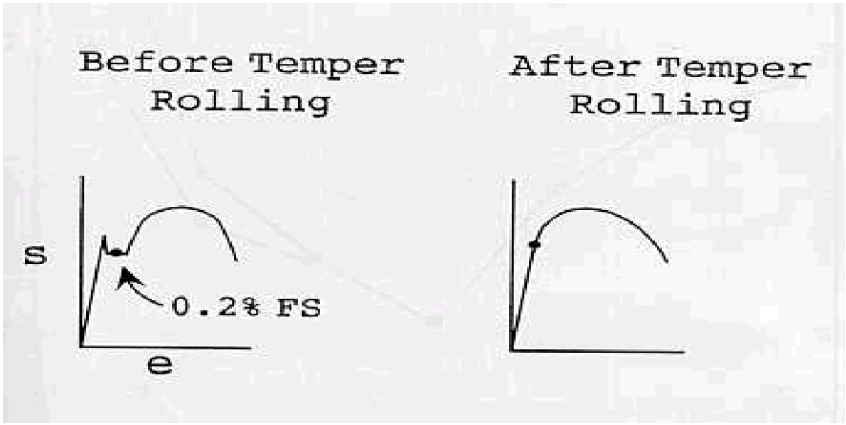

Fig 3.6: Effect of temper rolling on the yielding behaviour of BH steel [39]

Prestraining is considered to be responsible for amount of dislocation density and structure. As the prestraining is increased, so the dislocation density increases with possible potential of higher pinning effect in Cottrell atmosphere formation. The ageing temperature speeds up

the diffusion process and so the strain ageing process completes in less time as the temperature is increased. The effect of pre strain at 150 and 180 °C is shown in fig 3.7. It can be seen a yield strength increment of 20 MPa is achieved after a short time of ageing which is a result of Snoek and Cottrell atmosphere formation. However, the distinction between these two stages is not possible. With increase in pre strain level for a specific temperature, the contribution of the strength increment in 3rd stage decreases. The duration for first and 2nd stage of bake hardening decreases for the same level of deformation with an increase in ageing temperature. This becomes clear by a comparison of fig 3.7 (a) and (b).

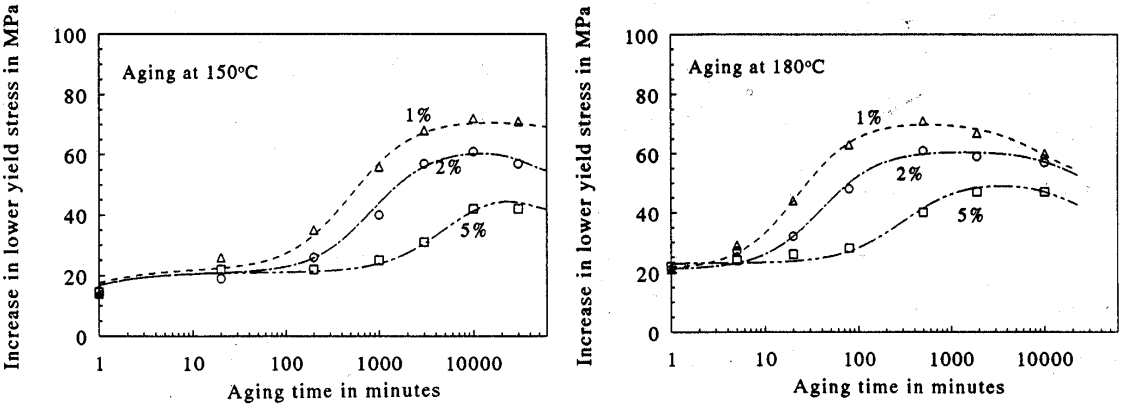

Fig 3.7: Effect of different levels of pre strain on the sample of ZStE180 BH when it is aged at **(a, left)** 150 °C, **(b, right)** 180°C [37]

The effect of pre straining on E modulus and baking effects are a bit inconsistent [58]. The finding of Round Robin Test conducted by Daimler and ThyssenKrupp Steel (TKS) are presented in table 3.2 and plotted in fig 3.8 (only TKS results) for a soft Interstitial Free (IF) steel (DX57), micro alloyed steel (H320 LA) , multiphase DP steel (HCT600X) and Residual Austenite (RA) steel (HCT700T). Tensile samples were prestrained in transverse direction. Baking treatment at 170°C for 20 minutes was applied for 2 % and 20% prestrain except for HCT600X for which the baking treatment was done at 15%. The standard deviation for the tested specimen was between 1 and 11 GPa. Although, effect of pre straining on all grades of steel was found to decrease the E modulus but the value of E modulus found by the two companies are slightly varying. This variation seems the result of lack of standardization for measurement of E modulus by tensile test [58]. The need of more accurate and highly standardized method for E modulus measurement is emphasized. As can be seen from the fig 3.8, E modulus restores to its original value for all grades of steel at 2% prestrain followed by baking treatment. For other prestrain and baking treatments, E modulus shows somehow a value in between before deformation and after deformation.

Table 3.2: Results of Round Robin Test on four grades of steel [58]

	IF				H320LA				HCT600X				HCT700T			
	Daimler		TKS		Daimler		TKS		Daimler		TKS		Daimler		TKS	
	E(GPa)	STD	E(GPa)	STD	E(GPa)	STD	E(GPa)	STD	E(GPa)	STD	E(GPa)	STD	E(GPa)	STD	E(GPa)	STD
0%	190,7	2,5	194,8	7,7	211,5	2,1	224,6	7,0	216,6	2,7	208,7	5,9	218,3	2,8	217,7	5,5
2%	177,7	1,8	170,3	2,6	189,4	5,8	202,4	1,6	191,8	4,0	190,6	1,8	200,3	2,0	195,7	5,9
2% + 170°C / 20 min.	193,3	0,5	190,0	9,7	212,5	1,4	223,6	4,8	214,5	1,1	213,1	3,8	214,3	4,0	217,6	3,6
5%	174,4	1,9	168,2	3,1	184,3	4,3	194,0	4,3	189,5	6,1	183,7	1,9	199,6	3,5	188,4	2,2
10%	169,4	3,0	165,1	0,8	181,0	1,6	181,9	2,0	179,8	6,0	178,9	1,1	186,2	3,6	180,7	5,7
15% (HCT600X) and 20% (rest)	163,1	0,2	165,7	2,7	179,5	1,7	186,1	4,4	179,9	1,8	181,0	1,8	177,4	2,5	181,3	0,7
20%+ 170°C / 20 min.	167,6	6,7	167,5	4,8	187,6	3,5	205,3	11,5	183,5	6,0	200,7	4,5	200,3	2,3	204,3	3,4

In the light of the theory presented for degradation and recovery, the recovery in E modulus for all grades of steel is understandable except IF steel. As the name suggests, this steel do not contain any free carbon and therefore the strain ageing phenomenon cannot takes place in this steel. But still, E modulus has restored at 2% prestrain for this steel. An orientation imaging microscopy (OIM) study of the sample has shown a strong localization of deformation within ferrite grains depending upon the grain orientation. The dislocation entanglement with grains can be seen at 2% prestrained in fig 3.9. The original microstructure is restored on baking heat treatment.

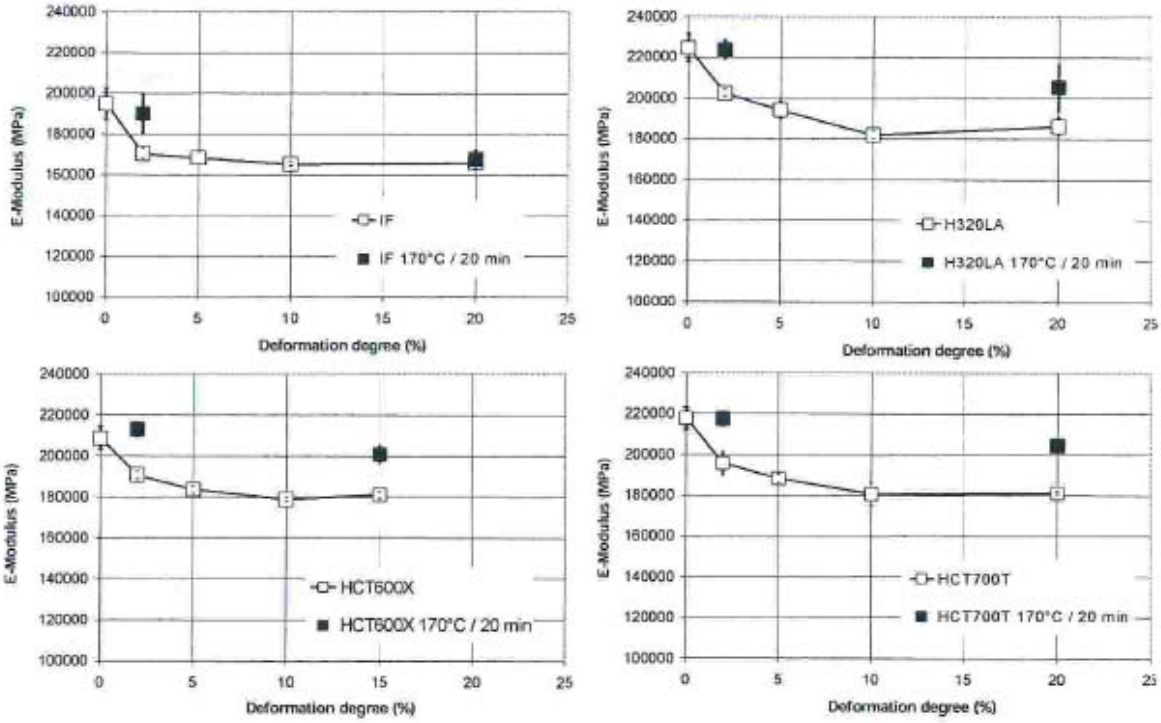

Fig 3.8: Effect of Prestraining and Baking treatment on different grades of steel [58]

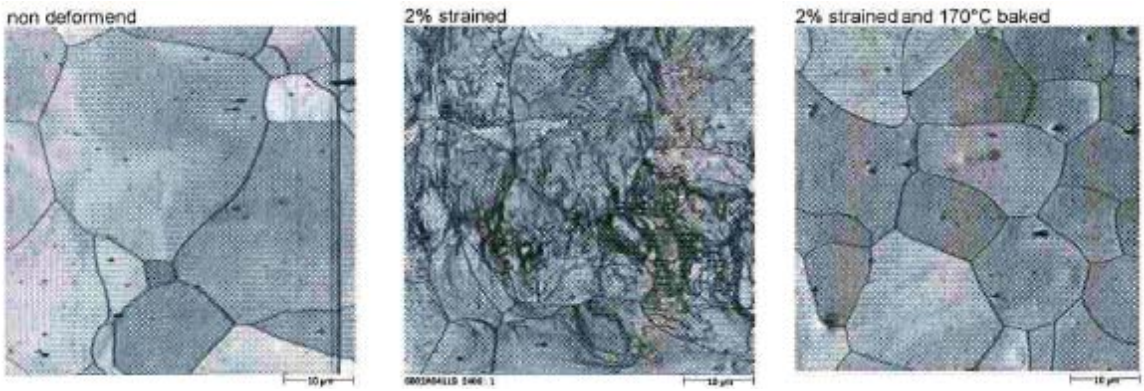

Fig 3.9: OIM images at non deformed, 2% pre strained and 2% pre strained followed by baking treatment [58]

Another recent research [59] has shown some contrast to the earlier study. E modulus is measured in three directions along the RD, at 45° and at 90° before and after baking treatment as a function of pre strain. As can be seen in fig 3.10 top figure, there is a full recovery in E modulus for the sample along RD at 5 and 15% while at 2%, the E modulus has a reduced value. For other two directions, there is a decrease at 2%, increase at 5% and another decrease at 15%. There could be many reasons for this contrast like the

difference in chemical composition, process and production variants from one company to another. Further research is necessary in case of IF steel. The same research [59] also shows full recovery in E modulus for BH, HSLA and DP/TRIP steels. Fig 3.10 (bottom figure) shows recovery in E modulus for BH Steel.

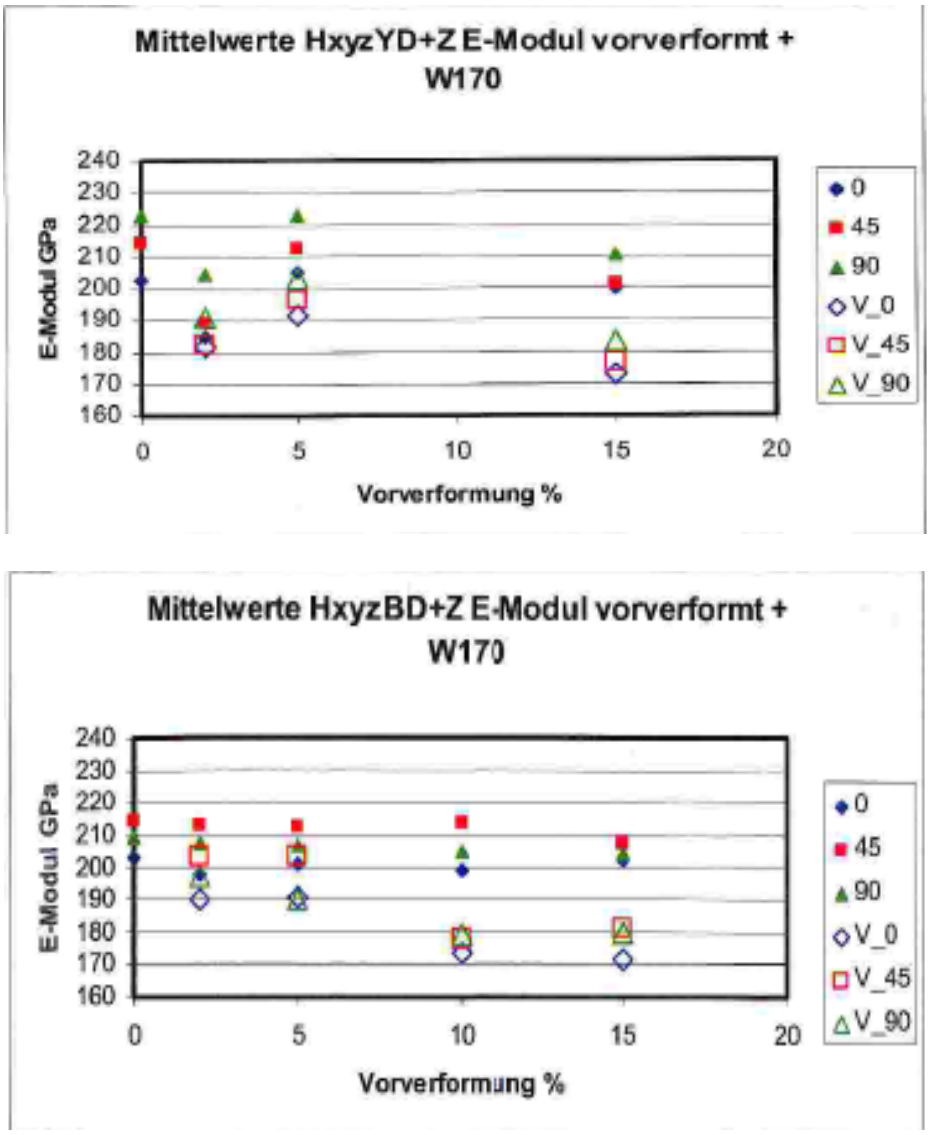

Fig 3.10: Effect of prestraining and heat treatment on IF steel (top) and BH steel (bottom). The hollow legend show prestraining without heat treatment and solid legend show prestraining accompanied with heat treatment [59]

3.5.3 Effect of Sample Orientation

During temper rolling of steel in production line, the so called “herringbone” structure develops which contains regions of deformed and non deformed material, which tends to be oriented across the strip width as shown in fig 3.11. This heterogeneous dislocation structure depends strongly on the temper rolling conditions such as tension/compression ratio, lubrication, diameter of rolls, sheet thickness etc. When the baking treatment is applied to the temper rolled specimen after 0% prestrain, the dislocation structure available for pinning is those generated by temper rolling and therefore only those dislocation will contribute to the yield strength increment which lies in the active slip plane. Therefore, the

yield strength increment resulting from baking will vary according to the dislocation density available in active slip plane. This is made clear by an overview of table 3.2 where the H180BD samples are baked in two directions i.e. in the direction transverse to rolling (TD) and in the direction of rolling (RD) without prestraining. Maximum bake hardening is obtained in TD direction, therefore, this direction can be considered as the direction of highest dislocation density. For both directions, bake hardening is sensitive to temperature.

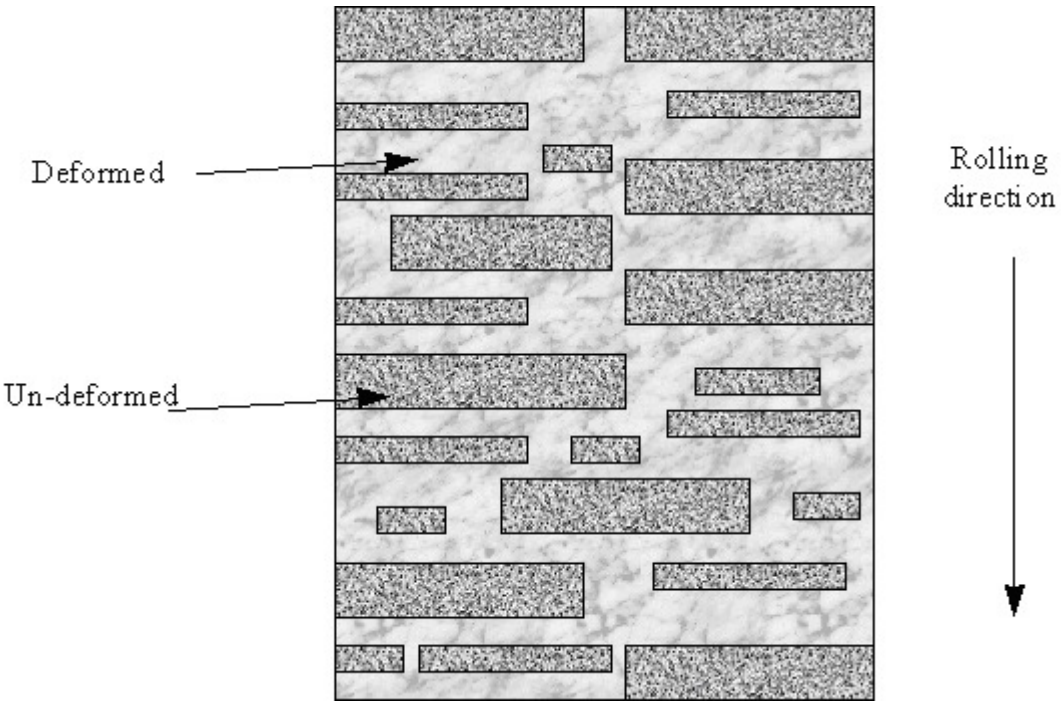

Fig 3.11: The schematic of herringbone structure developed during temper rolling [38]

Table 3.2: Bake hardening response after different temperatures and sample orientation after 0% prestrain [38]

Temperature (ºC)	$\Delta\sigma_{BH}$ **(MPa) in *TD***	$\Delta\sigma_{BH}$ **(MPa) in RD**
140	22	4
170	46	28
200	55	41
230	60	44

3.5.4 Effect of Primary and Secondary Deformation Direction

The direction of secondary deformation with initial pre straining plays an important role on the mechanical properties of BH steel. A difference in ageing response and yielding behaviour has been observed when the direction of secondary deformation is transverse when compared with a sample with secondary deformation in the direction of pre strain. As the diffusion of Carbon is same in both cases, the difference can be thought of the influence of different dislocation distributions introduced by the type of pre strain.
Figure 3.12 shows tensile curves of specimens cut in two directions from the bottom part of a stamped panel uni-axially deformed to 4% strain. The solid curve shows behaviour just after pre straining and the dashed curve shows the behaviour after baking at 170°C for 20 minutes. As can be seen, when the secondary and primary deformation direction is same,

an upper yield point accompanied by YPE appeared while no YPE is seen when the direction of secondary deformation is perpendicular to the primary direction of deformation even when the heat treatment is applied. Also, the yield strength is found lower and no strength increment is found when the direction of secondary deformation is perpendicular. This behaviour can be explained by the Bauschinger effect that aids activation of dislocation sources when the direction of straining is different from the direction of prestrain. The mechanism of the Bauschinger effect lies in the structure of the cold worked state. Orowan [60] described that during plastic deformation dislocation will accumulate at barriers in tangles, and eventually form cells. Upon removal of the load, the dislocation lines will not move because the structure is mechanically stable. However, when the direction of loading is reversed, some dislocations lines can move an appreciable distance at a low shear stress. This is because the barriers to the rear of the dislocations are not likely to be too much strong and closely spaced as those immediately in front. This results in initial yielding at a lower stress level when direction of loading is reversed [38, 56].

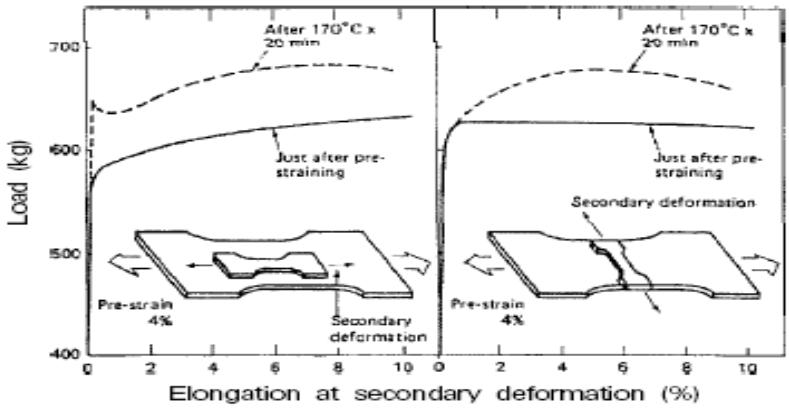

Fig 3.12: Effect of secondary deformation direction with Prestraining Direction (Rolling Direction) [56]

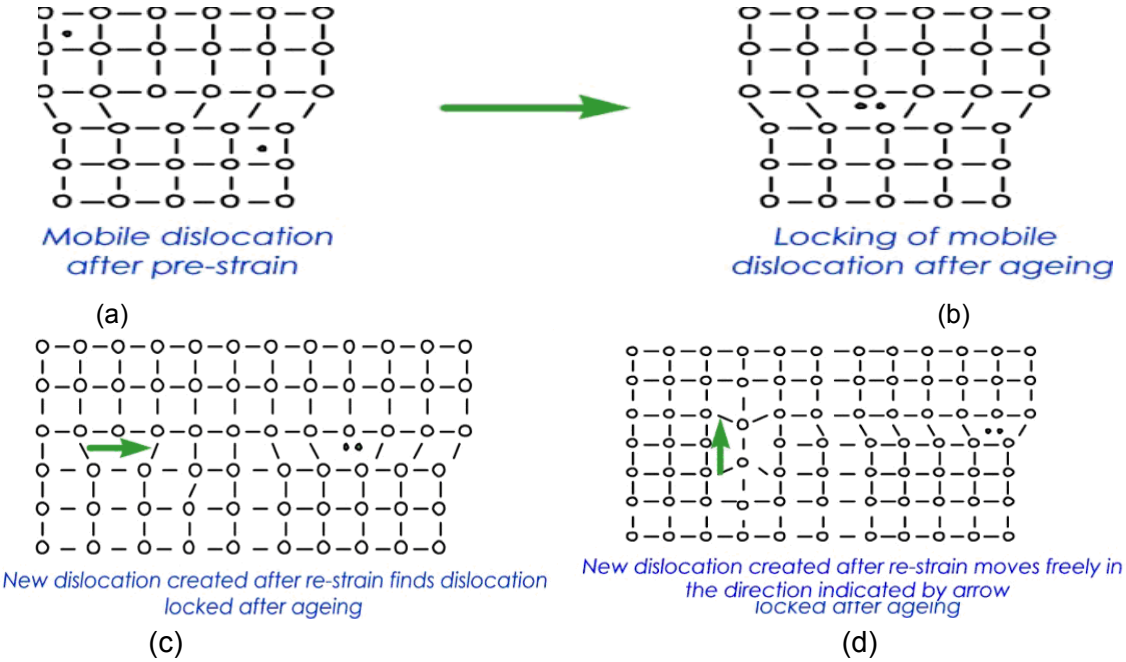

Fig 3.13: Mobile dislocation and its locking after ageing (a,b). When the direction of secondary deformation is (c) same, and (d) at right angle [38]

Exebio [38] presented metallographic explanation of this phenomenon. Mobile dislocations are locked by the ageing mechanism in which Carbon or Nitrogen interstitials diffuse to them. When the direction of secondary deformation is same, the deformation by means of newly created mobile dislocation takes place in the active slip system where it finds resistance to motion by the already locked dislocation and therefore causes an increase in yield strength (See fig 3.13(a), (b) and (c)). However, when the direction of secondary deformation is perpendicular, another slip system plays role in plastic deformation in which there is no resistance to movement of newly created mobile dislocation and hence there is no yield strength increment. (See fig 3.13(a), (b) and (d)).

3.5.5 Effect of Grain Size

The control of proper grain size is an important step for optimum bake hardenability. Variation of grain size affects distribution of carbon between the grain interior and the grain boundaries by changing the number of segregation sites at the grain boundary. The grain boundary provides low energy sites for interstitial carbon or nitrogen atoms and therefore interstitial atoms diffuse to it. As grain size increases, grain boundary area decreases and vice versa [60]. Higher amount of carbon can be stored in material with fine grain structure due to larger area of grain boundaries compared to large grain size with less grain boundary area. In case of a fine grain size, interstitials from grain boundaries can reach to dislocations in the middle of the grain earlier due to shorter distances.
Bake hardening depends on the grain size as well as the carbon and nitrogen concentration. This can be seen in fig 3.14. The effect of grain size is clear, the finer the grain the higher the bake hardenability. For a higher amount of carbon, the bake hardening is higher with decrease in grain size than for a low amount of Carbon. This can be seen in fig 3.15.

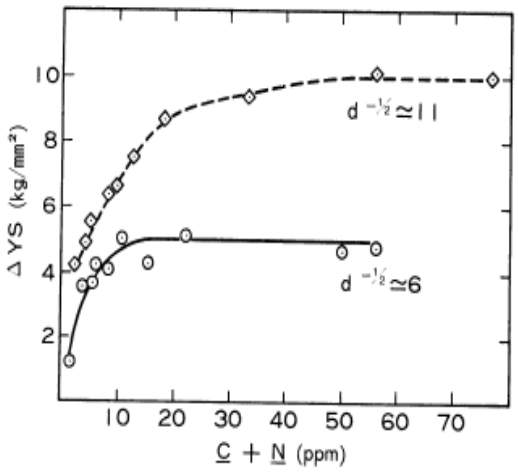

Fig 3.14: Effect of dissolved content (C+N) content on strength increment for two grain sizes [61]

The effect of grain refinement on the increase of bake hardenability depends on the location of solute carbon and the diffusion distance involved. The influence of grain size on the bake hardenability and carbon content can be understood by the fig 3.16. In case of low carbon content, the difference in grain size affects bake hardenability little as in this case the diffusion distances for carbon atoms (shown by arrow 1) is practically equal for small and large grains. This is clear by an overview of fig. 3.16(a) and (b). When the carbon content is high (as shown in fig 3.16(c) and (d)), the effect of grain size on bake hardenability becomes significant. In this case, the diffusion distance (shown by arrow 2) is important for bake hardening. Diffusion distance shown by arrow 3 (which is greater than arrow 1) in large

grain is far away from grain boundary and cannot contribute to bake hardening. This illustration makes clear why bake hardening is higher for smaller grains with higher amount of carbon content. The effect of grain size on E modulus is not reported yet in literature.

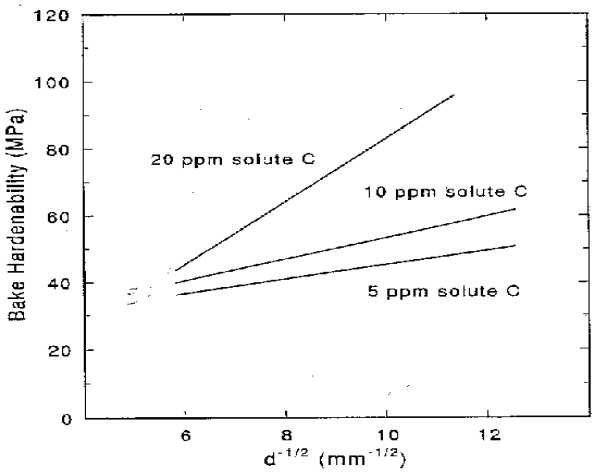

Fig 3.15: Strength increment for different concentration of Carbon as a function of grain size [61]

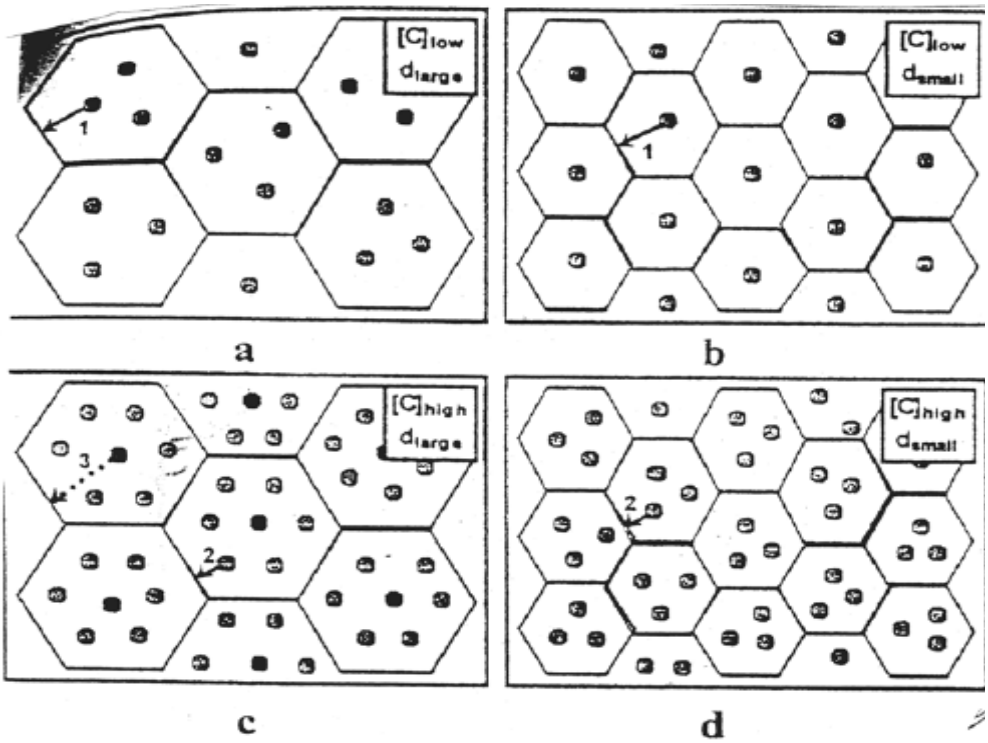

Fig 3.16: The effect of bake hardenability on grain size and carbon content [62]

3.6 Dislocation Structure

Transmission Electron Microscopy (TEM) studies have revealed a cellular dislocation structure and band type structure for the 0% and 2% prestrained samples with heat treatment at 230°C for 20 minutes respectively. This has been shown in fig 3.17(a) and (b) respectively for the samples baked at 230°C for 20 min without pre strain and with a prestrain of 2%. The direction of prestrain in this study was transverse to the RD. While De

[41] has observed the formation of cellular dislocation structure at 10% prestrained samples at RT for an ultra low carbon BH steel. The observation of cellular structure in BH steel at different prestrain and ageing conditions by Exebio [38] and De [41] could be due to the different input conditions of prestraining and heat treatment and the difference in chemical composition of the two BH materials.

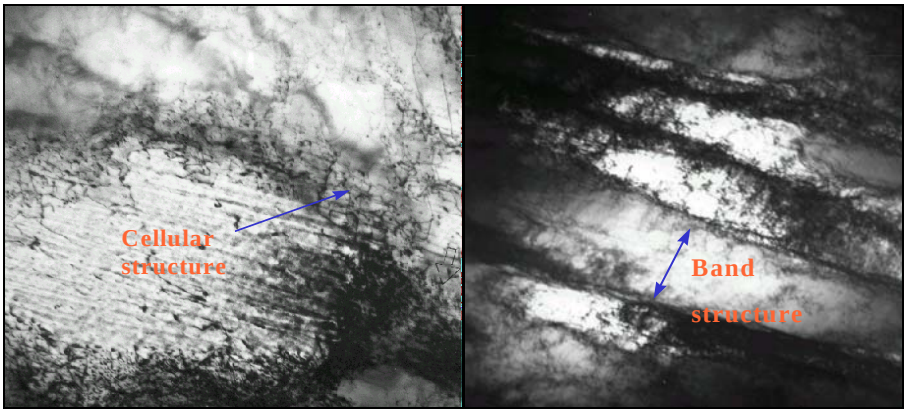

(a) (b)

Fig 3.17: TEM photograph of sample baked at 230°C-20 min and (a) 0% Pre Strain (b) 2% Pre Strain [38]

3.7 Model for Degradation

For accurate prediction of springback with numerical analysis, the significance of an accurate numerical model is clear from chapter 1. There are many numerical and material factors that need to be cared while developing a comprehensive mathematical model as discussed in chapter 1.

3.7.1 Previous Research

Until so far, there are very few models exists that predicts the degrading behaviour of E modulus in sheet metal forming in terms of material characteristics like dislocation density for example. Such types of models are necessary in order to fully understand the micro structural behaviour and changes when the material is subjected to plastic deformation. Most such models developed in literature are a function of many experimental unknowns. The unknown needs many experiments to find out, for examples, the models developed by Granato and Lucke [30,31] for E modulus degradation and internal friction. Therefore, these models are restricted only to literature and practically less useful.
There are some models developed which are extracted purely from experiments and hence their generalization to more materials can become a question. Two of such models will be discussed in this section.
As discussed in sec 1.7.3.3, Yang [25] found E-modulus of SPCE (Mild Steel) sheet metal as a function of plastic strain and found that there is more than 20 % decrease in E modulus after a plastic deformation of 0.25 (Fig 1.20). He found a mathematical relation for E modulus as a function of plastic strain from the experiments as follows

$$E = E_0(351\varepsilon^2 - 160\varepsilon + 93.8) \text{ ----------[3.3]}$$

Here ε is the plastic strain and E_0 is the initial Young's modulus. However, there seem some possible disadvantages associated with this model. For example, it can be seen that the model is a quadratic and hence after a certain minimum value of E, the E modulus predicted with this model will increase which is not realistic. Therefore it is useful only in certain range of measurement. Another problem is that since this model is based on the experimental results of only one material, therefore, such a model could only be useful for the same material in a certain specified strain ranges. Therefore this model is not a universal model.

Busche [65] did experiments on degrading behaviour of E modulus for different grades of steel like BH, DP, HSLA when prestrained up to 25% and developed the following mathematical relation

$$E_{\varepsilon} = \Delta E.e^{-C.\varepsilon.n} + E_{\infty} \text{----------[3.4]}$$

Here ***C*** is a correction factor with an initial guess of 1 ,***n*** is work hardening exponent and ***ε*** is the prestrain. E_{∞} is the value of E modulus at saturation. He also found experimentally the correction factor, initial and final saturated value for different steel such as
For Isotropic IF steel

$$E_0 = 208GPa, E_{\infty} = 171GPa; C = 0.8$$

For Micro alloys and BH steel

$$E_0 = 204GPa; E_{\infty} = 173GPa; C = 1.6$$

And for DP steel

$$E_0 = 211GPa, E_{\infty} = 172GPa; C = 3.2$$

This model seems better than Yang's model as it can predict Young's modulus for more materials when subjected to plastic deformation. However, the need for a generalized model in terms of its material characteristic is still not fulfilled.

3.7.2 Lems's Model

In sec 2.2 and 2.3 the theory of degradation and recovery has been presented. The bow model between two pinning points is the most famous for the possible explanation of this degradation. In FD loss, there is a phase lag due to some damping mechanism when the portion of dislocation between two fixed points oscillates rapidly under the application of external stress. In hysteresis model or strain amplitude dependent model, the breakaway of weak pinning point occurs when the strain amplitude exceeds a certain limit. It has been shown that the limit of FD and SA dependent is in the range of 10^{-7} -10^{-6} in sec 2.2.2.
The recovery of the E modulus in both models seems possible if the dislocation loop length could be shortened. This becomes possible in the Cottrell Atmosphere mechanism where Carbon atoms diffuse to the strain fields of dislocation and pin them.
The decrease of E modulus during plastic deformation and its recovery with time was shown by Lems[1][24] when he performed experiments on Copper, Gold and Silver. Lems proposed the following mathematical model for E modulus

$$-\frac{\Delta E}{E} = \frac{24\rho l^2}{1+24\rho l^2} \text{----------[3.5]}$$

Where ***ρ*** is the dislocation density, ***ℓ*** is the loop length of dislocation and ***E*** is the initial Young's modulus. From this expression it is evident that modulus changes are function of dislocation density and loop length. Therefore, to predict E modulus as a function of plastic strain, the corresponding dislocation density and loop length must be known. In this study, it will be tried to verify the Lems's model.

3.7.3 Calculation of Dislocation Density and effective Bake Hardening

Dislocation density can be calculated from flow stress by the use of the following equation

[1] In the present study, despite developing a new model, the strategy is kept to verify an earlier model developed for degradation of E modulus.

$$\sigma_f = \sigma_0 + \alpha G b \sqrt{\rho}$$ ----------[3.6]

Where σ_f is the flow shear stress and σ_0 is the back stress and or internal friction stress. ***G*** is the shear modulus and its values is 7.8×10^4 MPa and ***b*** is the burger's vector and its value is 2.5×10^{-10} m and α is a constant whose value is 0.82 and **ρ** has usual meaning of dislocation density.

However, it is difficult to know the changes in the loop length when material is strained to different levels. Therefore, experimental values of loop length for different level of plastic strain will be found out. Such type of experiments will be recommended to be done for other grades of steel. It will be recommended that a generalized model for loop length as a function plastic strain be developed in this way.

Mathematically, it is possible to see whether the bake hardening effect is complete or not. This can be done by calculating the diffusion distance of Carbon. From this diffusion distance, the minimum dislocation density can be calculated required for effective/complete bake hardening. Surely, if the magnitude of the dislocation densities as a function of pre - straining is equal to or higher than the minimum dislocation densities, then the bake hardening effect is effective.

For BH steel, diffusion process is temperature and time dependent. The temperature dependent diffusion can be calculated by the following expression [63].

$$D = D_0 e^{(-\frac{Q_d}{RT})}$$ ----------[3.7]

Where Q_d is the activation energy for diffusion and is equal to 80 kJ/mol and D_0 is a temperature independent pre-exponential and is equal to 6.2×10^{-7} m^2/sec for Carbon in α-Fe. ***R*** is the gas constant equal to 8.31 J/mol.K and ***T*** is the absolute temperature in Kelvin (K). Diffusion distance and minimum dislocation densities for various temperatures and baking times are calculated in sec 6.2.

4. EXPERIMENTAL PROCEDURE

4.1 Introduction

It has been described that degradation in E modulus values is due to increase in dislocation density. The density of dislocation density can be increased by plastic deformation. Plastic deformation takes place due to the motion of the dislocation. The recovery phenomenon is considered the reverse of increase of dislocation density i.e. the disappearance of dislocation by annihilation theory and immobilization of the dislocations by its interaction with other dislocations, point defects and solute interstitials. The most important steps of recovery are the Cottrell atmosphere formation and the Carbide precipitation. A proper heat treatment is therefore necessary for the prestrained material so that the free carbon interstitials diffuses to strain fields of dislocation, relax the strain fields of it and results in a shorter average loop length between pinning points in the so called Cottrell atmosphere. The next stage of recovery can take place by the formation of fine clusters of precipitates on saturated dislocation.
To observe the degrading behaviour, experiments are therefore designed such that the material is prestrained to different levels. And to observe the recovery phenomenon, experiments are designed with material by appropriate heat treatments so that the different stages of recovery described in sec 2.3 can be observed.
For determination of E modulus, both dynamic and static methods are selected. Same samples are used in both dynamic and static methods. The dynamic method selected for this investigation is Impulse Excitation Technique (IET) and the static method used is tensile test. Following layout will be followed in this chapter:

- Material
- Sample Preparation and Orientation
- Heat Treatment
- Mechanical Testing

4.2 Material

The material used in this investigation is low carbon based H220BD grade. The *H* denotes cold rolled flat products of high strength for cold forming, *220* the minimum proof strength $R_{p0.2}$ in N/mm^2, *B* bake hardened and D that the material is hot dip galvanized. The chemical composition and mechanical properties are presented in table 4.1 and 4.2.

Table 4.1: Chemical Composition for H220BD

Grade	C	Mn	Si	Altot	Alzo	N	P	S	Nb	V	Ti	Cu	Sn	Cr	Ni	Mo	B
H220BD	1.4	638	52	53	49	2.1	72	10	0	1	1	11	1	30	39	6	1.1

Note: All values are in 10^{-3}%

The as-received material was produced in the year 2006 and was in size of 960x500 mm to accommodate storage in the freezer. The temperature of the freezer was kept at -15°C to avoid ageing of the material. To be sure that the material has not aged, it was tested both theoretically and experimentally.

Table 4.2: Mechanical Properties of H220BD, measured with Tensile Test (Uni Axial). Date of test. 31st May 2006

Property	**Average**	**0°**	**45°**	**90°**
$R_{p0.2}$ (MPa)	248	239	254	243
R_m (MPa)	361	349	372	352
A_g (%)	18.6	20.6	17.2	19.2
A_{80} (%)	32.4	38.5	28.3	34.6
R	1.395	1.655	0.917	2.09
N	0.168	0.18	0.162	0.17
BH_0 (MPa)	32	25	32	41
BH_2 (MPa)	46	43	48	44

Theoretically, the relation between ageing [time (t), temperature (T)] at room temperature (t_{RT}, T_{RT}) and at higher temperature (t_H, T_H) is given by Hundy's relation [66,67] and is given below

$$\log\left(\frac{t_{RT}}{t_H}\right) = \frac{Q_d}{2.3R}\left(\frac{1}{T_{RT}} - \frac{1}{T_H}\right) \text{----------[4.1]}$$

for $T_H \leq 373$ K (100 °C). Here time is in units of hours and temperature in Kelvin. The value of Qd/(2.3R) is 4185.6 for carbon in α iron. According to this relation six month storage at room temperature (~22°C) can be simulated by ~four hours at 100 °C. Table 4.3 shows ageing time for some low as well as high temperatures using this relation. Storage time is kept 3* months at ~22°C. (This is Corus's warranty period for stability of non ageing at room temperature for BH steel.)

Table 4.3: Calculated time of ageing at different temperature levels for BH steel

	Temperature [°C]	Temperature [K]	Time [hrs]	Time [min]	Time [months]	Time [yrs]
Room	22	295	2188.8	131328	3	0.25
Elevated	100	373	1.959228	117.5537	2.69E-03	2.24E-04
Elevated	140	413	0.149816	8.988939	2.05E-04	1.71E-05
Elevated	180	453	0.018039	1.08233	2.47E-05	2.06E-06
Lowered	0	273	32722.81	1963369	44.85	3.73
Lowered	-20	253	575416.5	34524991	788.67	65.72

Experimentally, three samples of the as-received material were tensile tested until failure. The absence of the YPE or Luders's band confirmed that materials had not aged. The material in the as received condition was sheets of dimensions 960x500x0.6984 mm with 500 mm side in the rolling direction (RD). To avoid ageing of the material, these sheets were being stored in the freezer at temperature of -15°C.
The sheets were cut into smaller dimensions of 250x120 mm with 250 mm direction in the RD direction and were given plastic strain in RD at different levels of 0, 2, 6, 10, 14 and 18% as shown in fig 4.1.

* Corus's warranty to customers :(This is the time Corus gives to its customers for steel not to age at room temperature.

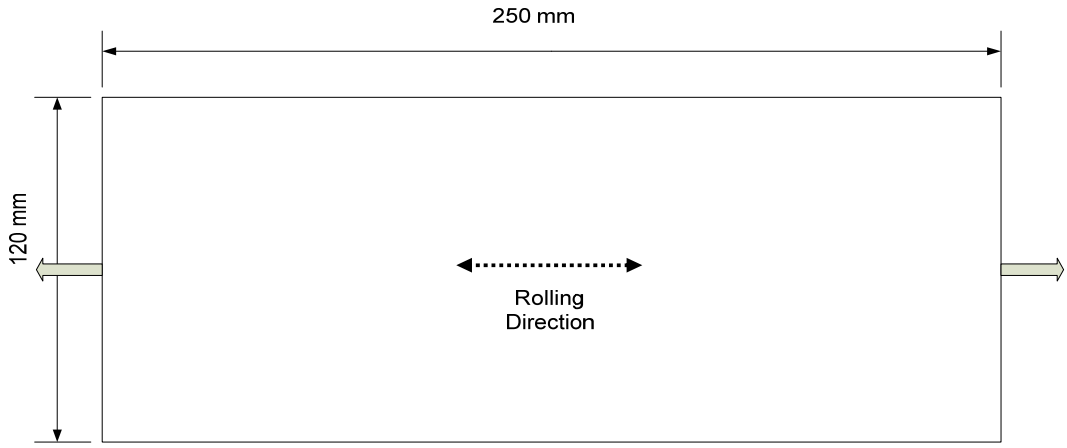

Fig 4.1: Pre Straining orientation with respect to RD.

During straining, E is not known exactly and therefore elastic strain cannot be determined exactly. This could be solved by iterative testing but this was deemed too time consuming and also the error made is very small. Therefore, in this study, the prestraining was performed by using total plastic strain rather the true plastic strain. The error induced in this way will be constant for all specimens because total plastic control is used on all samples of the same dimension and same material. In actual cases, due to elastic strain contribution, if the material is desired to be strained to a level (ε_t), then it is strained to the level of true plastic strain (R_{TrS}) rather than the total prestrain level (R_{ToS}). The situation is schematically represented in fig 4.2.

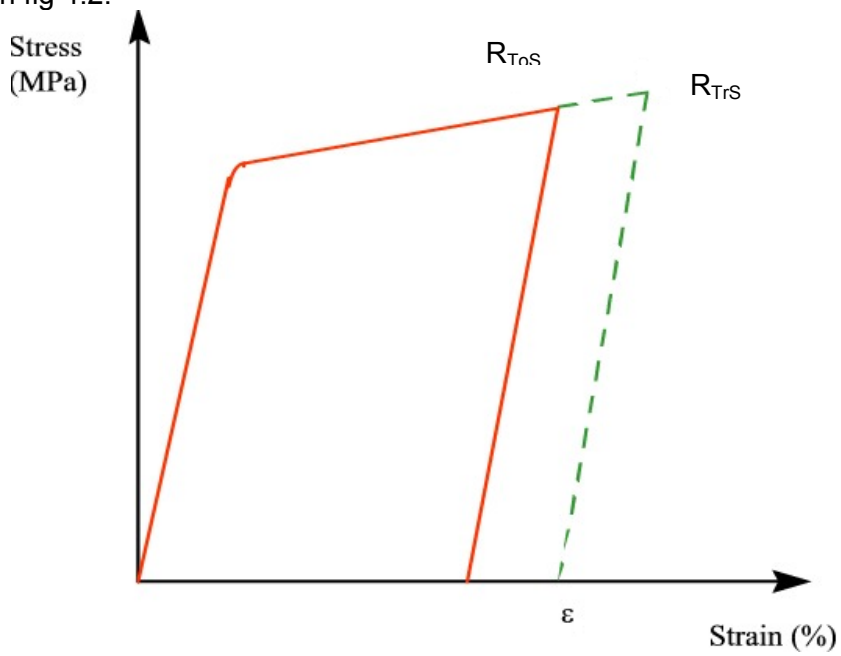

Fig 4.2: Schematic illustration of stress at total prestrain (R_{ToS}) and true plastic strain (R_{TrS})

4.3 Sample Preparation and Orientations

Same samples are being used for both dynamic and tensile tests. E modulus is measured for both methods one after the other. To determine the as-received mechanical properties like E modulus, R_p and R_m, three samples were tested in tensile test until failure. The following sections give details of the sample preparation used for both tests.

4.3.1 IET Samples

From the prestrained strips, rectangular samples of dimensions 230x30 mm were sheared with 230 mm dimension in the RD as shown in fig 4.3 with 230 mm dimension in the RD.

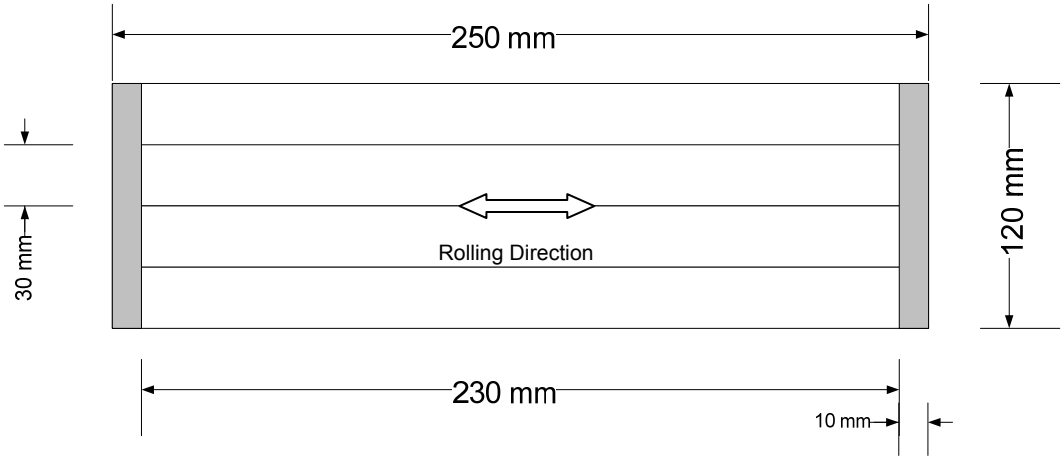

Fig 4.3: Orientation of sheared samples for IET

4.3.2 Tensile Samples

After IET testing, same rectangular samples are used for tensile testing. Tensile samples were machined from the rectangular samples. The shape of the tensile samples is shown in fig 4.4 and its dimensions are given in the table 4.4.

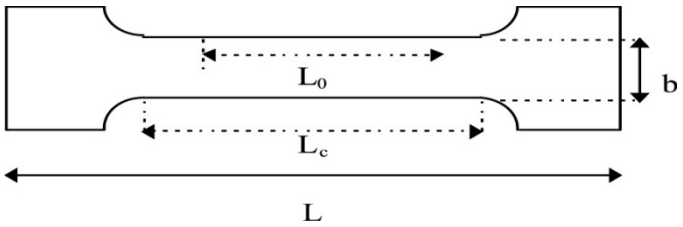

Fig. 4.4: Tensile sample dimensions

Table 4.4 : Dimensions of tensile specimens

Width (b) (mm)	Original Gauge Length (mm)	Parallel Length (mm)	Test Piece total length (mm)
20	80	120	230

4.4 Heat Treatment

To see the effect of bake hardening on Young's modulus, samples were subjected to varying combination of heat treatments and times before being tested dynamically and statically. For heat treatment, Tamson T2500 silicon based oil bath are used in which the specimens were fried to the desired temperature and time. For each bake hardening condition, three samples were prepared to determine standard deviation and give an estimate of the test reproducibility. Samples are heat treated according to the details given in Table 4.5.

Table 4.5: Details of experiment and their coding

	Baking Process		Level of prestrain					
Series	T (ºC)	t min	0%	2%	6%	10%	14%	18%
1	0	0	0%-0°C-0 min	2%-0°C-0 min	6%-0°C-0 min	10%-0°C-0 min	14%-0°C-0 min	18%-0°C-0 min
2	160	20	0%-160°C-20 min	2%-160°C-20 min	6%-160°C-20 min	10%-160°C-20 min	14%-160°C-20 min	18%-160°C-20 min
		10	0%-160°C-10 min	2%-160°C-10 min	6%-160°C-10 min	10%-160°C-10 min	14%-160°C-10 min	18%-160°C-10 min
3	180	20	0%-180°C-20 min	2%-180°C-20 min	6%-180°C-20 min	10%-180°C-20 min	14%-180°C-20 min	18%-180°C-20 min
		10	0%-180°C-10 min	2%-180°C-10 min	6%-180°C-10 min	10%-180°C-10 min	14%-180°C-10 min	18%-180°C-10 min
4	200	20	0%-200°C-20 min	2%-200°C-20 min	6%-200°C-20 min	10%-200°C-20 min	14%-200°C-20 min	18%-200°C-20 min
		10	0%-200°C-10min	2%-200°C-10 min	6%-200°C-10 min	10%-200°C-10 min	14%-200°C-10 min	18%-200°C-10 min
5	230	20	0%-230°C-20 min	2%-230°C-20 min	6%-230°C-20 min	10%-230°C-20 min	14%-230°C-20 min	18%-230°C-20 min
		10	0%-230°C-10 min	2%-230°C-10 min	6%-230°C-10 min	10%-230°C-10 min	14%-230°C-10 min	18%-230°C-10 min
Number of samples			9	9	9	9	9	9

4.5 Mechanical Testing

As discussed in previous sections, for determination of E modulus one dynamic method and one static method is selected. E modulus was calculated with both methods, the details of which are given below. The samples were kept in Freezer at a temperature of -15°C and were only taken out when it was being tested.

4.5.1 Impulse Excitation Technique (IET)

IET test facility is not available at Corus, Ijmuiden and therefore, rectangular pre strained samples were transported to TU Delft for testing. The total time for transportation is around one and a half hour from Corus (Ijmuiden) to TU Delft. Since the samples are sensitive to heat, therefore, they were placed in between ice blocks and then packed in an insulated bag to avoid to a big extent of heat transfer. After IET testing, the samples were transported back to Corus the same way.

Impulse Excitation Method (IET) is one of the dynamic method which covers determination of the dynamic elastic properties of elastic materials at ambient temperatures. All elastic materials (steel and other materials) posses specific resonant frequencies. Dynamic E modulus is determined using resonant frequencies in flexural mode of vibration. The test set up is shown in fig 4.5. For measurement of vibration, laser vibrometer was used.

4.5.1.1 Principle of Laser Vibrometer

The measurement of laser vibrometer is based on Laser Doppler Principles and evaluates the light scattered back from a moving/vibrating object. The Laser Doppler Vibrometer (LDV) consists of a two beam laser interferometer which measures the frequency or phase differences between an internal reference beam and a test beam. The most common type of laser in an LDV is Helium-Neon laser [68]. In most commercial vibrometers, a known frequency shift (of the order of 30-40 MHz) is added to one of the beams generated by means of a Bragg cell.

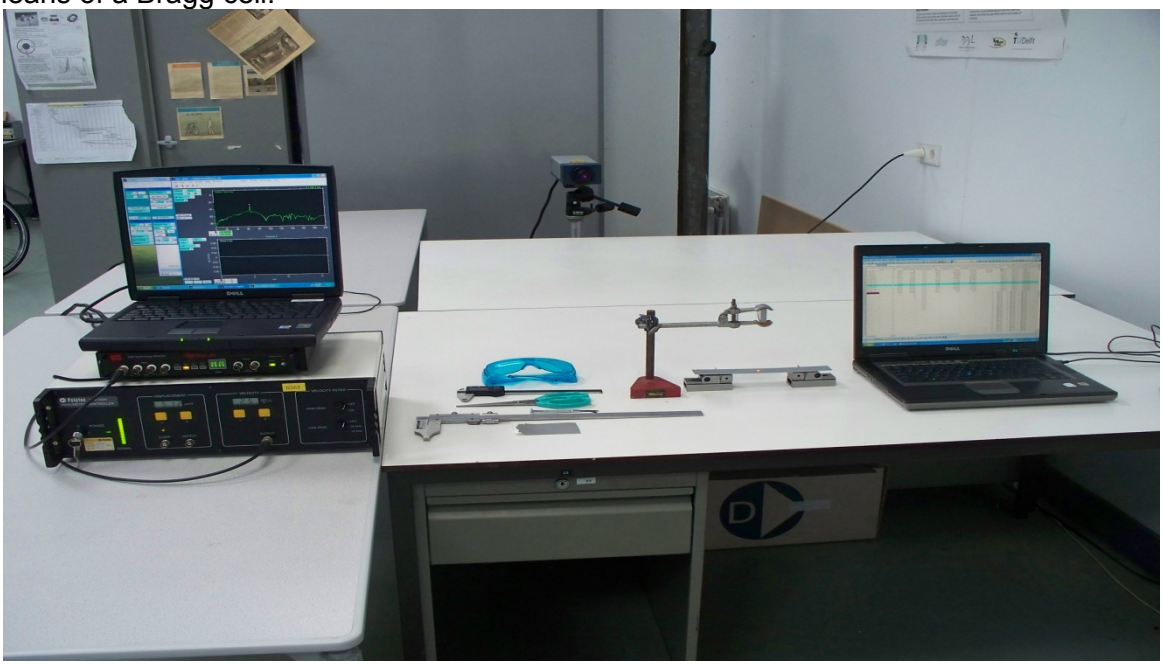

Fig 4.5: Experimental Set up of IET

Figure 4.6 shows a schematic of a typical laser vibrometer. The beam from the laser with frequency f_o is divided into a reference beam and a test beam with a beam splitter. The test beam then passes through the Bragg Cell, adding a frequency shift f_b. This frequency shifted beam is then directed to the target. The motion of the target adds a Doppler shift to the beam given by $f_{d..}$ Light scatters from the target in all directions but some portions of the light is collected by the LDV and reflected by the beam splitters to the photo detector. This light has a frequency equal to $f_o+f_b+f_d$. This scattered light is combined with the reference beam at the photo detector. The initial frequency is very high ($>10^{14}$ Hz), which is much higher than the response of the detector, therefore, the detector does respond to the beat frequency between the two beams which is at f_b+f_d. The output of the photo detector is a standard frequency modulated (FM) signal, with the Bragg Cell frequency as the carrier frequency and the Doppler shift as the modulation frequency. This signal can be demodulated to derive the velocity vs. time of the vibrating target.

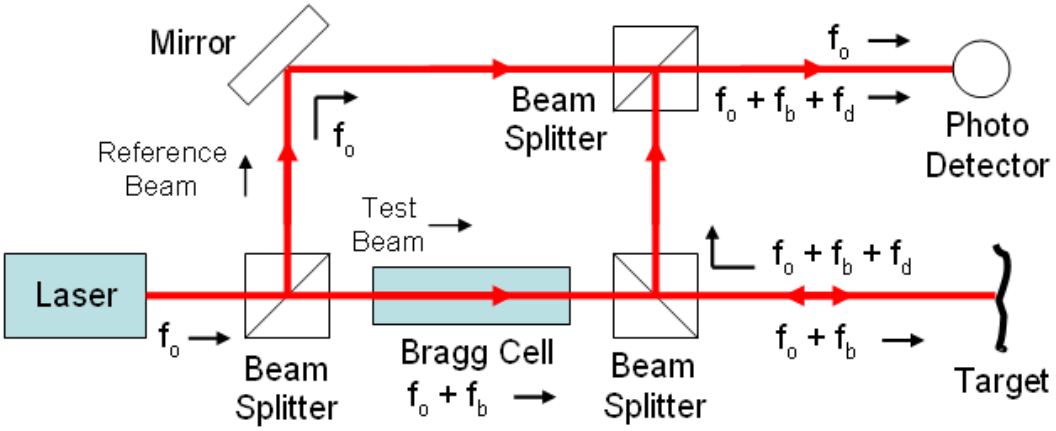

Fig 4.6: Principle of Laser Based Vibration [69]

Unlike traditional contact vibration transducers, laser-based vibration transducers require no physical contact with the test object. Non-contact vibration measurements with very high spatial resolution are possible with such a scanning system and can lead to significant improvements in the accuracy and precision of experimental model models. Commercial instruments can measure velocities ranging from a few μm s−1 to 1000 mm s−1 for vibration frequencies from 0.01 Hz to a few MHz.

4.5.1.2 Method of measurement and modification in support system

The procedure for the determination of E modulus is adopted according to norm ASTM E-1876-07 [70] and NEN-EN 843-2 [71]. For IET, accurate measurement of geometry is important as described in [23,70,71]. Table 7.6 shows error induced in the calculation of results by 0.1 percent error in dimensions and mass of the samples. Therefore, machined surface (with flat and smooth surface) should produce better results than un-machined surfaces (rough and non smooth surface) to avoid any possibility of non-parallelism of opposite edges. Another caution that can be taken is to measure dimensions of the samples with accurate gauges. In this work, the length and width were measured with a digital vernier calliper accurate to two decimal digits in millimetres. Thickness and mass were measured with a thickness gauge and a mass balance accurate to 3 decimal places in millimetres. The resolution of the acquisition system was kept at 0.06 Hz

The samples were tested for out of plane flexure as shown schematically in fig 4.7. The transducer (transducer's laser point) was placed at the point of maximum sensitivity at antinodes (point of maximum amplitudes) of the samples. Supports were placed on the nodal points at a distance of 0.224 times the length of the specimen. . Laser vibrometer in combination with commercial acquisition software SigLab® was used for the measurement of frequency in bending mode.

Knife edges were used for the support (shown in fig 4.8). The exciting impulse is imparted by lightly striking the specimen with a suitable implement with most of its mass concentrated at the point of impact and should have sufficient mass to induce measurable mechanical vibrations. For this purpose, a precision screw driver meeting the required condition was used.

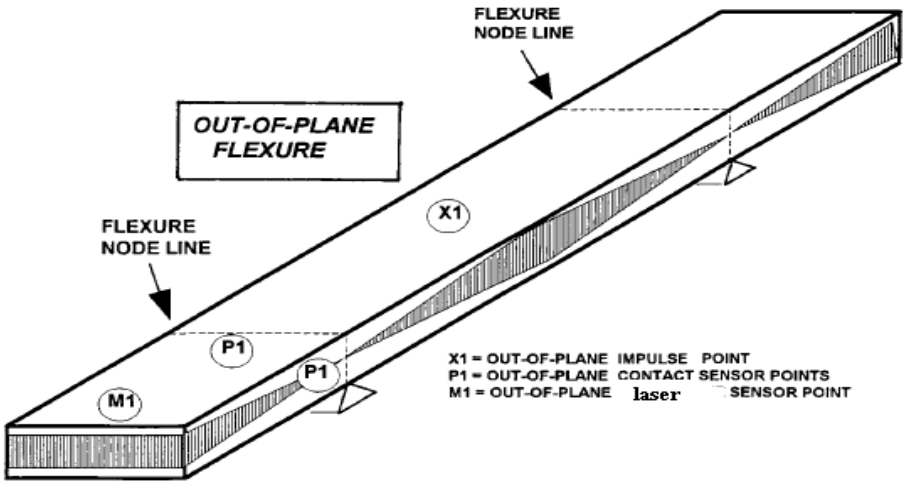

Fig 4.7: Rectangular sample tested for out of plane flexure

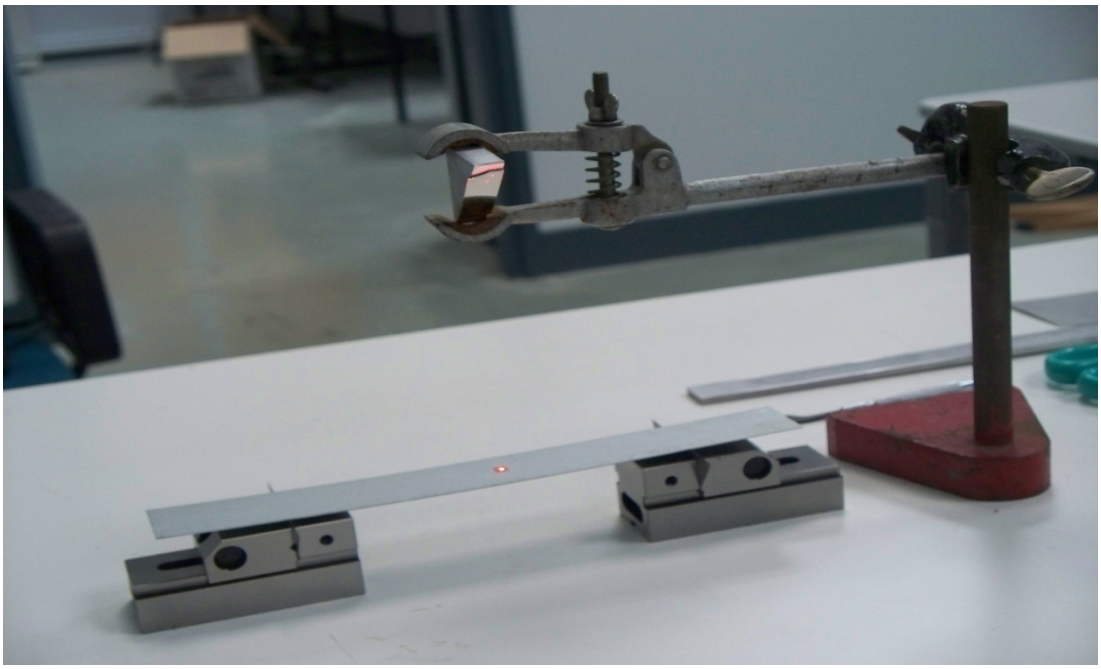

Fig 4.8: Knife Edged Support System

After measuring a couple of samples, it was noticed that some of the samples were not perfectly flat (distorted). Such samples when placed on the knife edged supports become unstable and may thus cause a change of boundary condition which may affect resonant frequency. For confirmation, two extra samples were taken which were perfectly flat and hence were stable on the support system and their frequencies were measured. Now the both the samples were twisted purposely from the ends in opposite direction and hence the samples were made distorted. Their frequencies were measured again and as a surprise it was noted that there was a difference (decrease) of 10 Hz from their original resonant frequency.

Therefore, the support system was modified to the rubber band hanging system which is perfect even for distorted samples due to elastic flexibility of the rubber band and restarted the measurement of samples. This modified support system is shown in fig 4.9.

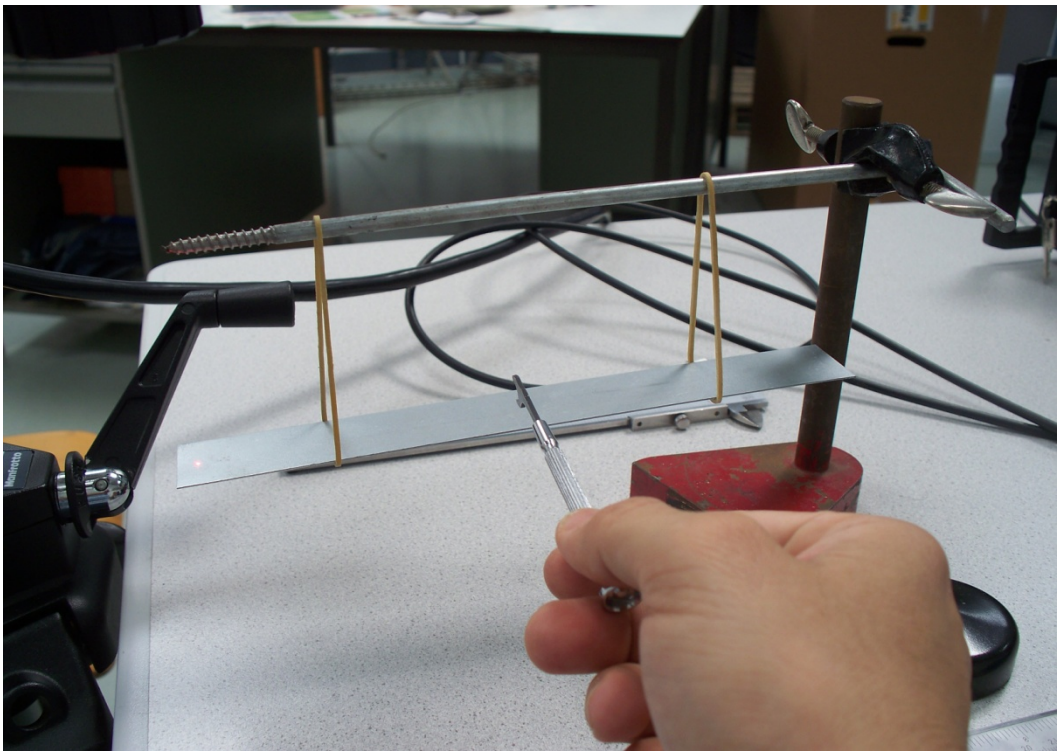

Fig 4.9: Rubber band Support System (Modified)

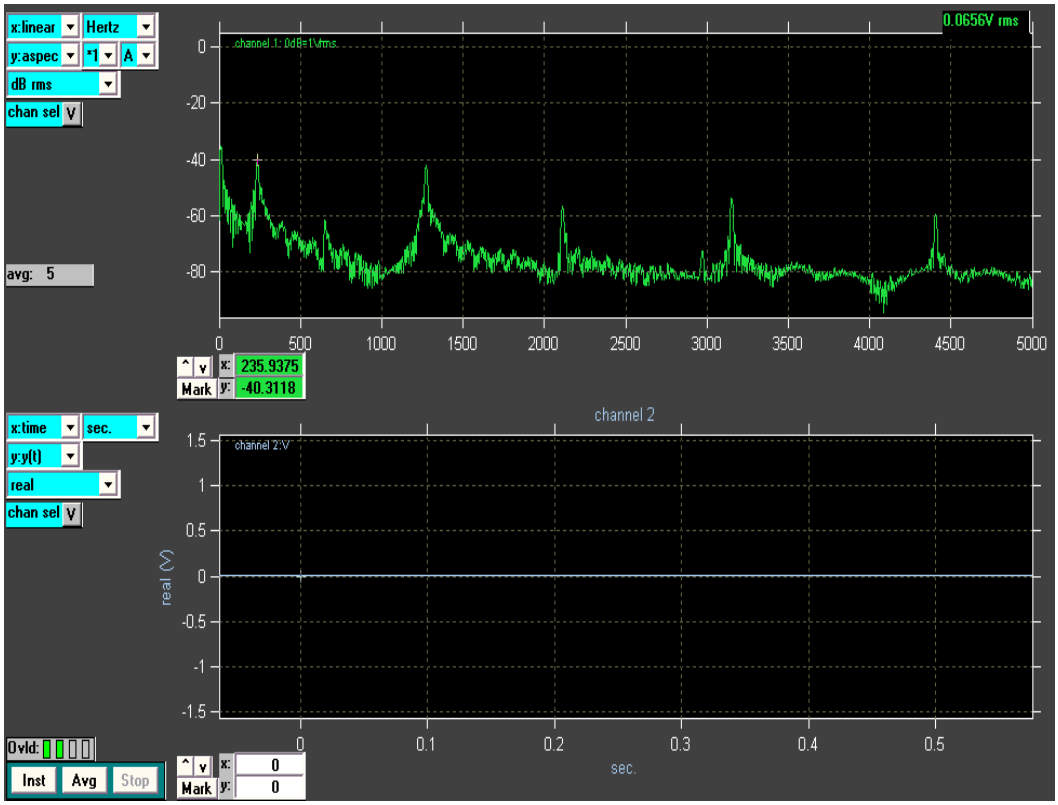

Fig 4.10: Output of SigLab® User interface showing frequency on horizontal axis vs. amplitude on vertical axis

4.5.1.3 Post Processing

As discussed above, the laser vibrometer was coupled with commercial software SigLab® which displays the results of vibration graphically with frequency vs. amplitude as shown in fig 4.10. The x axis value corresponding to the first peak is the required frequency in bending mode. The E modulus can now be calculated as [70,71]

$$E = \frac{0.9465(mf_f^2 L^3)T_1}{bt^3}$$

Where
E= Young's modulus in Pa
m=Mass of the samples, gr
b=width of the samples, mm
L=Length of the sample, mm
t= thickness of the samples, mm
f_f= fundamental resonant frequency of samples in flexure, Hz and
T_1= Correction factor for fundamental flexural mode to account for finite thickness of sample
For sample with L/t≥20, T_1 is simplified and is given by

$$T_1 = [1 + 6.585(\frac{t}{L})^2]$$

4.5.2 Tensile Testing

Tensile samples were machined from the samples dynamically tested according to the dimension given in table 4.4. All samples were taken from the original sheet in the RD. To avoid room temperature ageing, all the samples were stored in deep freezer at temperature equal to -20°C until required for testing.
Tensile testing was performed on a Schenck tensile testing machine with a 100 kN maximum load capacity, according to ISO 7500/1 and NEN-EN 10002-2 standards at a nominal strain rate of 1.7×10^{-4} per second. Tension testing of all samples in this way was carried out until failure.

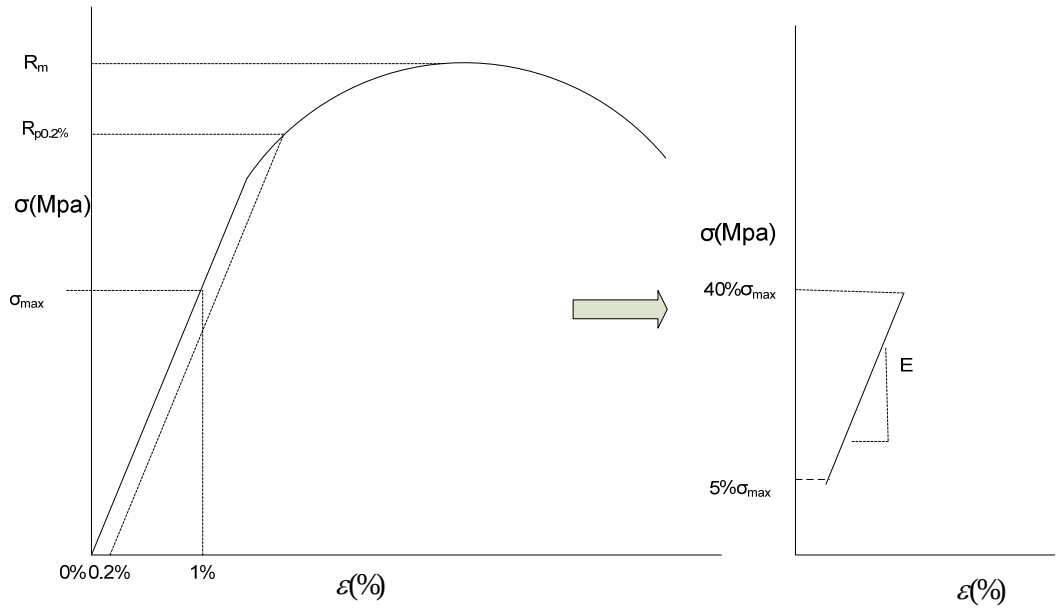

Fig 4.11: Standard method for determination of E modulus from tensile test data

From the data obtained in MUS files, E modulus is calculated according to the ASTM standard E111 [76]. For most loading systems and test specimens, effects of backlash, specimen curvature, initial grip alignment, etc, introduce significant errors in the extensometer output when applying a small force to the test specimen. Measurements shall therefore be made from a small force or preload, known to be high enough to minimize these effects, to some higher applied force, still within either the proportional limit or elastic limit of the material. In our case, these limits are set according to CORUS standard i.e. from the stress-strain data, maximum stress (σ_{max}) is found for strain ranging from 0 to 1%. Now stress strain diagram is drawn for the stress strain in the range of 5% σ_{max} to 40% σ_{max}. E modulus is now found from the linear regression of the calculated stress strain curve. This is illustrated in fig 4.11.

Change of E modulus due to work hardening after prestrain can be calculated as

$$\Delta E_{wh} = E_t - E_{as}$$

where E_t is the E-modulus value after a certain amount of prestrain and E_{as} is the E modulus of the as received material.

Change of E modulus due to baking treatment can be calculated as

$$\Delta E_{bh} = E_b - E_t$$

where E_b is the E modulus after baking treatment. This is schematically represented in fig 4.12.

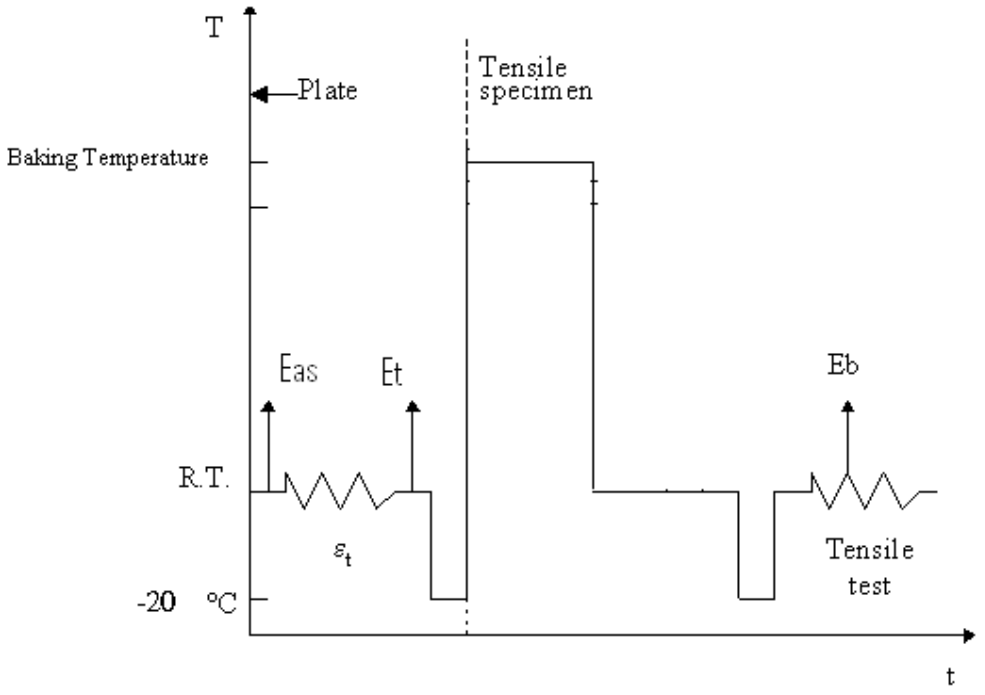

Fig 4.12: Schematic Representation of Work Hardening and Bake Hardening and Tensile Testing

4.5.3 Retesting

Due to a problem (which will be described in chapter 6 and 7), samples were retested with tensile test only. Samples were prestrained to 0%,2%,4%,6%,8%,10%,14% and 18%. After this half of samples were retested in tension test until failure and another half were tested in tension test until failure only after allowing them to age at room temperature for 24 hours. To have a lower standard deviation, six samples of each input conditions were taken except the 0% prestrain level. For the 0% prestrain, only four samples were tested.

5. RESULTS

5.1 Introduction

The results of static and dynamic methods will be presented in this chapter according to following structure:

- As received properties
- Influence of Pre Strain on As received material (Dynamic and Static Methods)
- Influence of Pre Strain on the Heat Treated Samples (Dynamic Testing)
- Influence of Pre Strain on the Heat Treated Samples (Static Testing)

5.2 As-Received properties

In order to determine the as received mechanical properties of the material, it was tested both statically and dynamically i.e. tensile test and IET. A true stress-strain tensile curve for the as received material and after bake hardening treatment at 180 °C for 20 min after a prestrain of 6% is shown in fig. 5.1.

For the as received sample, a continuous yielding of the H220BD materials suggests that there was no natural strain ageing or Lüders bands. While the presence of YPE for the sample, which is 6 % prestrained followed by heat treatment at 180 °C for 20 min, shows that the materials has strain aged. The yield strength increment by baking and prestraining is more clearly visible for this curve which is combined contribution of both work hardening and baking.

The mechanical properties of table 5.1 are approximately the same as were measured for the material at the time of production given in table 4.2 in rolling direction (RD).

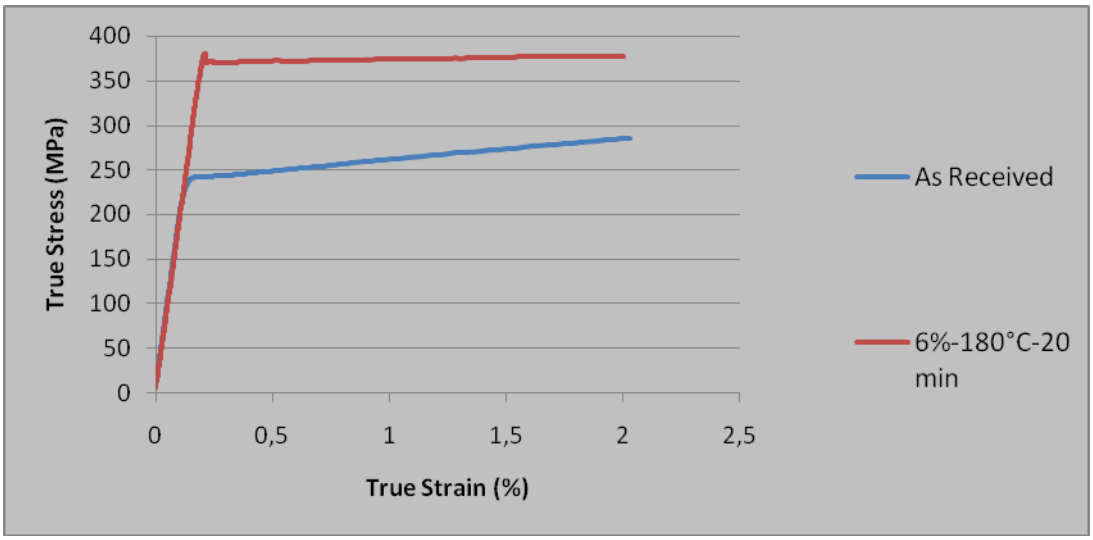

Fig 5.1: True stress-true strain curve for the as received material

Table 5.1: Mechanical properties measured of as received material

Mechanical Properties	**0.2% Proof Strength $R_{p\ 0.2}$ [MPa]**	**Tensile Strength R_m [MPa]**	**Elongation A_{80} [%]**	**Plastic Strain Ratio r_{90}**	**Strain Hardening Exponent, n**	**E Modulus by Tension Test [GPa]**	**E modulus by IET [GPa]**

Average	241	351	39	1.657	0.183	193	192

5.3 Influence of Pre Strain on the As-Received material

Reference to [23] and theory, it was expected that E modulus will decrease as the level of pre strain increases on the as received material. However, it was found both statically and dynamically that E modulus values do not degraded significantly for different prestrain levels until 18% prestrain (as shown in fig 5.2). Slight variation (in the range of 1 to 2 GPa) for different prestrain level was found but since it was under the error bars, those values can be assumed constant. This behaviour was unexpected and strange. It was however found and will be shown in sec 6.3.1 that the phenomenon of strain ageing has already started in those samples. To eliminate the uncertainty of the initial experiment for the samples without heat treatment, retesting was done with only tension testing. The design of the retesting has been discussed in sec 4.5.3 in which half of the samples were tested without ageing and another half of the samples were tested in tension test until failure after allowing them to age for 24 hours. The retesting results are shown in fig 5.3. Application of 2% prestrain decreased E modulus to 170 GPa- a decrease of approximately 11.5% from the as received value of 192 GPa. The E modulus remains at this reduced level for further prestraining up to 18%. The results of aged specimens show the restoring phenomena and E modulus is restored fully at 10% (approximately equal to 20 GPa) and an increasing trend is found for higher prestrain levels. On the other levels of prestrain for aged specimens, the value of E modulus remained at reduced level from the as received value. But E modulus values in this range of prestrain showed significant recovery from the non aged samples approximately equal to 16 GPa. For 0% prestrain, no significant change has been noticed for both types of ageing condition. These results confirmed the high sensitivity of the BH samples especially after prestraining. The deviating behaviour in fig 5.2 can now be understood well due to large time of exposing to the room temperature after prestraining during transportation and measurement with IET testing. More explanation of this deviated behaviour will be given in sec 6.3.1

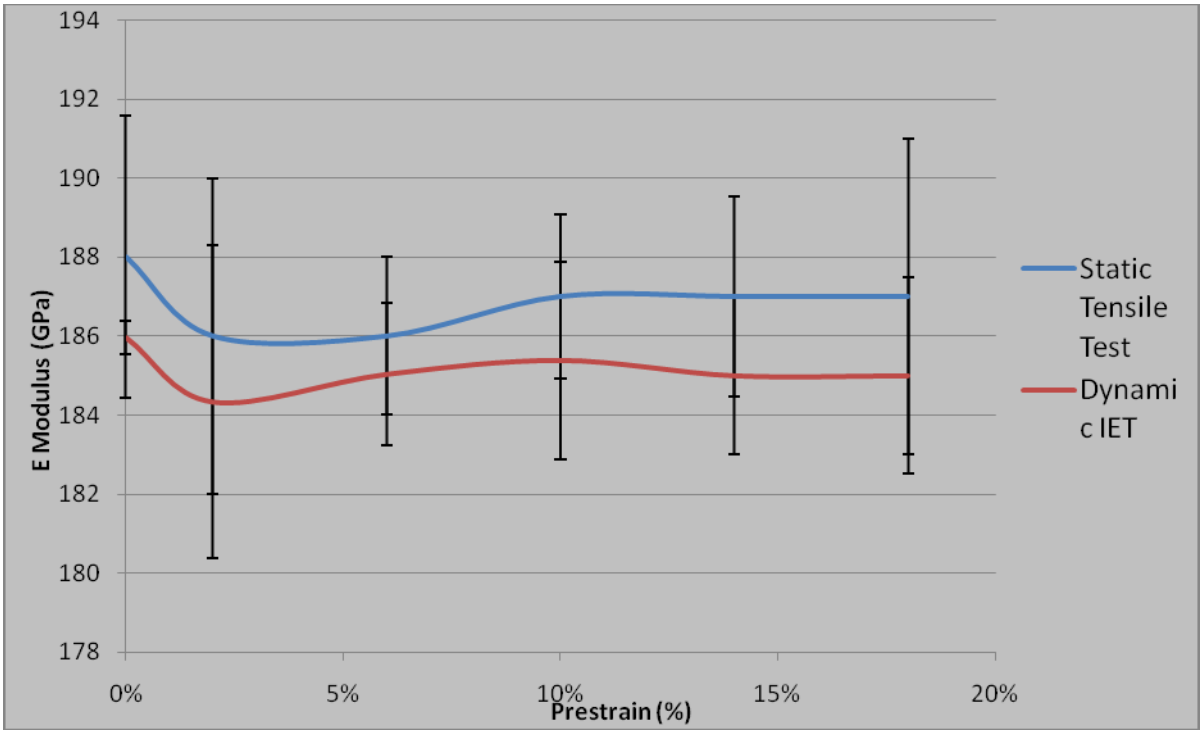

Fig 5.2: Effect of Pre Strain measured on non heat treated material

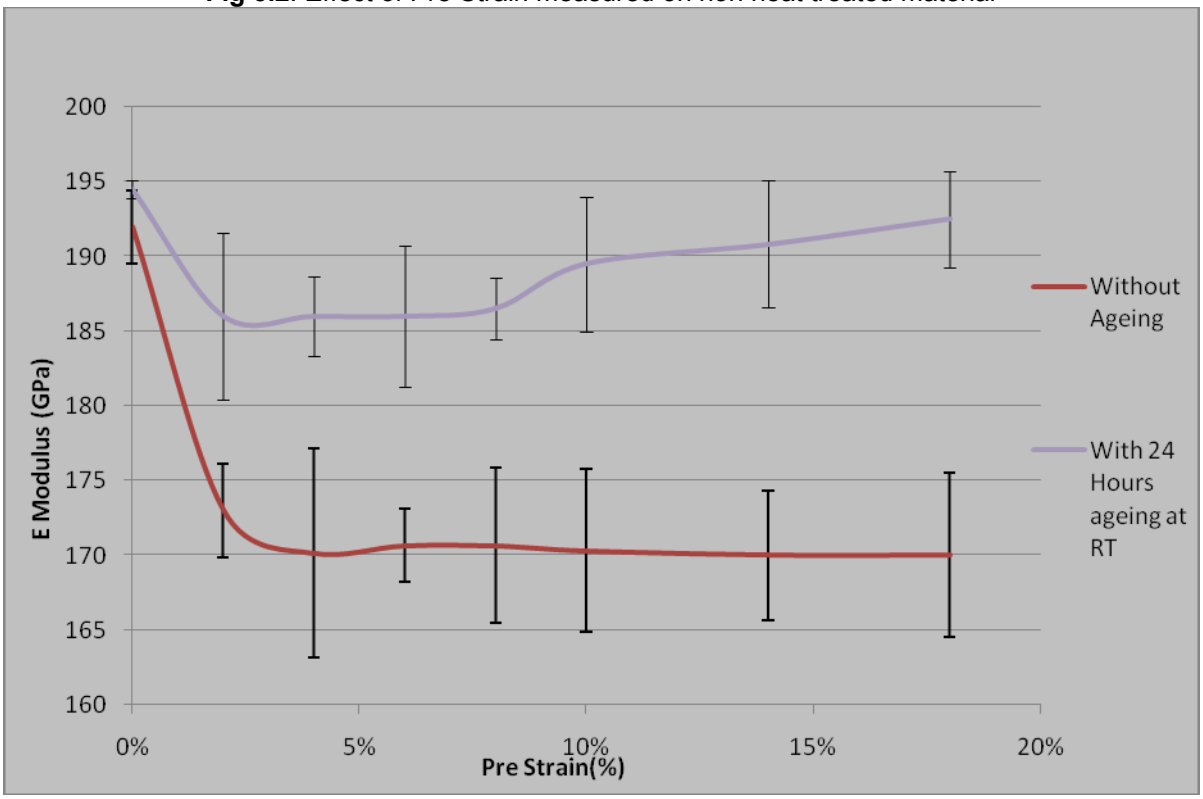

Fig 5.3: Effect of Pre Strain on samples without ageing and ageing for 24 hours at RT (Only Tensile Tested)

5.4 Influence of Pre Strain on the Heat Treated Samples (Dynamic Testing)

For the Impulse Excitation Technique (IET) method, as described in the previous chapter, rectangular samples, supported by rubber bands, were vibrated in flexure mode by hitting them on antinodes with a metallic impulser (see fig 4.9). Dimensions and mass were

carefully noted for each sample and mechanical resonant frequencies were measured with a non contacting laser vibrometer. E modulus was calculated by the mathematical relation provided in the previous chapter.

Figure 5.4 and 5.5 shows average E modulus values measured by this method for 20 minutes and 10 minutes respectively. Non heat treated sample results are those which are tensile retested. The difference of E modulus for non aged and of different heat treatments is very clear. Heat treated samples of all temperatures have shown full recovery for all levels of prestraining. Aged specimen for 24 hours has shown a gradual recovery.

The results for different heat treatments are not distinguishable. In most cases, the values of E modulii corresponding to different heat treatments are overlapping and within the error bars of standard deviation. There is a minute gradual increase in E modulus value up to 6% prestrain level followed by a decrease for 200°C and 230°C treatments only for both 10 and 20 minutes of baking. For other heat treatments, this trend is not consistent. There is no significant difference found between the curves of different temperatures baked for 10 and 20 minutes.

As discussed in previous section, the curve of aged specimen for 24 hours showed gradual recovery for different levels of prestraining and at 10% prestrain, E modulus has fully recovered and an increasing trend is found for further increase in prestrain. At 10% and higher prestrain there is no significant difference found for aged and different heat treated E

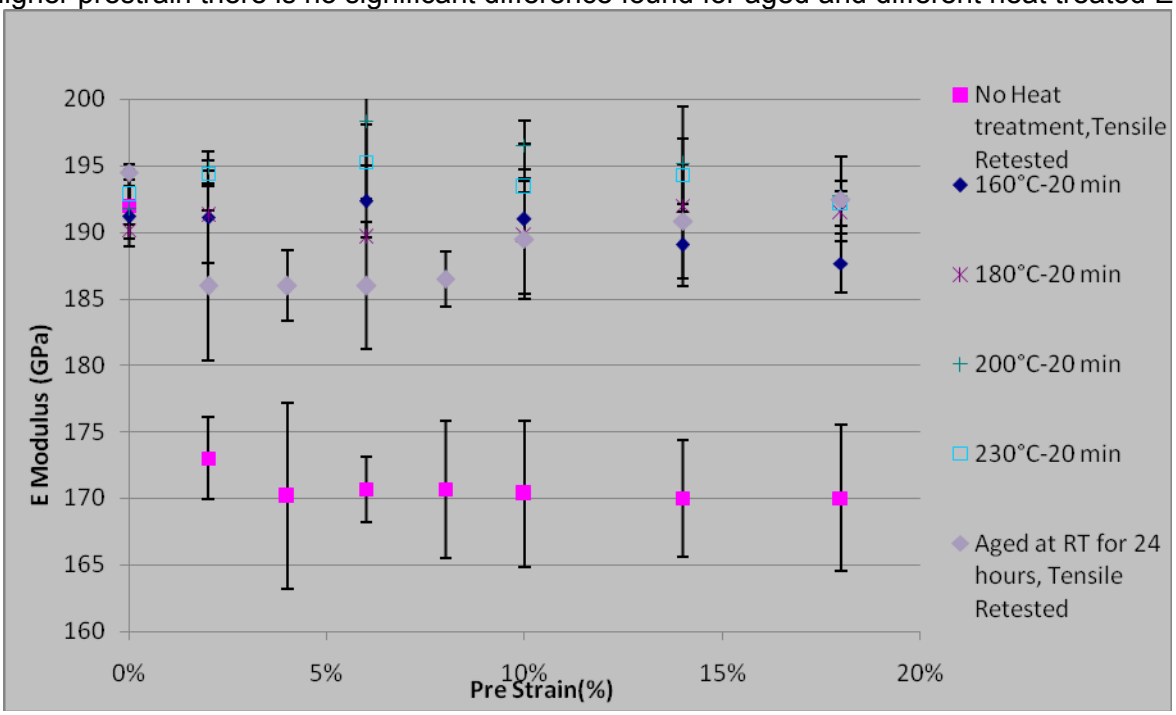

Fig 5.4: E-Modulus measured by IET against prestrain for different heat treatments for 20 minutes

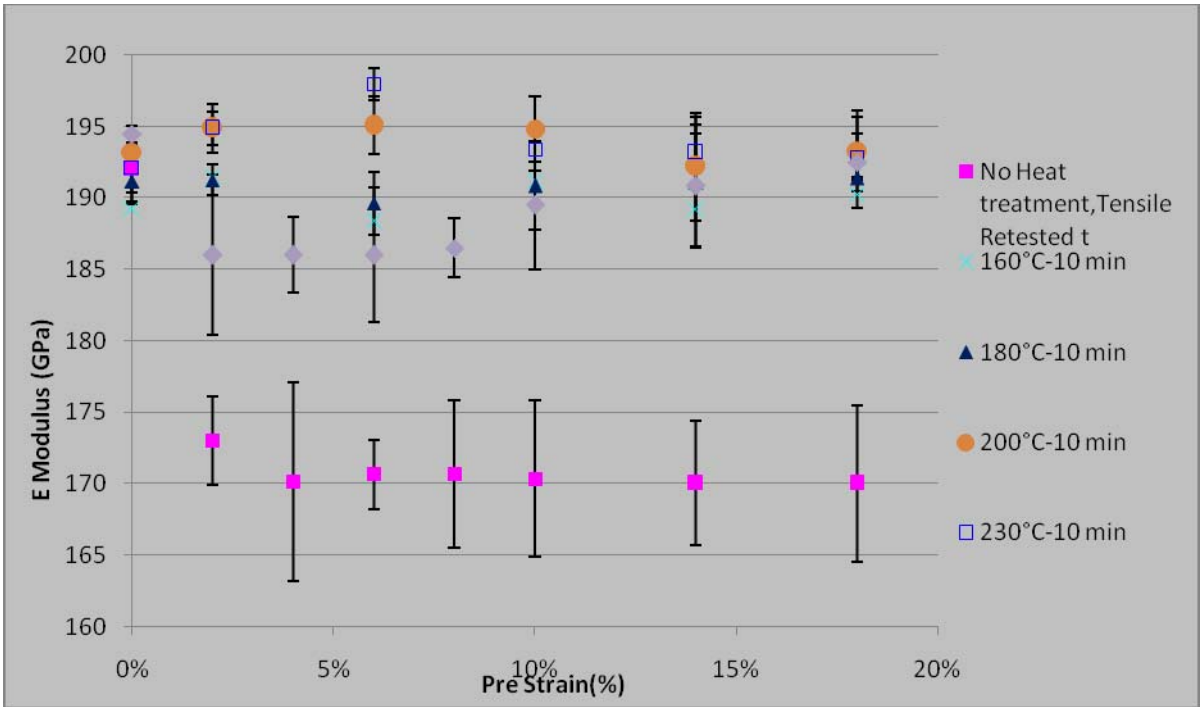

Fig 5.5: E-Modulus measured by IET against prestrain for different heat treatments for 10 minutes

modulii values. All the heat treated samples has shown a quick recovery for all levels of prestrain and the influence of prestrain is clear only for the 24 hours aged sample.
Keeping in view, the slight variation of E modulus among different prestrain levels for baked specimens, mostly within the standard deviation error bars, one may arrive at a conclusion that in fact the E modulus values are constant for any specific heat treatment temperature. To see, whether it is the case or not, E modulus values are averaged for each temperature range and plotted against temperature. This resulting graph can be seen in fig 5.6. The dependence of baking time is again not proved as most of the values are overlapping for any specific temperature. From this figure, a very slight continuous increase with temperature is however noticed.

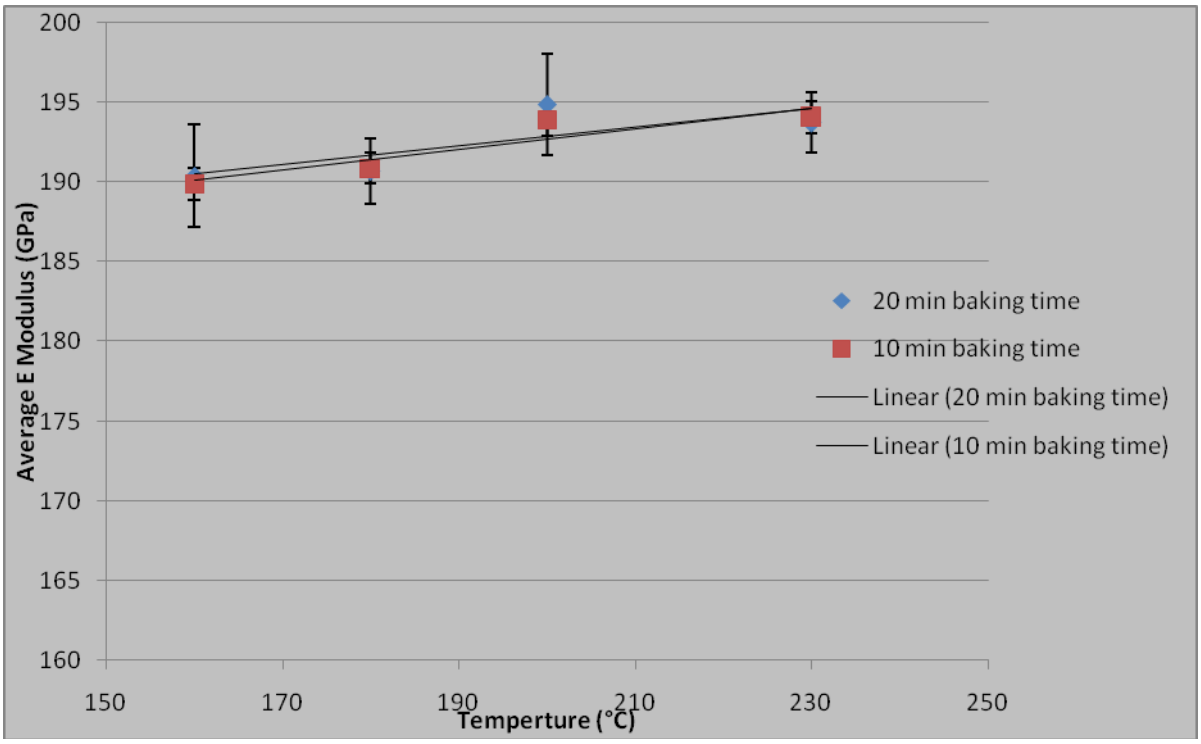

Fig 5.6: Average dynamic E modulus against temperature for 10 and 20 minutes

5.5 Influence of Pre Strain on the Heat Treated Samples (Static Testing)

The results of tensile test are shown for baking time of 20 and 10 minutes in fig 5.7 and 5.8 respectively. The first thing that comes to mind, like the results of dynamic experiments, is that heat treatment has fully restored the E modulus.

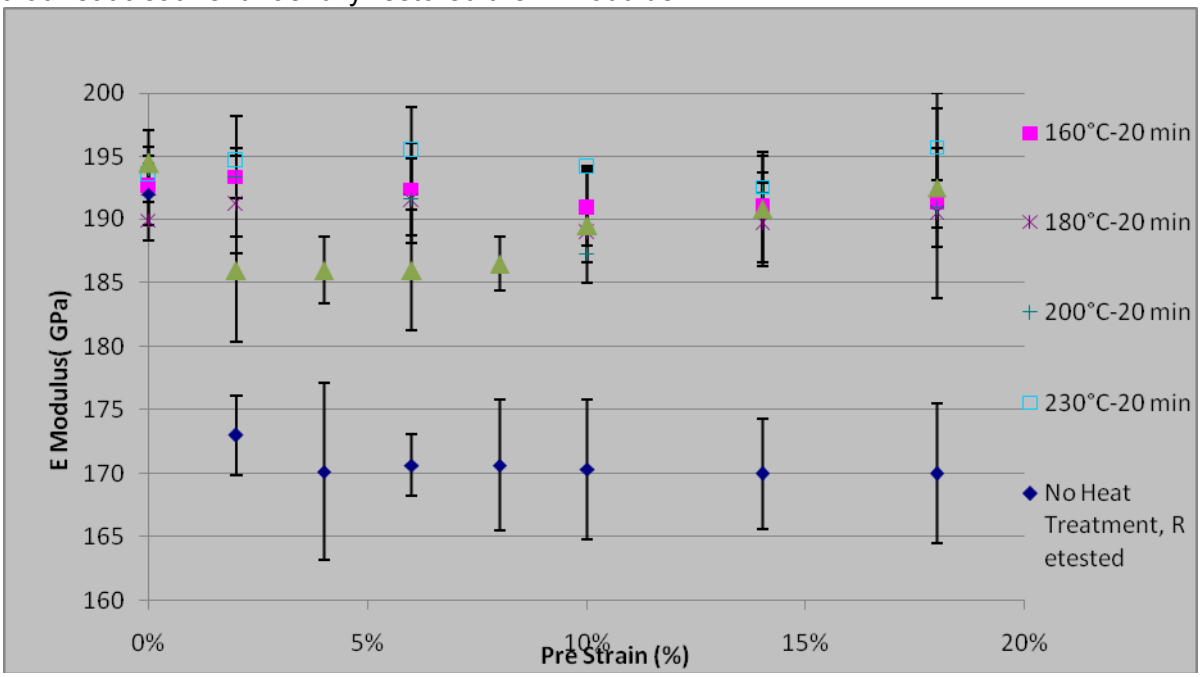

Fig 5.7: E-Modulus measured by tensile test against prestrain for different heat treatments for a baking time of 20 minutes

.

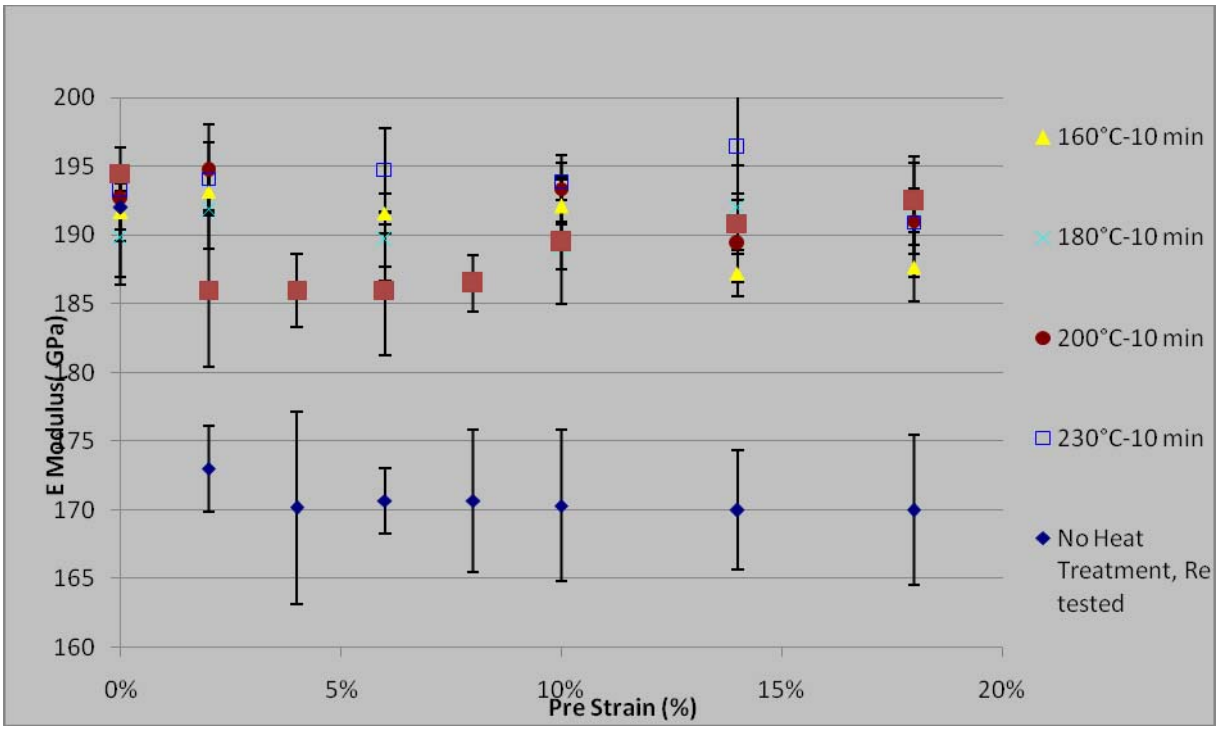

Fig 5.8: E-Modulus measured by tensile test against prestrain for different heat treatments for a baking time of 10 minutes

Again, the difference between E modulii values for different heat treatment is not distinguishable and most heat treated values are overlapping and within the standard deviation error bars. With some exceptions, in general the standard deviations with tensile test are found higher than the IET results.

The slight gradual increase in E modulus values with prestrain up to 6% and then a decreasing trend is found only for 230°C and 20 minutes. No trend is found with other heat treated values. The dependence on baking time is also not distinguished. At 10% and higher prestrain levels, there is no difference found for aged samples of 24 hours and different heat treated samples. All the heat treated samples has shown a quick recovery for all levels of prestrain and the influence of prestrain is clear only for the 24 hours aged sample. Since, for all heat treated E modulus values, prestraining produces very marginal difference which is hardly distinguishable, therefore, E modulus values can be assumed constant for any specific temperature. Therefore, the values for any definite temperature ranges are averaged and plotted against temperature. The result can be seen in fig 5.9 for both 20 and 10 minutes baking time.

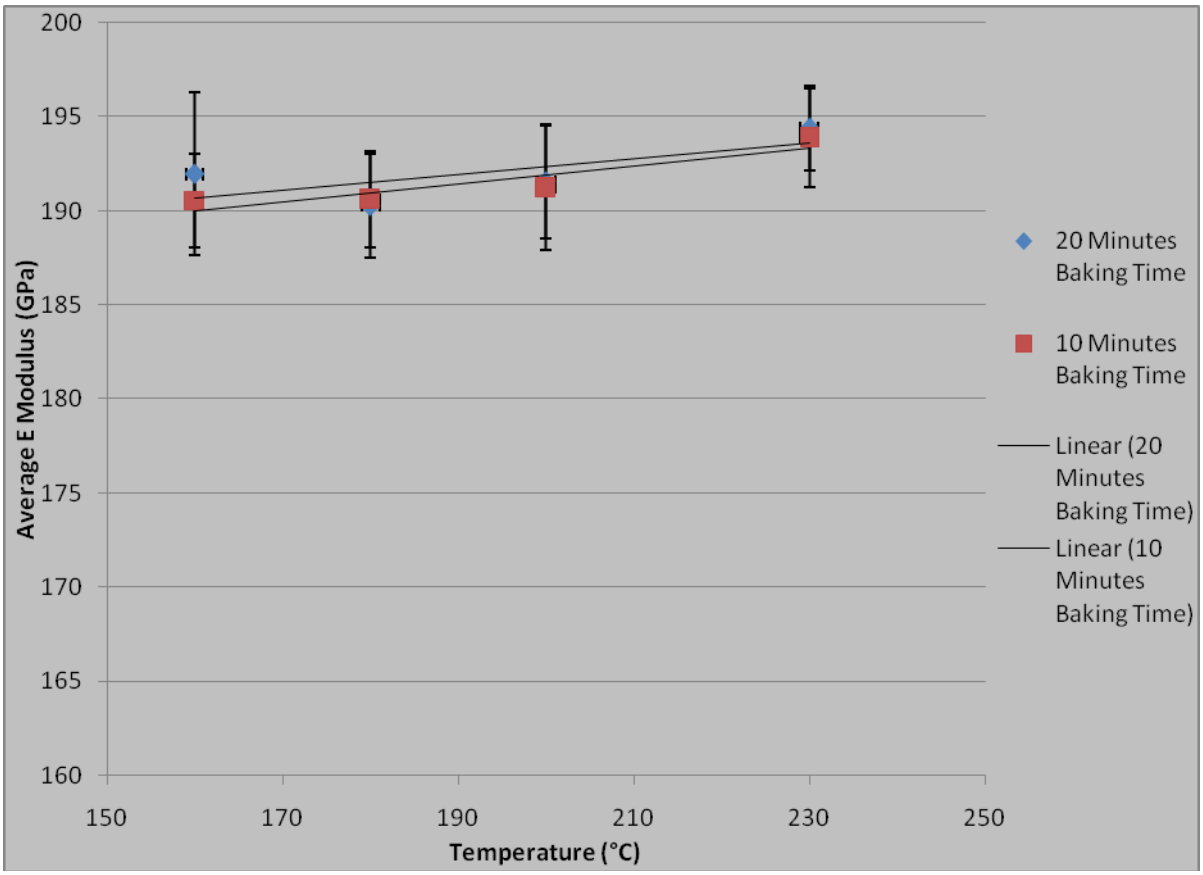

Fig 5.9: Average Static E modulus against temperature for 10 and 20 minutes

Interestingly, this is the same result as found in fig 5.6. Only the average values for 200°C is a bit marginally lower but this could be due to the high standard deviation. Therefore, again we have found a slight continuous increase in E modulus with temperature.

6. DISCUSSION OF RESULTS

6.1 Introduction

The results presented in Chapter 6, will be discussed in this chapter according to the following order

- Dislocation Density and Loop Length
- Influence of pre straining
- Influence of Baking Temperature and Time
- Error Analysis and Difficulties of Measurement
- Comparison of Measurement Methods

6.2 Dislocation Density and Loop Length

Dislocation density can be calculated from the equation (3.6). The dislocation density is calculated assuming the initial values for dislocation density as 10^{12} m^{-2} [38] and is shown in table 6.1. The dislocation densities for different levels of prestrain with the assumption of initial dislocation density as 10^{12} closely matches with another literature for the H180BD grade [38] against our material H220BD.

Table 6.1: Calculated dislocation density using two values of initial dislocation densities

Pre Strain	ρ [10^{12} m^{-2}]
0%	1
2%	10.98
4%	24.96
6%	36.41
8%	45.18
10%	51.26
14%	58.68
18%	61.49

Table 6.2: Diffusion distance and minimum dislocation density for the respective baking conditions

Condition	T [°C]	Time[sec]	√(Dt) [microns]	ρ [10^{12} m^{-2}]
24 hours at RT	20	86400	0.02	3400
160°C+10 min	160	600	0.29	12
160°C+20 min	160	1200	0.41	6
180°C+10 min	180	600	0.47	4.5
180°C+20 min	180	1200	0.67	2.3
200°C+10 min	200	600	0.74	1.8
200°C+20 min	200	1200	1.04	0.92
230°C+10 min	230	600	1.35	0.55
230°C+20 min	230	1200	1.91	0.27

As described in sec 3.8.1 the minimum dislocation density required for complete bake hardening effect can also be calculated. This can be done by employing the equation (3.7) and multiplying the diffusion by the respective ageing time. The minimum dislocation density computed in this way is shown in table 6.2. A comparison of table 6.1 and 6.2 shows that

with the exception of 2% pre strain and baking at 160°C for 10 minutes, the actual dislocation density is always greater than or equal to minimum dislocation. Figure 5.3 shows full restoration of E modulus at 10% prestrain level for aged specimen for 24 hours at RT. It can be inferred from this behaviour that the minimum dislocation density required for effective bake hardening has been met at 10% prestrain level. However, it will be shown in later sections that actually there is more room for bake hardening. The ineffective bake hardening for ageing at 24 hours RT is also clear by the comparison of minimum dislocation density required and actual dislocation density. From table 6.2 it can be seen that the minimum dislocation density for 24 hours ageing at RT is $3.4x10^{15}$ m^{-2} and the actual calculated dislocation density equal at 10% prestrain from table 6.1 is $51.26x10^{12}$ m^{-2}. Due to a big difference in these two figures, the bake hardening can be understood as ineffective.

After calculation of dislocation density, the second most important variable is the average dislocation loop length at different prestrain levels. The loop length is needed to estimate E modulus for a specific prestrain level by the use of Lems's model given in equation (3.5). The dislocation density calculated earlier is total dislocation density and is composed of mobile and immobile dislocation densities. In Bergrstom model [64], the density of mobile dislocation is assumed constant and that of immobile dislocation density increases with prestrain. The variation of immobile dislocation density is determined by four dislocation processes, i.e. the creation, the immobilization, the remobilization and the annihilation of dislocation. Due to simultaneous occurrence of all these process, it is very difficult to estimate the loop length for any specific plastic prestrain level. Therefore, it is recommended to go in the reverse direction and estimate the loop length by giving input of variation of E modulus and calculated dislocation density in the Lems model. Loop length is calculated for various prestrain levels using Lems's model and is presented in fig 6.1. From this figure, it can be seen that the loop length at 2% prestrain level decreases on further prestraining and saturates at 0.01μm

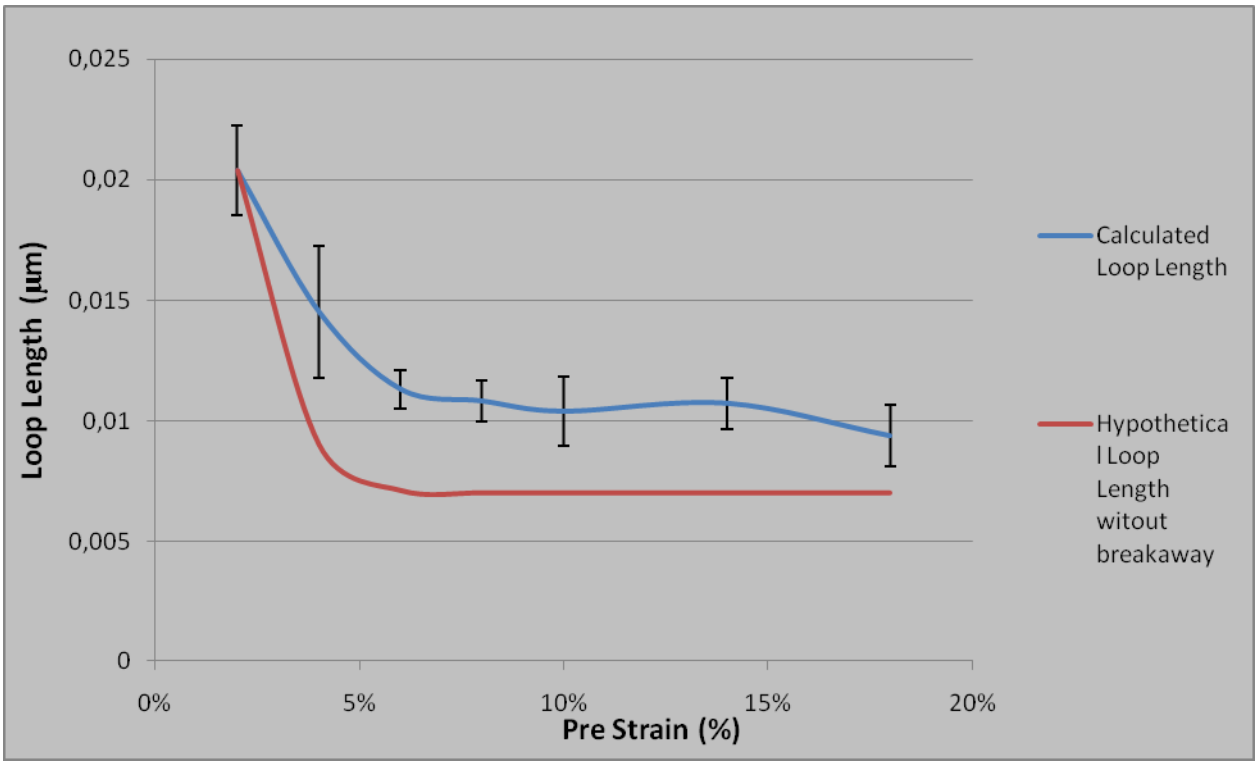

Fig 6.1: Calculated Loop length using Lems's model [24] for change in E modulus

The most plausible explanation of this situation could be that on prestraining the dislocation density increases considerably as shown in table 6.1. In this process, dislocation intersects other dislocations and also the interstitial point defects and hence become pinned. On further prestraining, the dislocation density further increases and hence further reduction in the loop length takes place. However, as can be seen from the figure, the loop length at 4% and higher prestrain saturates and there is no further noticeable decrease noted.
The decrease of loop length however seems to contradict the model of strain amplitude dependent modulus defect presented in sec 2.2.2 in which the loop length increases when breakaway stress reaches resulting in breaking of weak intermediate points. But it is possible that after 2% prestrain, the breakaway stress limit has reached and the breakaway of the weak pinning point took place. In that particular case, the red curve in fig 6.1 shows the loop length without breaking of the weak intermediate points. It is also possible that after initial decrease in loop length up to 4% prestrain level, the reduction in loop length by the increase of dislocation density and the increase in loop length by breakaway is somewhat equal and the net effect of these two events is to cancel each other's effect and therefore, the loop length saturates.
More research is recommended to be done by carrying out such experiments on other grades of steel. It will be interesting to observe the shape of loop length in other grades of steel when prestrained to different levels. In this way, it may become possible to generalize the loop length as a function of prestrain. The calculated dislocation density and the generalized loop length can then be used to estimate the E modulus for any level of prestrain for any material. Implementation of such E modulus model in FE analysis will thus result in an accurate prediction of springback before carrying out any specific sheet metal forming operation.

6.3 Influence of Pre Strain

During tensile prestraining, the dislocation structure will become more homogenous throughout the sheet thickness and will be oriented according to specific deformation path. During pre straining, the dislocation density increases. The increased dislocation density induces stress fields which are the driving force for the migration of impurity atoms. Hence, the carbon atoms diffuses to the stress fields of dislocations and therefore results in higher pinning and a higher bake hardening and recovery.
Also when the secondary load direction after baking (for heat treated samples) or without baking (for non heat treated samples) is same, the pinning is more effective as described and explained in sec 3.5.4. The reason for this is that because most of the immobilized dislocations lie in the active slip plane.

6.3.1 Non Heat treated samples

The influence of pre strain on as received or non heat treated samples results in a decrease of E modulus. This is found in many literatures [24,27-32,52, 65,39,58]. Two examples for BH grade ZStE 180 BH and H220BD from some recent studies is shown in fig 6.2 and 6.3 respectively. In these studies, E modulus is measured in three directions 0°, 45° and 90°relative to the RD. The difference of E modulus values in three directions for any specific pre strain level could be due to the dislocation structure development which is the results of the direction of pre and secondary deformation. In all three directions, E modulus has decreased with only exception of increase in E modulus values at 2% pre strain in fig 6.2 only. Up to 15% prestrain, E modulus values has decreased to 16% from the as received value to 175GPa from 208 GPa (as received value) and to 170 GPa from 202 GPa (as received value) in fig 6.2 and 6.3 respectively.

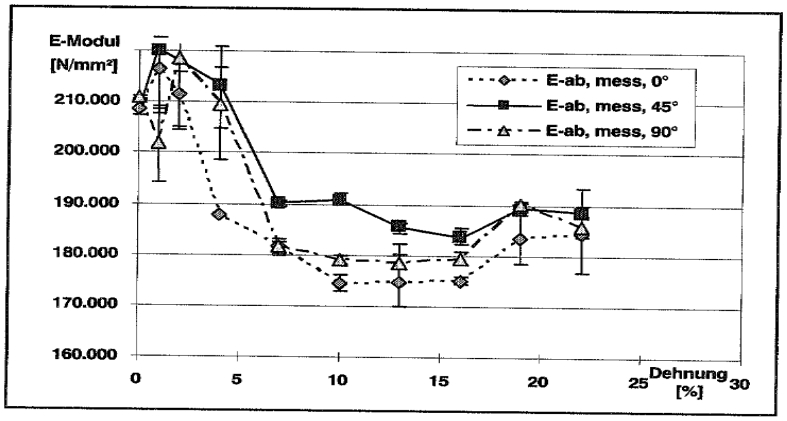

Fig 6.2: E Modulus degradation as a function of pre strain at 0°, 45° and 90° to RD for ZStE 180 BH [65]

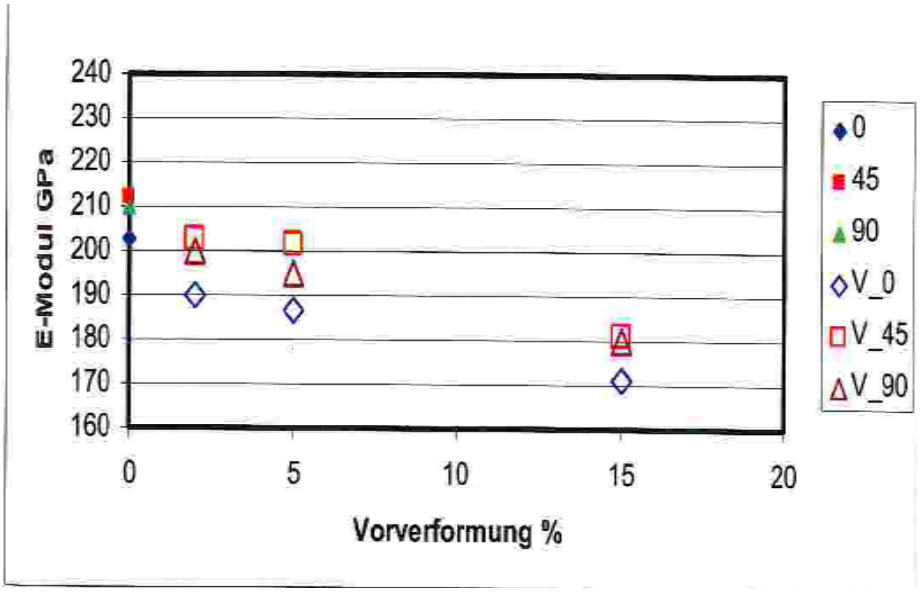

Fig 6.3: E Modulus degradation as a function of pre strain at 0°, 45° and 90° to RD for H220BD [59]

These observations were in contrast to our initial results for non heat treated samples which do not show any degrading behaviour in both types of experiments i.e. static and dynamic. To investigate the reason of the deviation in our first experiment, true stress and true strain curves of non heat treated samples are plotted on the same graph for different prestrain levels and is shown in fig 6.4. It can be seen that all hardening curves are overlapping, which is a good reason for the authenticity and accuracy of the results. The most interesting point in fig 6.4 is the appearance of YPE for all samples beyond 2 % pre strain. It means all samples except 0% and 2% are strain aged without any heat treatment. This strain ageing phenomena is therefore responsible for the recovery observed in the non heat treated samples.

The reason of the unexpected strain ageing phenomenon can be explained by the unavoidable exposing of the prestrained material to RT during transportation to Delft and back as the facility for IET is not available at Corus plant. The total transportation time was around three and half hours. During dynamic testing, although, the samples were kept in freezer at low temperature (-15°C) during storage but at the time of test the sample were again exposed for some time to room temperature.

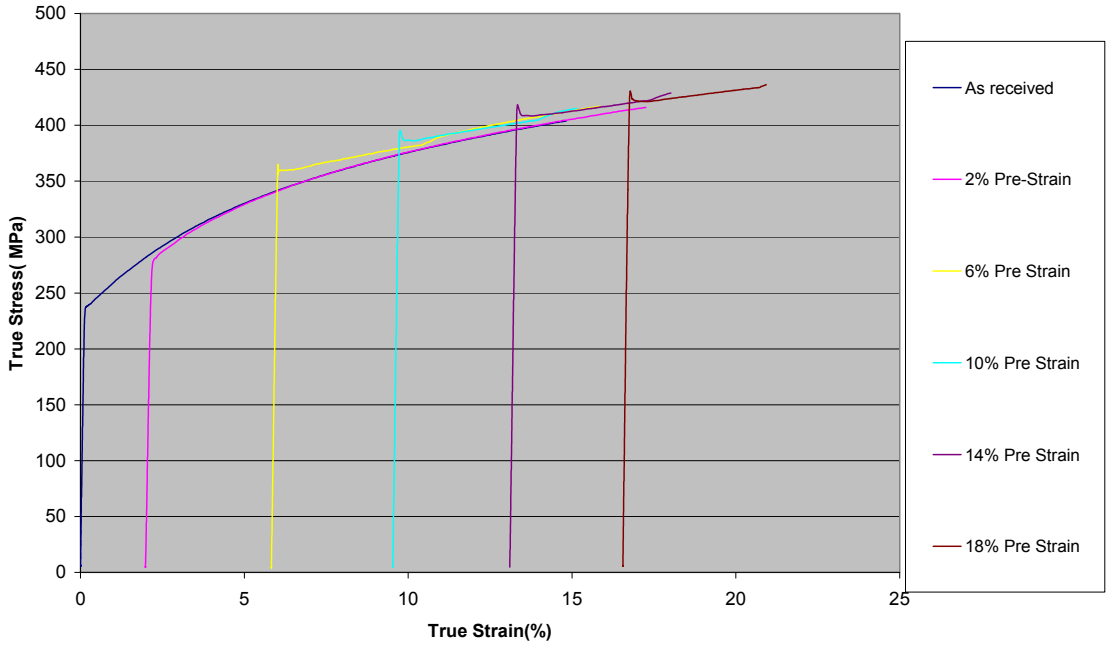

Fig 6.4: True stress strain curves for different levels of prestraining indicating start of strain ageing phenomena beyond 2% prestrain levels without any heat treatment (Initial Experiments)

However, the degradation in E modulus is proved when samples were retested as shown in fig 5.3. Figure 6.5 shows a comparison of the true stress and strain curves of our first experimental results with non degrading behaviour and the hardening curves of the retest for non heat treated samples. The thicker lines show results of retest and the thinner lines the result of initial experiments. Unlike, the first result, no strain ageing phenomenon has taken place for the retested material at all level of prestraining which is visible by the absence of YPE for all prestrain levels. And this is the reason that the result of retesting showed significant reduction of E modulus. As discussed before, a reduction of 11.5% has been observed for 2% and higher prestrain levels.

It would also be very interesting to observe the difference in hardening curves of retested samples with 24 hours ageing with results of our initial experiments. This comparison is shown in fig 6.6. From fig 5.3 we can see that E modulus has recovered to as received value at 10% and higher prestrain values for aged curve. From this observation, it was expected that at 10% and higher prestrain values for the aged retested sample, YPE will show up but as can be seen, YPE is not visible. A careful and magnified comparison of fig 6.5 and 6.6 for without aged and aged sample show some difference in flow stress at 10% and higher prestrain values. This is made clear in fig 6.7 in which the flow stress for all three conditions i.e. initial experiment values and retested results without ageing and with 24 hours ageing at RT are plotted versus prestrain. From this figure, it can be seen that no heat treatment curve of our initial experiment show deviations from other two curves beyond 2% prestrain value. We know from fig 5.3, that recovery in our E modulus for our initial experiment also started at the same level. So again it is proved that the bake hardening causes the recovery in our initial experiments.

Another interesting observation from the fig 6.7 is that up to 8% prestrain, the values of flow stress without ageing and with ageing are same. In this range of prestrain, however, we have seen a gradual or partial recovery in E modulus which can be seen in fig 5.4. Flow stress values at 10% and 18% show marginal increase from non aged samples in fig 6.7. In this level of prestrain including 14% prestrain, there is an increasing trend found in the E

modulus form fig 5.3. From these observations, it seems that E modulus is very sensitive to ageing than the flow stress.

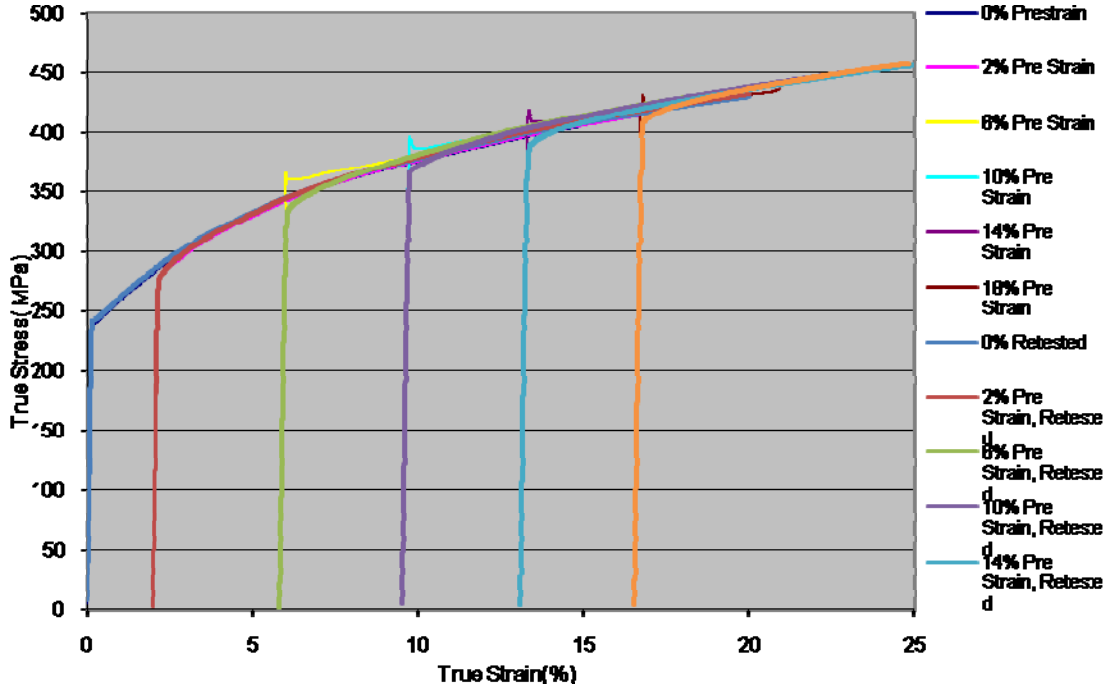

Fig 6.5: Comparison of the hardening curves of first experiment and retested only for non aged material

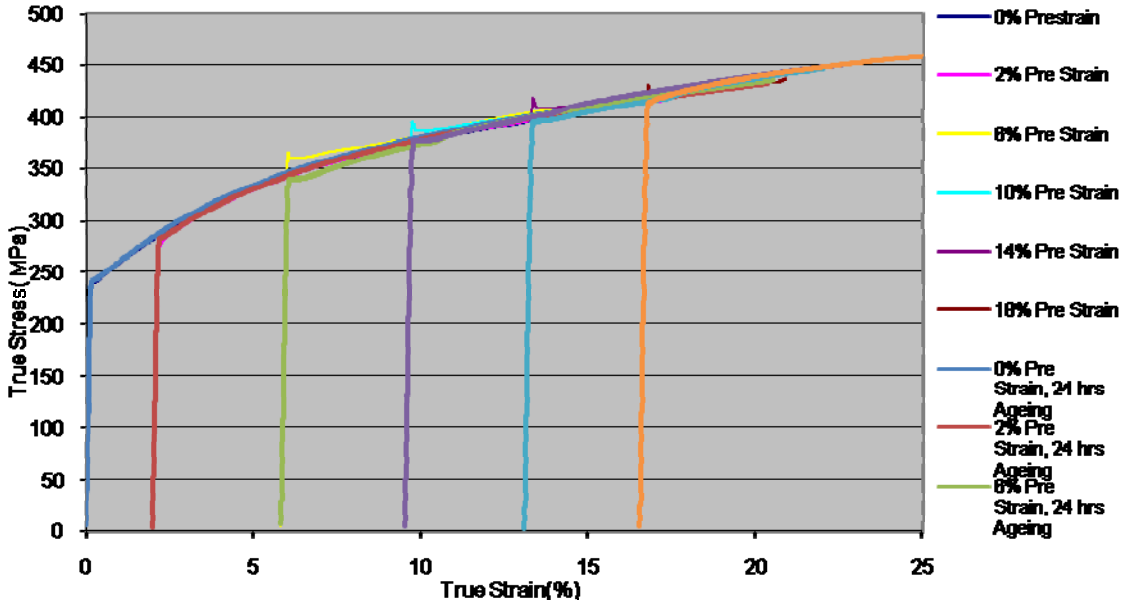

Fig 6.6: Comparison of the hardening curves of first experiment (without heat treatment) and retested samples with 24 hours ageing at RT

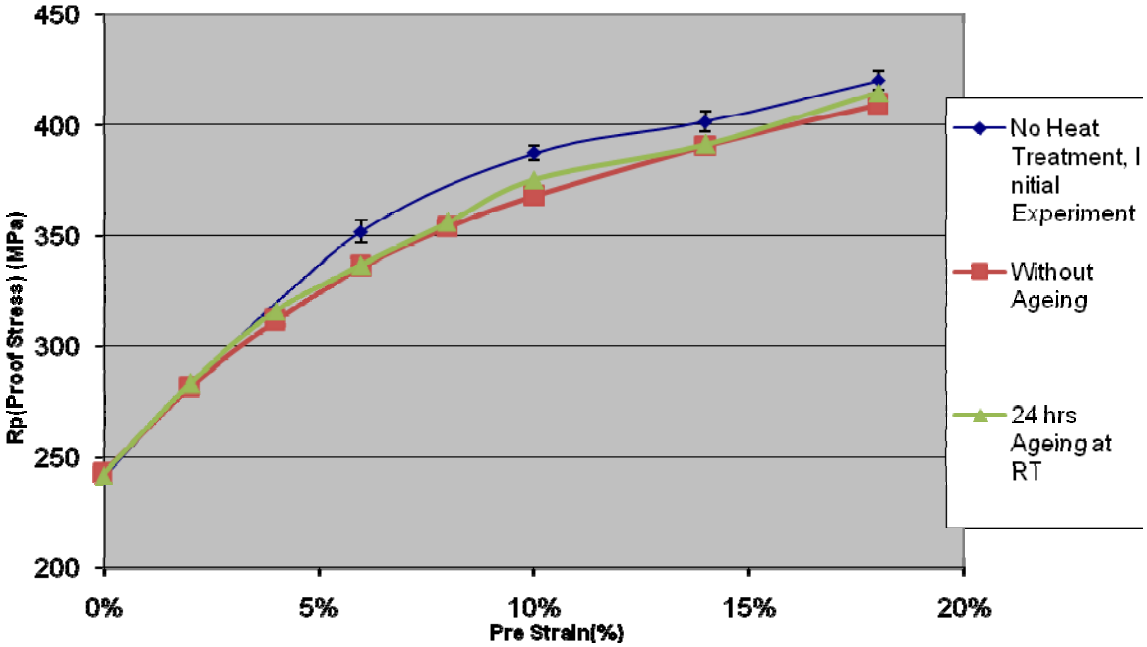

Fig 6.7: Flow Stress for different input conditions

The restoring gradual recovery as a function of prestrain for aged specimens in figure 5.3 shows the very high sensitivity of recovery to ageing unlike the flow stress as it has been pointed out that recovery in E modulus is more sensitive than the yield strength increment by baking. The reason of high sensitivity of prestrained BH samples to heat is understandable. As stated in sec 2.3.2, plastic deformation introduces local stress fields in the vicinities of dislocations. These changes in the stress fields are the driving force for the migration of impurity atoms. We also know that plastic prestraining results in a big increase of dislocation densities. So the ultimate result would be the creation of very high stress field due to increase in the dislocation densities. On the other hand, diffusion is a temperature dependent phenomenon and an increase in temperature results in a higher speed of diffusion. Therefore, the higher stress field around dislocation and higher speed of diffusion resulted in the start of strain ageing phenomenon. This is the main reason for the absence of degrading behaviour of E modulus in our initial results.

Whether the degradation of E modulus by prestraining is frequency dependent (FD) or strain amplitude dependent (AD) is still not known. The type of degradation can be known by the internal friction study which is not done in our case. And also it is not important to know which type of degradation took place.

6.3.2 Heat treated samples

Figures 5.4, 5.5, 5.7 and 5.8 show the effect of heat treatment on E modulus values. Heat treatment has fully restored the E modulus for all heat treatments. This observation is in agreement with the previous research e.g. like in fig 3.8 and 3.10 for BH steel. The effect of baking and prestraining on yield strength increment is more dominant and distinguishable. However, E modulus shows full recovery for any level of heat treatment and after recovery the effect of prestraining is least distinguishable. Therefore, the effect of prestraining on E modulus is visible only when the E modulus has not fully restored like in fig 5.3 for aged specimens at RT.

Since dynamic and tensile test results are almost the same for E modulus and also less standard deviation is found for dynamic results, therefore, only dynamic IET results will be consulted for discussion. As discussed, after recovery the distinction between E modulus values corresponding to different heat treatment is difficult as most of the values are under the standard deviation bars.

As described, the effect of heat treatment and prestraining is more distinguishable for yield strength increment. This can be observed by inspection of the fig 6.8 and 6.9 where hardening curves of 160°C and 230°C both for 20 minutes are compared with as received (retested) hardening curves. It can be seen that the higher the temperature of heat treatment, the higher is the YPE and the upper yield point (R_{bH}). The hardening curves for one temperature level are always overlapping with other prestrain levels which mean there is no reason to distrust the experiments.

E modulus restored fully for aged condition for 24 hours at 10% prestrain and higher. Beyond this level of prestrain, there is hardly any difference between aged specimens and heat treated samples. By only looking into the recovery curve of E modulus for aged conditions and for heat treatment curves, one might become of the opinion that the treatment of prestrain of 10% and higher at RT is equivalent to at least 160°C to 180°C for both time of baking and that the former treatment is sufficient for complete bake hardening. However, this opinion can be misleading and is clarified by the comparison of yield stress for different treatments of ageing and heat treatment shown in fig 6.10. At 10% prestrain, the total yield strength (R_p)increment between the lowest heat treatment i.e. 160°C for 10 minutes of baking and the aged condition for 24 hours is 24 MPa and becomes 33 MPa for highest heat treatment i.e. 230°C and 20 minutes of baking. The difference in R_p between aged (24 hours aged at RT) and non aged sample at 10% level of prestrain is only 7 MPa. The baking R_p at lowest heat treatment is 31 MPa and 40 MPa for highest heat treatment level.

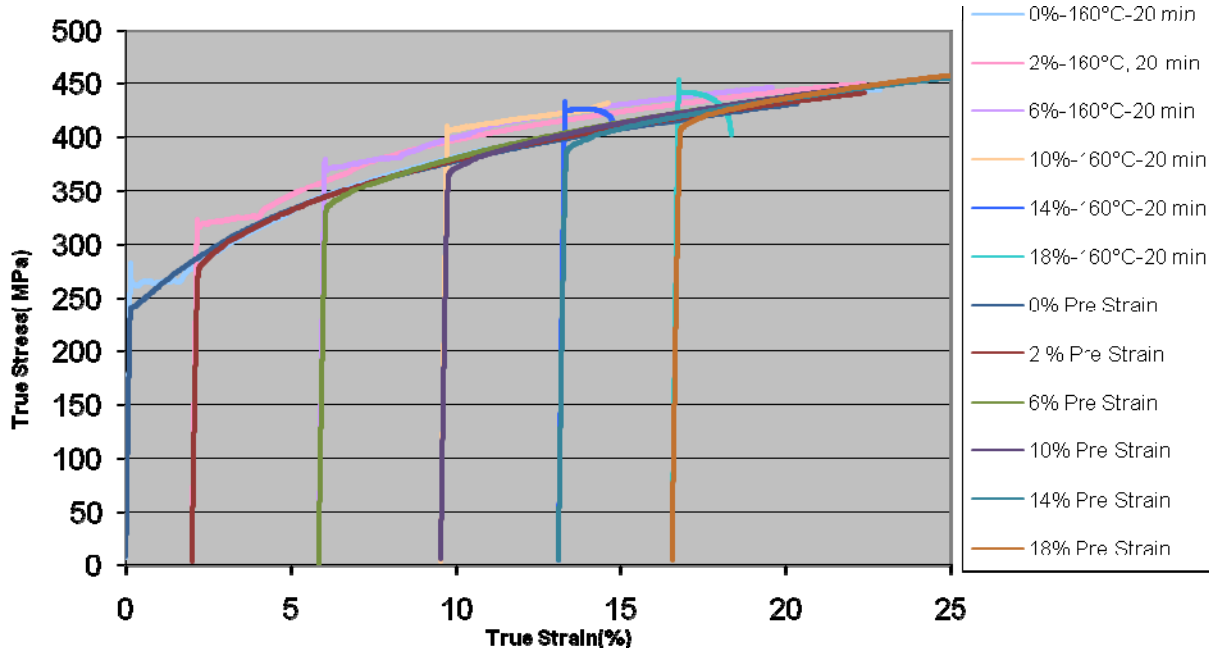

Fig 6.8: Comparison of hardening curves for non heat treated samples with heat treated sample at 160°C for 20 minutes

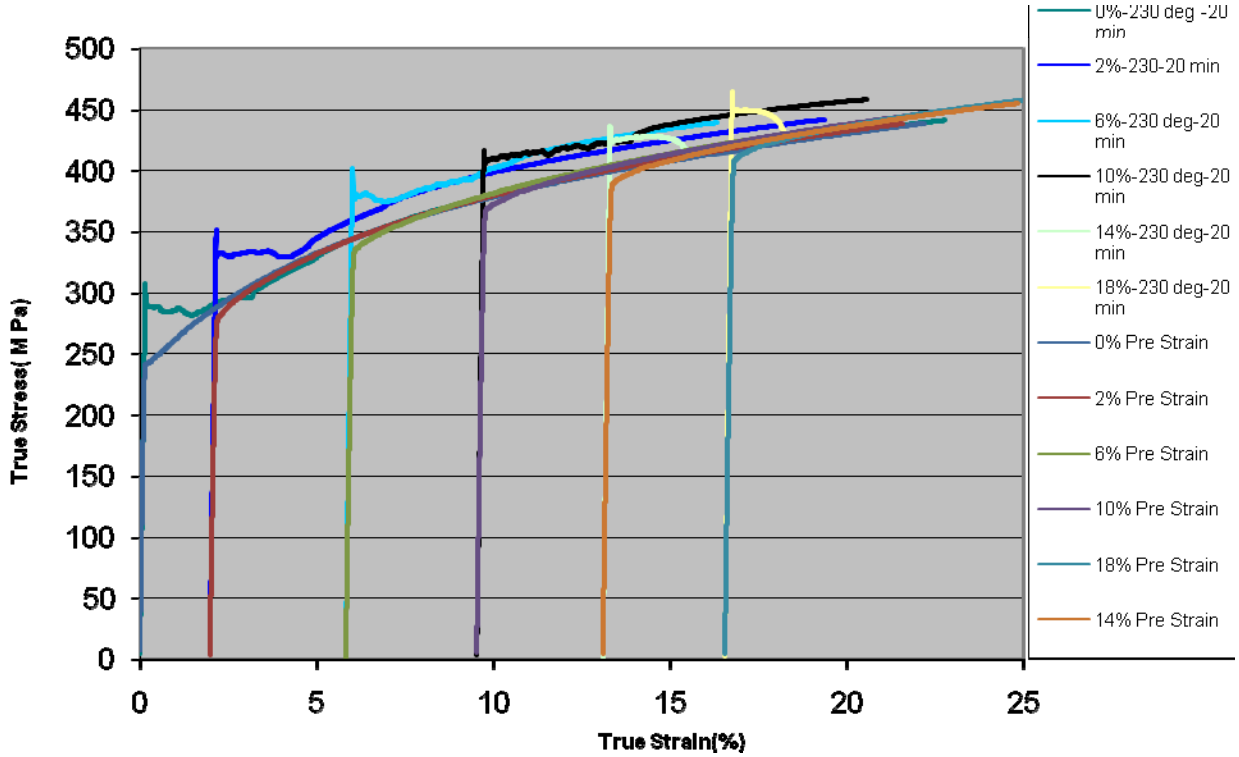

Fig 6.9: Comparison of hardening curves for non heat treated samples with heat treated sample at 230°C for 20 minutes

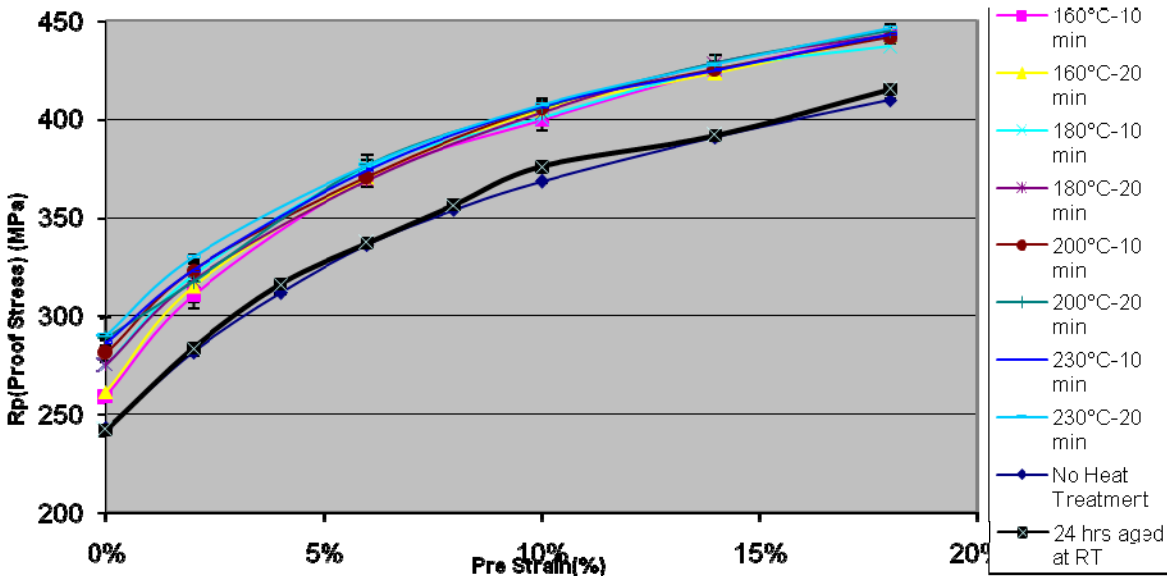

Fig 6.10: Flow Stress versus different levels of pre straining for non heat treated samples and at different heat treatments

From this observation, it can be concluded that the maximum extent of E modulus to different heat treatment is to restore it fully but there cannot be significant increase in E modulus after restoration by the different levels of prestrain and temperatures like the flow strength increment which increases very significantly by the application of variation of heat

treatment and prestrain levels. This is because there is a physical constraint for E modulus which is explained below.

On an atomic scale, E modulus is manifested as a function of interatomic bonding force (F) (or the stress σ) and interatomic distance r (or the strain ε) in the state of equilibrium and can be written as

$$E_a = \frac{\sigma}{\varepsilon_a} \quad \text{----------[6.1]}$$

The macroscopic elastic strain is manifested as small changes in the interatomic spacing and the stretching of interatomic bonds. Therefore, the magnitude of E modulus is a measure of the resistance to separation of adjacent atoms i.e. the interatomic bonding forces. When a material is prestrained, then in addition to interatomic separation, there is an additional strain caused by dislocation. In the that particular case, the effective E modulus becomes as

$$E_{eff} = \frac{\sigma}{\varepsilon_a + \varepsilon_d} \text{----------[6.2]}$$

Due to this dislocation strain, the E modulus reduces when prestrained to different levels. Baking at different temperature causes diffusion of carbon to those dislocations, pin them and hence the contribution of dislocation strain is minimized and therefore the original E modulus restores and this is the reason for the maximum extent of the restoration of E modulus.

Two mechanisms are responsible for the minimizing the effect of dislocation strain. The first is the contribution caused by the interstitials atoms which transfer to energetically favourable positions at the dislocations. This is accompanied by disappearance of the lattice strains around these atoms and a significant strain relaxation in the dislocation core. The second contribution is related to the change of average dislocation segment length between dislocation pinning points.

With application of a small prestrain, the driving force of strain ageing causes the diffusion of solute carbon content provided the material is given enough time at a certain temperature. A considerable magnitude of mobile dislocations thus will be pinned down effectively by solute carbon. When the pre strain level is increased further, more mobile dislocation will be created to continue plastic flow and thus raising the flow stress and causing recovery in E modulus.

If the level of pre strain is too large, the density of mobile dislocations will be too large so that the pinning of solute carbon will not be as effective as with low pre strain level. This fact becomes clear by a comparison of fig 6.8 and 6.9. Up to 6% increase in pre strain level, YPE and R_{bH} are higher for higher temperature, but pre strain higher than 6% causes no significant increase in YPE and R_{bH} and these two values are almost the same in these two temperature ranges. In those regions of higher prestrain, the fraction of "total strength increment[2]" is majorly dominated by the work hardening rather than the bake hardening increment. Pinning effect in those regions will not be much strong even though the driving force for strain ageing may be higher. The less effective bake hardening effect after 6% prestrain is also clear from fig 6.10 for the value of R_p. Beyond 6% prestrain level, the R_p values for different temperature ranges (only heat treated curves) are hardly distinguishable and are mostly within the standard deviation bars. The effective bake hardening up to 6%

[2] Total yield Strength In a BH steel is equal to sum of flow strength increment caused by work hardening and bake hardening.

prestrain level is not clearly visible for E modulus. The reason of this less effective bake hardening beyond 6% is given in sec 6.3.3.
More research is required to be done especially dynamic test with higher resolution and accuracy. Some research has shown dynamic IET with a higher resolution (10-4 Hz [73]) for the study of ageing of BH steel.

6.3.3 Carbide Precipitation

The ternary cementite in pure alpha iron precipitates as spherical coherent particles. Calculated Time Temperature Precipitation (TTP) diagrams verified with ageing experiments with different alloying composition are a useful way for knowing the existence of precipitation as a function of temperature, prestrain and time of ageing. An example is shown in fig 6.11. This figure can be used as a rough guide for the existence of precipitation. From this figure, it can be seen that at temperature of 200°C and 230°C for 10 and 20 minutes, the precipitation stage must have taken place.

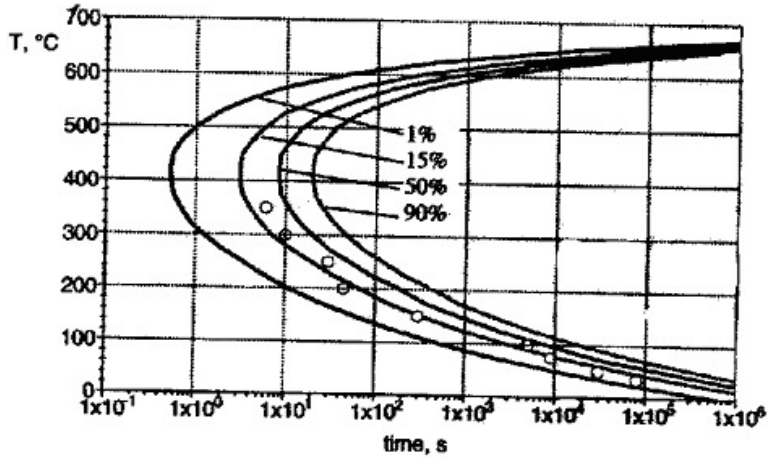

Fig 6.11: Calculated TTP diagram for cementite (Fe_3C) precipitation in ferrite. Experimental points taken from [74] for 15% Carbides precipitated in steel with additional mass contents of 0.02% P and 0.35% Mn.

In the literature two types of precipitation have been recognized, i.e. ε carbides or high temperature carbides which precipitate in the temperature range of 90°C to 250°C and low temperature carbides which precipitate at temperatures below 90°C. The effect of increase in recovery due to carbide precipitation is not clear in our experiments, however, the slight continuous increase in average E modulus values visible in fig 5.6 could be due to this carbide precipitates.
For a fixed amount of carbon, more carbon will be consumed in Cottrell atmosphere when the level of prestrain is higher. This will render less carbon available for carbide precipitation stage and consequently will result in reduce strength increment and recovery in precipitation stage. This is illustrated in fig 6.12. This hypothesis is in agreement with our experimental results for yield strength increment only. This is also found by De [41,42] when he carried out experiments on ultra low carbon BH steel when prestrained up to 10%. In this study, the strength increment by the Cottrell atmosphere formation and precipitation stage took place only after 1% prestrain level. For higher prestrain levels at 2%, 5% and10%, the precipitation stage was absent. The absence of this stage is attributed to the extremely low amount of carbon which is all almost consumed in the Cottrell atmosphere and hence no free carbon is left for the precipitation stage.
However, on the other hand, it is also well documented that extremely small amount of carbon is required for saturation of dislocation. In most literature, the occupancy of one

carbon atom per atomic plane is considered enough for saturation of dislocation. Using equation (3.2), for the highest calculated dislocation density of 61.5×10^{12} m^{-2}, only 0.5 ppm of carbon content is required for saturation. However, in other literature, there is a bit higher amount of carbon described sufficient for saturation such as 1 ppm of carbon is described enough for only an initial dislocation density of 10^{12} m^{-2}. This discrepancy can be understood if we keep in mind that equation (3.2) is valid for the supposition of one carbon atom per atomic plane. However, in actual, there could be more carbon atoms per dislocation line. This can be understood by the way that when there is a strain field, free carbon atom will be diffusing to it from all direction due to strain field associated with it and hence more than one carbon atom can diffuse per one dislocation.

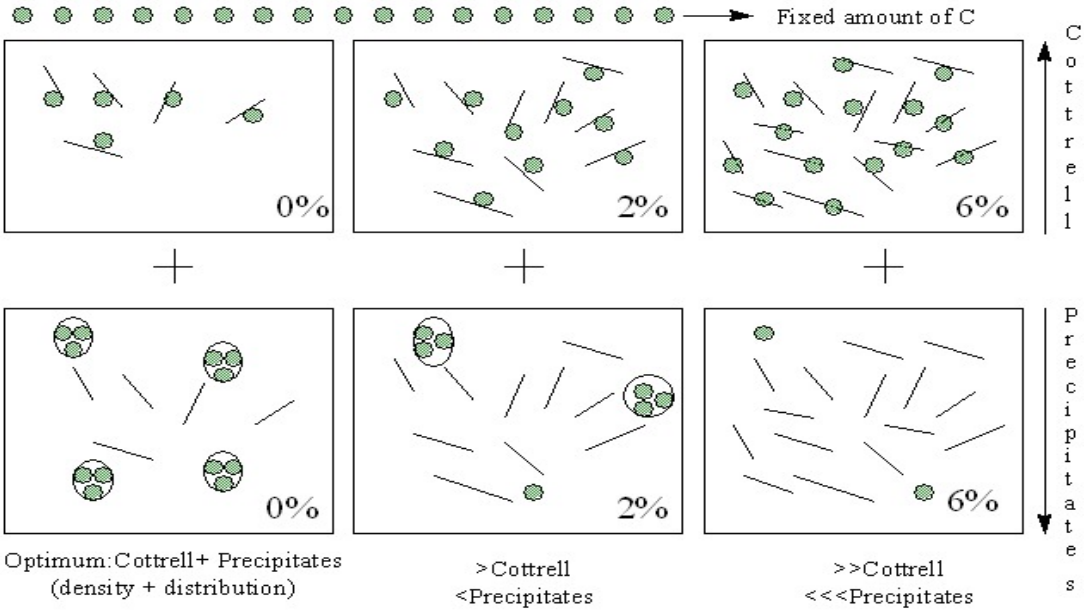

Fig 6.12: The Effect of increase of Pre Strain on contribution of strength increment by Cottrell atmosphere and Precipitation stage for a fixed amount of carbon [38]

From this hypothesis, the situation of higher dislocation density described in sec 6.2 can also be understood. Even when the carbon content is high enough for saturation of all dislocation at a higher level of dislocation density, there remains possibility of dislocations without pinning. Those dislocations will be those which are furthest from any free carbon atom as all the carbon content is consumed for saturation of nearby dislocations. From this explanation, it is easy to understand why at a higher prestrain level, the bake hardening is not as effective as it is on lower values of prestrain. In literature, the range of carbon contents described sufficient for saturation of dislocation is in the range of 5-25 ppm [37,38]

6.4 Influence of Baking Temperature and Time

To some extent, the influence of baking temperature has been discussed in the last section. Variations on ageing response can take place depending upon the baking temperature and time of baking. Method and equipment of heat treatment is also important. In our experiments, an oil bath has been used in for heat transfer. Fluid (oil or water) heating has been described as an efficient and effective heat treatment and is also described elsewhere [73]. Variation of heat treatment can affect the bake hardening as the underlying mechanism is controlled by diffusion which is sensitive to temperature.

Results of E modulus for different temperatures shows hardly any dependence on baking time and E modulus values were almost the same for both 10 and 20 minutes of baking time

for any specific temperature. The average E modulus values for a specific temperature however showed a continuous slight increase trend in E modulus values, which is visible in fig 5.6 and 5.9 for dynamic and static test respectively. The maximum bake hardening in yield strength was in the range of 34 to 48 MPa for different levels of prestrains and heat treatments. The bake hardening for lowest and highest heat treatment has been shown in table 6.3. The same range of bake hardening is reported by other researches also [38,41,42].

Table 6.3: Bake Hardening for lowest and highest heat treatment

Pre Strain	$BH_{160°C\text{-}10min}$ [MPa]	$BH_{230°C\text{-}20min}$ [MPa]
0%	16	47
2%	29	48
6%	34	40
10%	31	39
14%	34	37
18%	33	36

A TEM study for H180BD has shown that carbides formed at this temperature are ε carbides [38]. Although, carbides can also form at temperatures below 200°C, it is assumed that this precipitation will be too small and sparsely distributed that its contribution is not distinguishable.

The results of both bake hardening strength increment and E modulus variation undermine the effect of baking time, but show sensitivity to heat treatment temperature. Therefore, the Hundy's equation (equ 4.1) is not appropriate to describe the equivalence of baking time and temperature in these experiments. More research is needed especially in other time ranges of baking.

The investigation on BH steel for E modulus is quite a new topic and there remains the need of further research for different influencing factors like the effect of prestraining and secondary straining direction, effect of orientation, effect of grain size, which were discussed in chapter 3. Further, the material in our experiments was assumed isotropic, in practice; however, this assumption is not quite true. Anisotropic nature develops in sheet metal during rolling in production lines. Accurate dynamic methods which can determine E modulus in different directions to RD exists e.g. the Ultrasonic Method and Resonant Ultrasound Spectroscopy (RUS) briefly discussed in initial literature survey [23]. The need of further research by these methods is emphasized. Even with the assumption of isotropic nature, the need is there for research to be done with high accuracy methods which could be the use of high precision extensometer in tensile test and the use of high resolution in the IET method.

6.5 Error Analysis and Difficulties of measurement

In this section possible error induced in the results will be discussed. Standard Deviation with static method is found larger than the dynamic method. In the following, error analysis of both methods of measurement will be presented one by one, but before this strain distribution along the samples length will be discussed.

6.5.1 Strain Distribution

In the experiments of this work, the total strain was used for measurement. In order to know the real strain state, the work of Schouten [75] is referred who did strain distribution

experiments on bake hardenable steel grade H180BD. The mechanical properties of his material are given in table 6.4

Table 6.4: Mechanical properties of H180BD [75]

R_p [MPa]	R_m [MPa]	A_{80} [%]	r-value	n-value
200	305	42.3	2.15	0.215

Sample dimension taken in this study were 320x120x0.7 mm and were strained to deformation level of 2,4,6 and 8% with a tensile test machine. The samples were provided with an electro-chemically applied grid with a distance of 2 mm dots. After deformation, the grid was measured again with the help of software Phast. A set of 11 pictures from different angles were taken to calculate the strain. Each sample consisted of ±9000 points. Fig 6.13 and 6.14 show the 2D plot and Forming Limit Diagram (FLD) for the strip deformed to 2% and 8% respectively. The major and minor strain in the centre of the samples is shown in table 6.5. In FLD plots, horizontal axis represents the minor axis with a scale of 0 to -0.10 to and the vertical axis represents the major strain with a scale of 0 to 0.10.

Table 6.5: Major and Minor strain measured in the centre of the samples [75]

Prestrain ε_t (%)	Major strain in the centre	Minor strain in the centre
2	0.01 ± 0.01	-0.02 ± 0.01
4	0.03 ± 0.01	-0.04 ± 0.01
6	0.05 ± 0.01	-0.05 ± 0.01
8	0.07 ± 0.01	-0.06 ± 0.01

An ellipsoidal yellow red region of 200x100 mm dimensions was found in the 2D photographs for each level of pre strain. Fig 6.15 show the strain profile of major strain (blue lines) for the strip prestrained to 8%. It is clear that the line that represents the strain in the centre of the sample (maj c) has a uniform deformation of 8% from 50 to 270 mm along the strip length. While the other two blue lines namely major-b and major-o, which represent the strain at approximately 40 mm distance from either side of the centre, have uniform deformation from 90 to 210 mm along the strip length. Therefore a uniform distribution of 100x100 mm should be expected in the centre region of the samples.

Keeping in mind the conclusion just mentioned, it can be inferred that uniform deformation area in the tested samples should also be approximately 100x100 mm in the centre. (In fact, this area could be more as sample lengths in this work are 250 mm compared to 320 mm length of the study while width of the sample remains the same in both studies). With this conclusion, the uniform deformation area in our experiments is shown in fig 6.16. So each sample is uniformly deformed in the centre.

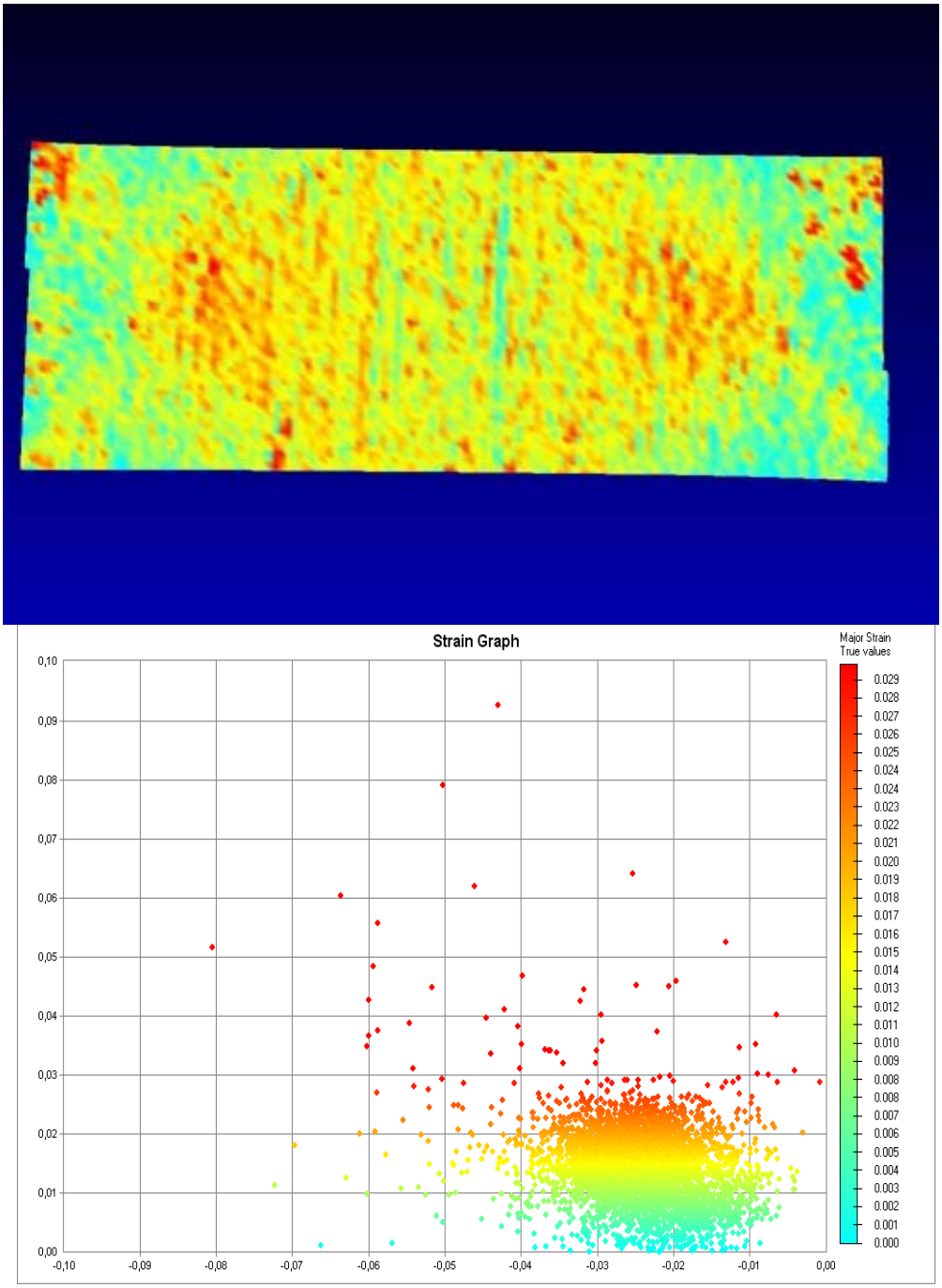

Fig 6.13: (top) 2D photograph (bottom) FLD diagram of the sample pre strained to 2% [75]

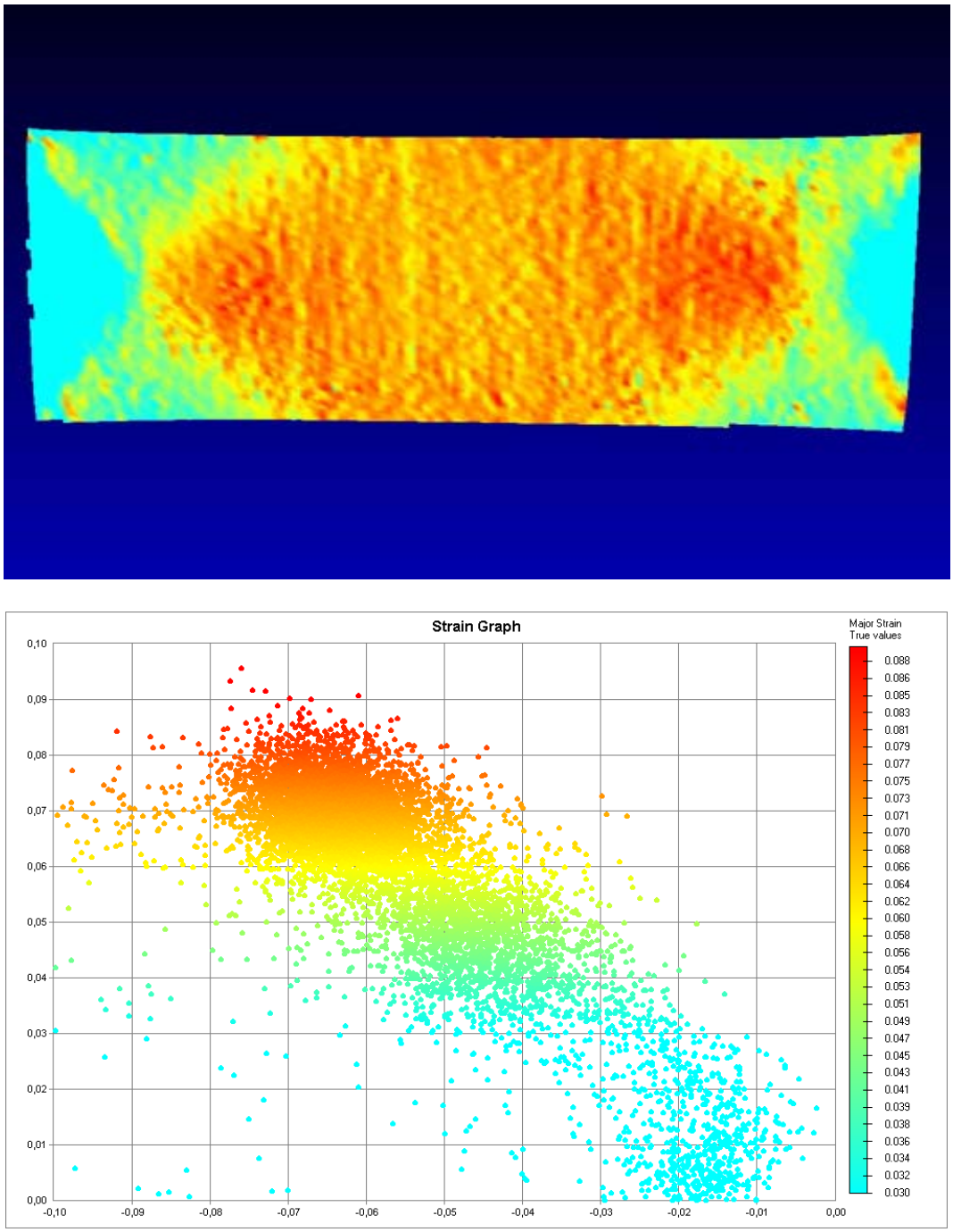

Fig 6.14: (top) 2D photograph (bottom) FLD diagram of the sample pre strained to 8 % [75]

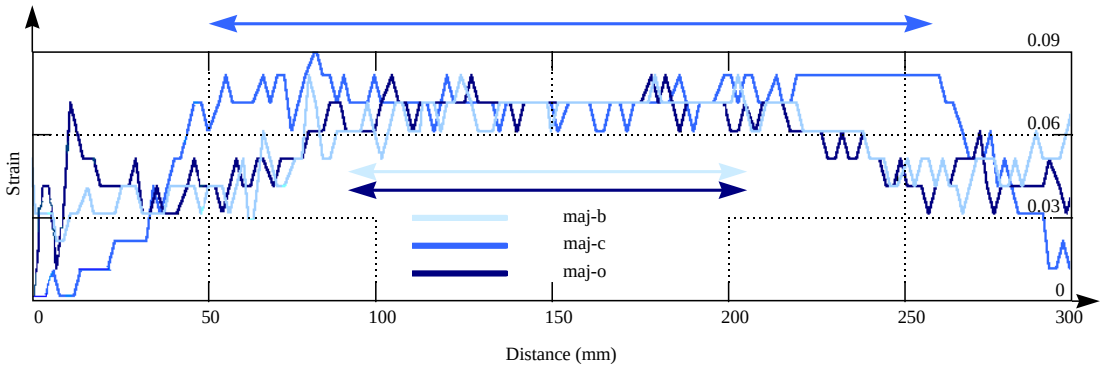

Fig: 6.15: Section plot for strip pre strained to 8% [75]

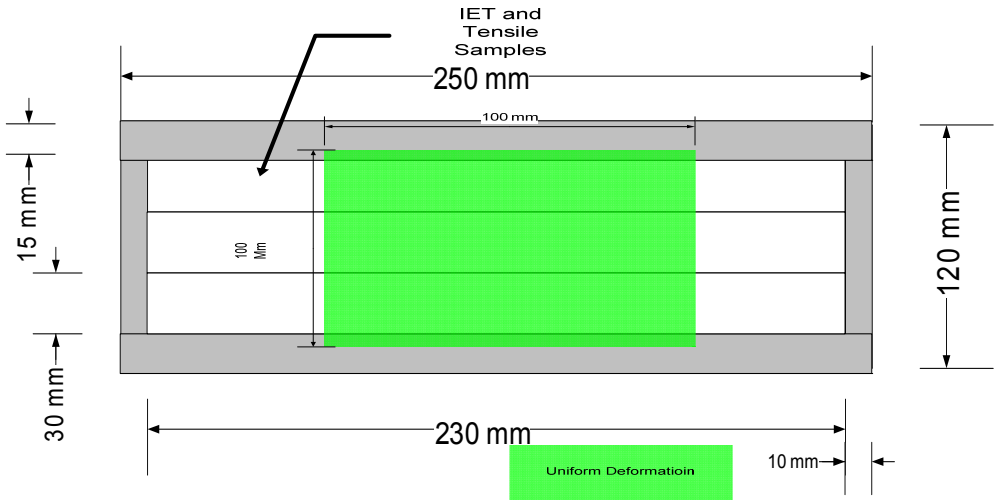

Fig 6.16: Uniform Deformation area of IET and Tensile Samples after Pre Strain

6.5.2 Impulse Excitation Test (IET)

The standard deviation found with IET is on general lower than the static tensile test method. It is described in the sec 4.5.1 that IET is sensitive to dimensions of the samples and mass. Besides this, the accuracy with which the frequency of the sample is measured is also important. Table 6.6 shows percent error in calculation of E modulus when a 0.1% error is induced in the measurement of the input parameters. From an overview of the table it is clear that accurate measurement of length and thickness is most important for accurate calculation of E modulus. In our case, thickness was measured with a digital thickness gauge accurate to 3 decimal places in millimetres and thickness was measured on five equidistant points and then an average value was used for calculation of the E modulus. However, for measurement of length a manual vernier calliper was used, so accuracy in terms of length may occur affecting the accuracy of the results. Frequency measurement is another important input parameter which can affect the accuracy of calculation by 0.2 % for measurement error of 0.1%. For this purpose a laser vibrometer was used with a resolution equal to 0.063 Hz. This means if actual frequency of the sample were less than this resolution, then the laser vibrometer could make an error in frequency up to 0.1 %. For width measurement, a digital vernier accurate to two decimal places was used and an average value of two ends of the samples was used in the final calculation of E modulus. The fact that the samples were not machined but sheared may induce some geometrical errors in terms of length and width. Mass of the sample was measured with a digital mass balance accurate to four decimal places in gram.

Table 6.6: Effect of variable error on modulus calculation [70]

Variable	Measurement Error	Variable Exponent in Modulus Equation	Calculation Error
Frequency (f)	0.1 %	f^2	0.2 %
Length (L)	0.1 %	L^3	0.3 %
Mass (m)	0.1 %	m	0.1 %
Width (b)	0.1 %	b^{-1}	0.1 %
Thickness (t)	0.1 %	t^{-3}	0.3 %
Diameter (D)	0.1 %	D^{-4}	0.4 %

6.5.3 Tensile Test and its standardization

For the determination of E modulus, the lack of standardization has been felt. Except the US standard ASTM E111-04 [76], there is no European standard or DIN standard available. The results of tensile test showed relatively higher standard deviation and lack of standardization is one of the reasons for high variation of results. The indication error of the extensometer used in this study was 0.6 μm and the measurement uncertainty equal to 0.2% which is equal to 0.15 μm. To know the magnitude of error, some eight examples are taken randomly and compared with Proof stress (R_p) and Ultimate Tensile Strength (R_m) values in table 6.7.It can be seen from this table that standard deviation for E modulus is higher in 4 cases when compared with the standard deviation of Rp and Rm (namely at example 1,2,3 and 7) and is greater from one value and less than the other in one case (example 4) and less in other three examples. It is recommended that for determination of E modulus with uniaxial tensile test, three samples are not sufficient and at least 5 samples of each condition should be simulated to get a lower standard deviation. The magnitude of error for the case of E modulus is in fact much larger if one keep in mind that error for E modulus is the units of giga Pascal (10^9)while that of other two properties is in mega Pascal (10^9).

Table 6.7: Comparison of experimental measured E modulus, Rp and Rm for Error Analysis.

Example No.	Pre Strain	Heat Treatment	Property	Sample 1	Sample 2	Sample 3	Standard Deviation
1	0%	No Heat Treatment	E Modulus(GPa)	190	191	186	2.65
			R_p(Mpa)	241	240	240	0.58
			R_m(Mpa)	351	350	350	0.58
2	6%	No Heat Treatment	E Modulus(GPa)	186	186	176	5.77
			R_p(Mpa)	350	358	348	5.29
			R_m(Mpa)	372	375	369	3.00
3	6%	180°C and 20 min	E Modulus(GPa)	193	190	178.56	7.62
			R_p(Mpa)	369	370	368	1.00
			R_m(Mpa)	389	391	389	1.15
4	10%	180°C and 20 min	E Modulus(GPa)	189	185	187	2.00
			R_p(Mpa)	405	401	403	2.00
			R_m(Mpa)	408	408	411	1.73
5	6%	200°C and 20 min	E Modulus(GPa)	188	190	195	3.61
			R_p(Mpa)	380	379	371	4.93
			R_m(Mpa)	393	398	390	4.04
6	10%	200°C and 20 min	E Modulus(GPa)	186	185	186	0.58
			R_p(Mpa)	406	407	405	1.00
			R_m(Mpa)	411	410	408	1.53
7	6%	230°C and 20 min	E Modulus(GPa)	203	196	192	5.57
			R_p(Mpa)	377	379	374	2.52
			R_m(Mpa)	394	396	391	2.52
8	2%	230°C and 20 min	E Modulus(GPa)	193	195	194	1.00
			R_p(Mpa)	331	329	336	3.61
			R_m(Mpa)	372	372	374	1.15

A European Round Robin test with 91 testing laboratories has shown that in many cases E modulus of steel with tensile test has not been determined with sufficient accuracy [58]. The scatter band of modulus data in those tests on round steels specimens was found even larger than our measured values. Many factors influence the results like elongation is measured with cross head separation and not with high resolution extensometers. Another important factor is the lack of standards for testing procedure and evaluation. Some influential factors which may contribute to accuracy of E modulus are tabulated in table 7.10. Further standardization of the method is in progress as described by Borsutzki [58].

Table 6.8: Possible Influences on Young's Modulus in Uniaxial Tensile Test [58]

Testing Machine ➢ Clamps ➢ Extensometers	Measuring values: Load, Elongation, Initial Cross section, Initial measuring Length ➢ Mechanical or hydraulic grips, alignment ➢ Resolution, precision, conditions of slits…
Test Parameters	Pre Load, Stress Rate, Measuring Frequency, Temperature
Test Software	Finding of the linear part, Regression
Material Condition	Deformation(Skin Pass levelling, stretching, straightening), residual stress state, texture
Specimen Fabrication	Tolerances, Micro Cracks, Residual Stresses

6.6 Comparison of Measurement Methods

It has been described that E modulus measured with IET produced less variation in results than the tensile test. The hitting of sample by impulser and its frequency measurement by the laser vibrometer hardly takes 30 to 40 seconds. In tensile test, the actual time of operation is around one minute in tensile test after mounting in the jaws. IET is a non destructive method unlike the tensile test and the same sample can be and has been used for tensile test after testing with IET. Tensile test is a universally accepted method and with one experiment of tensile test, mechanical properties like R_p, R_m, R_t, E modulus, A_g and others properties can be obtained. Further to this, the phenomenon of YPE can only be detected from a stress strain curve obtained with the tensile test. It also gives information about work hardening, its exponent (n) and Lankford's coefficient.

A problem encountered with tension testing is the lack of standardization for determination of E modulus. The E modulus values in tensile test are software calculated which is based on the method described in sec 4.5.2. i.e. slope of the data between 5 to 40% of maximum stress where the maximum stress is taken from the strain range between 0 to 1% strains. There were some cases in which this range of data was not a straight line but curved from which it was difficult to determine E modulus. In those cases, other data ranges were taken for a more linear portion of the data. It means software calculated values should not always be trusted and stress strain chart should be drawn and then it has to be decided which portion of the data should be taken. This is a time consuming process unlike the dynamic

testing where you need to just plug the measured frequency in the relation of E modulus. Due to high standard deviation, it is recommended that at least 5 samples be used with tensile test in order to get a lower standard deviation. Another step for improving accuracy can be the use of high resolution extensometer and a better quality of clamps to avoid any slippage during testing.

The error in IET can be reduced if the resolution of the laser vibrometer is refined to 10^{-4} Hz as Vasilye [73] has done in his studies while doing dynamic test. Further to this, it is also recommended that machined samples be used for IET. This will reduce the geometry related uncertainties and there will be no need to measure the dimensions of each sample separately which can save productive time. Since BH steel is sensitive to heat, therefore, a machining method should be used which do not produce heat or produce very localized heat. Use of Abrasive Water Jet Machining and Electrode Discharge Machining could be a solution to this problem.

CONCLUSION AND RECOMMENDATIONS

CONCLUSIONS

1. Plastic deformation in the uni-axial tension caused a 10%-12% reduction in E modulus in the prestrain range of 2% to 18% for the H220BD.
2. Heat treatment restored the original E modulus of the material after prestrain.
3. BH steel is extremely sensitive to ageing at especially after prestraining and especially the recovery phenomenon in E modulus is more sensitive to ageing at RT/heat treatment than the yield strength increment.
4. The mechanism of recovery or bake hardening in BH steel is considered to be a three stage process characterized by Snoek Effect, Cottrell Atmosphere formation and ε carbides precipitation. Among these, Cottrell atmosphere formation is most significant for recovery.
5. Carbon diffusion to the strain fields of dislocation in Cottrell atmosphere is the governing mechanism for recovery.
6. The effect of prestrain on recovery of E modulus is more clear and distinguishable until the E modulus has not restored such as for the aged sample. After restoration of E modulus, the effect of prestrain on recovery is hardly distinguishable.
7. The maximum extent of E modulus is the full recovery by the application of different ageing and heat treatments due to the physical constraint. This is unlike yield strength increment which results higher strength for higher temperature of baking.
8. Impulse Excitation Technique (IET) which is a dynamic method is a non destructive method and same samples can be used in subsequent tensile test which is a destructive method. Accuracy of the methods can be improved by the use of higher resolution of laser vibrometer and siglab® in IET and a higher resolution extensometer in tensile test.
9. The dynamic method's experimental setup is simple and cheaper unlike the tensile test's experimental setup like the Universal tensile test machine. However, with one test of tensile test, more information can be obtained unlike the IET.
10. Like the yield strength increment in BH steel, restoration of E modulus also shows only temperature dependence and no baking time dependence (baking time used in this study).
11. E modulus is a function of dislocation density and average dislocation loop length and can be estimated at any prestrain level by the knowledge of exact figures of dislocation density and average dislocation loop length.
12. Dislocation density can be calculated from flow stress equation (which is done in this study) or with the use of Bergstrom's model.
13. Loop length has to be calculated experimentally as is done in this study.

RECOMMENDATIONS

1. Loop length as a function of prestrain should be found for other grades of steel so that a model can be developed for loop length as a function of plastic strain. .
2. The accuracy of experientially found loop length dictates the use of high accuracy method of E modulus measurement. As described before, this can be done by the use of higher resolution of laser vibrometer in dynamic IET method and extensometer in static tensile test.
3. Due to high sensitivity of the BH material to ageing, when experiment needs to be done for this material, a non heat producing method of machining should be employed for shearing/ cutting and making of the samples. At the very least the temperature/time history should be known, therefore, it is recommended to measure these parameters during machining at least once.
4. The measurement time in IET can be reduced significantly if the rectangular samples are made exactly of the same size and dimensions. In this way, the individual time for measurement of dimension and its mass can be saved. It can be concluded that the cutting of rectangular samples with shearing machine is not a good option as the sample sheared by this method are not accurately rectangular (i.e. the parallelism of opposite side is not very accurate). A punched sample would probably be better in this respect.
5. The support system in IET depends on the flatness of the samples. If samples are distorted even very marginally, the boundary condition can differ by the use of rigid knife edged supports because in that case some points of contact line are not in contact with support. In such cases, rubber band support method should be employed.
6. To cater for the anisotropic nature of E modulus along different directions, it should be measured along different directions by accurate static methods like Tensile Test with higher resolution extensometer and dynamic methods like Ultrasonic Pulse Echo Method, Resonant Ultrasound Spectroscopy (RUS).

Appendix

A.1 Tensile Test Machine Schematics

Some basic components of tensile test machine are shown in fig A.1.1. During tensile test, length and width of the samples and force and cross head displacement is measured as a function of time and the test is carried out until the fracture. The data is stored in MUS-file of a tensile test and mechanical properties like R_p,R_t,R_{eH},R_{eL},A_e,R_m,A_g,A_{gt},A_{50}, A_{80}, n and r are found from this data. These properties are defined in Appendix A.2.

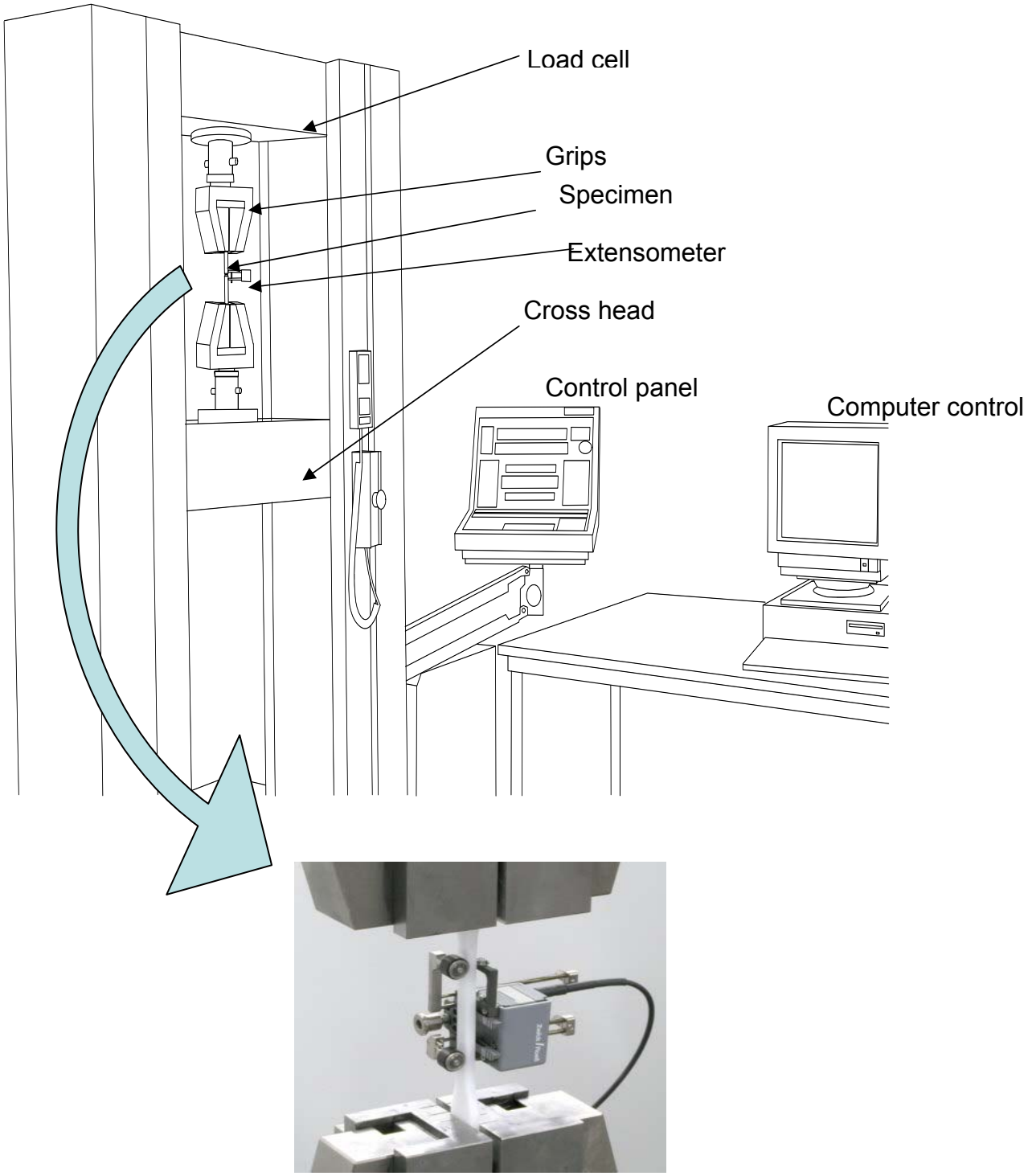

Fig A.1.1: Essential Components of a Tensile Test Machine [77]

A.2 Basic Stress Strain Parameters

Some basic and important stress strain parameters will be illustrated through stress strain diagrams.

Yield Strength ($R_{p0.2\%}$) and Yield Strength ($R_{t0.5}$):

At the start of the curve there is an elastic part after which plastic deformation starts. The point where the material starts to deform plastically is the yield point denoted by R_p. Normally R_p is defined at the stress at 0.2% plastic strain. The plastic strain is determined by fitting a line through the elastic portion of the curve and intersection of this line with a line parallel to the elastic fit line at 0.2% strain. This is most widely used strength measures for metals. If elastic correction is not used to define the yield point and instead total strain is used then the yield point is not indicated by the R_p but with the R_t parameter. R_t and R_p are shown on a stress strain diagram in fig A.2.1.

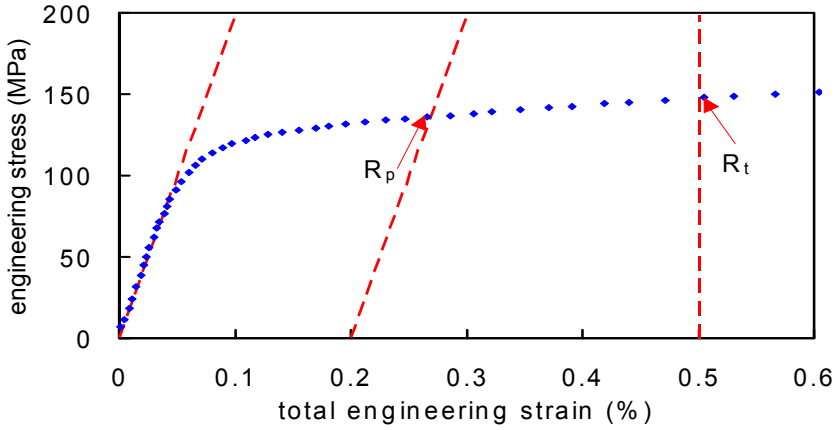

Fig A.2.1: Definition of $R_{p0.2}$ and $R_{t0.5}$ [77]

Upper Yield Strength (R_{eH}) and Lower Yield Strength (R_{eL}):

Some materials show an elongated yield point such as the Bake Hardenable steel used in this study. This yield point shows a plateau before the usual hardening occurs. This elongation can be characterised by a peak followed by a flat area. Two parameters define the high and low point of the yield elongation. Upper yield strength is the maximum value of stress just prior to first decrease in force and the lower yield strength is the lowest value of stress during plastic yielding ignoring transient effects. These two parameters are illustrated in fig A.2.2.

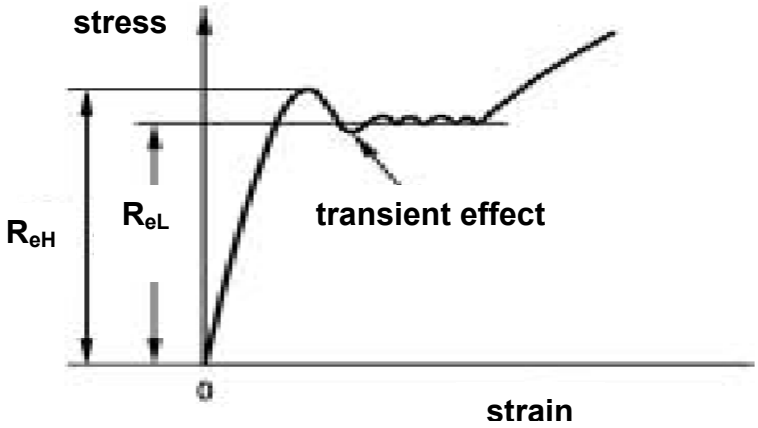

Fig A.2.1: Definition of R_{eH} and R_{eL} [77]

Yield Point Elongation (A_e)

Yield Point Elongation (YPE) is the strain between R_{eH} and intersection of line through yielding (b) and line corresponding to highest slope of curve at start of uniform work hardening (c) and is shown in fig A.2.2. The yield point elongation does not have to be horizontal but can also occur at a slope.

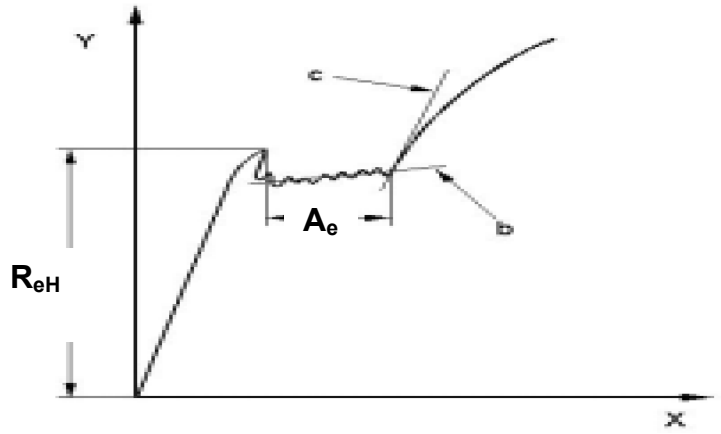

Fig A.2.1: Definition of A_e [77]

Tensile strength (R_m), Uniform Elongation (A_g and A_{gt}):

The Tensile strength (R_m) value is the stress at the maximum of the engineering force-extension curve. This values is not the maximum of the true stress – true strain curve. The plastic strain at the maximum force point has been defined as A_g while the total strain at this point is defined by A_{gt}.

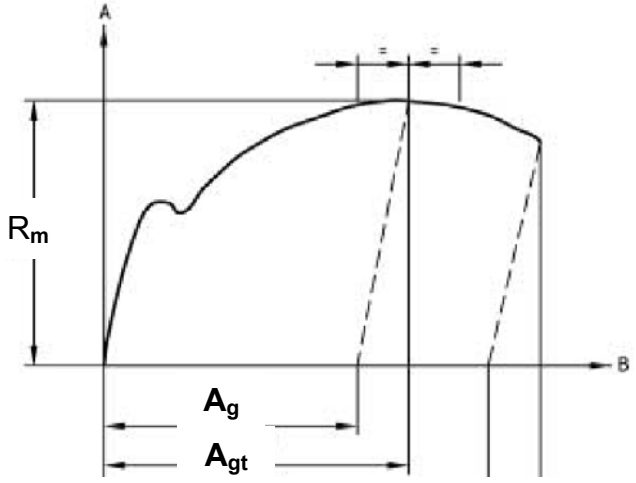

.

Fig A.2.2: Definition of terms R_m, A_g and A_{gt}

Fracture Strain (A_{80}) or (A_{50}):

The final point of the tensile curve is the point where the specimen fractures. The fracture strain is determined from the length of the specimen including the necked region. This means that the fracture strain contains a part where the strain is at A_{gt} level, while in the neck region the strain is a lot higher. Therefore, the calculated fracture strain is an average of the maximum uniform strain and the strain distribution in the neck. This means when a larger specimen is used, the contribution of the uniform strain will be higher and therefore, when the fracture strain is specified the original gauge length of the specimen has to be

stated like A_{80} and A_{50} where the subscript shows the gauge length of the tensile sample. Fracture strain is shown in fig A.2.5.

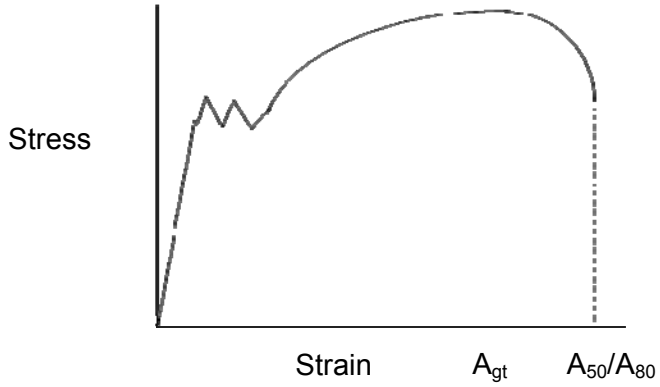

Fig. A.2.5: Definition of A_{50}/A_{80}

Plastic Strain Ratio (r):

This is the ratio between the strain in width direction to the strain in thickness direction. For isotropic material, both strains will be equal and the r value will be 1. In tensile test, strain in thickness direction is not measured, therefore, to calculate the strain in the thickness direction; it is calculated from the strain in width and length direction with the assumption of constant volume. Figure A.2.6 shows the strains in three directions i.e. length, width and thickness.

$$r = \frac{\varepsilon_{width}}{\varepsilon_{thick}}$$

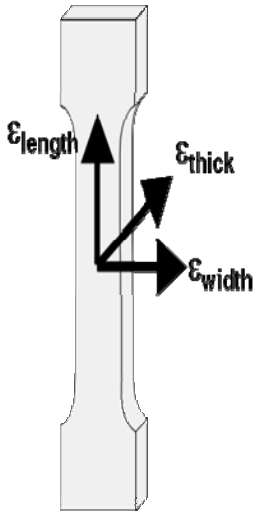

Fig. A.2.6: Strain in three directions

Strain Hardening Exponent (n):

The strain hardening exponent (also called strain hardening index), denoted by n, is a materials constant which is used in calculations for stress-strain behaviour in work hardening. It is calculated from the relation between true stress and true strain by applying the Ludwik-Nadai relation which is

$$\sigma = C\varepsilon^n$$

In this relation, σ represents the applied stress on the material, ε is the strain and C is the strength coefficient. “n” and “C” are determined from this relation using linear regression. The value of the strain hardening exponent lies between 0 and 1. A value of 0 means that a material is perfectly plastic while a value of 1 represents a 100% elastic material. Most metals have an n value between 0.10 and 0.50. n value may change with strain level. Fit region could be 10-20% strain, 6-8, .., 18-20%. The strain limits are not fixed but ranges are given like n2-20/Ag. Normally, lower limit is the end of yield elongation and the upper limit is Ag.

REFERENCES

1) Schelkle,E, “CAE Simulations What are the Challenges in the Future?”, autosim 2006
2) Lingbeek, R.A, “Virtual Tool Reworking- New Strategies in Die Design Using Finite Element Forming Simulations”, ISBN: 978-90-77172-38-4, NIMR, 2008
3) K. Fukizawa, S. Koike and K. Shibata: Material Japan., 39 (2000), 17
4) Burchitz, I, “Improvement of Springback Prediction in Sheet Metal Forming”, ISBN: 978-90-365-2656-2
5) Wagoner, R.H/Li. M “Simulation of Springback: Through-Thickness Integration”, International Journal of Plasticity 23(2007), pp 345-360
6) Livatyali. H/ Altan, T, “Prediction and Elimination of Springback in Straight Flanging using Computer Aided Design Methods Part 1. Experimental Investigations”, Journal of Materials Processing Technology 117, pp 262-268, 2001
7) Yang,D.-Y/Oh.S.I/Huh,H/Kim, Y.H, Proceedings of the 5th International Conference and Workshop on numerical simulation of 3D sheet metal forming processes, NUMISHEET2002, Korea, 2002
8) T. Kuwabara, Y. Asano, S. Ikeda, and H. Hayashi. An evaluation method for springback characteristics of sheet metals based on a stretch bending test. In Kergen R., Kebler L., Langerak N., Lenze F.-J., Janssen E., and Steinbeck G., editors, Proceedings of IDDRG 2004. Forming the Future. Global Trends in Sheet Metal Forming, pages 55 – 64, Sindelfingen, Germany, 2004.
9) L.M. Smith, F. Pourboghrat, J.W. Yoon, and T.B. Stoughton, editors. Proceedings of the 6th international conference and workshop on numerical simulation of 3D sheet metal forming processes, NUMISHEET 2005, Detroit, MI, U.S.A., 2005.
10) Lingbeek, R.A/ Meinders, T, “Towards efficient modelling of macro and micro tool deformations in sheet metal forming”, Proceedings NUMIFORM conference, pp 723-727, 2007
11) Dingle, M.E/Hodgson, P.D/ Cardew-Hall, M.J, “Effect of global and local stiffness on blankholder pressure in draw die forming”, SAE World Congress, 2001
12) Keum, Y.T/Ahn, I.H/Lee,I.K/Song, M. H/ Kwon, S.O/Park, J.S, “Simulation of Stamping Process of automobile panel considering die deformation”, Proceedings NUMISHEET 2005, pp 279-286, 2002
13) Meinders, T/Konter, A.W.A/ Meijers, S.E/ Atzema, E.H/ Kappert, H, “A Sensitivity Analysis on the Springback Behaviour of the Unconstrained Bending Problem”, International Journal of Forming Processes, pp 272-277, Vol A, Numisheet 2005
14) Aretz. H, “Applications of a new plane stress yield function to orthotropic steel and aluminium sheet metals”. Modelling and Simulation in Materials Science and Engineering, 12(3):491–509, 2004.
15) Geng, L/ Wagoner, R.H, “Role of Plastic Anisotropy and its Evolution on Springback”, International Journal of Mechanical Sciences 44, pp 123-148, 2002
16) Pijlman, H.H/Huetink, J/ Meinders, T/ Carleer, B.D/ Vegter, H, “The Implementation of the Vegter Yield Criterion and a Physically based Hardening Rule in Finite Elements”
17) Hill.R, “Constitutive modelling of orthotropic plasticity in sheet metals”. Journal of Mechanics and Physics of Solids, 38:405–417, 1990.
18) Hosford. W.F. “A generalized isotropic yield criterion”. Journal of Applied Mechanics, Transactions of the ASME, 39:607–609, 1972.
19) Barlat.F/ Maeda.Y/ Chung.K/ Yanagawa.M/Brem.J.C/Hayashida.Y/. Lege.D.J/ Matsui K./ Murtha.S.J./ Hattori.S./ Becker R.C./ Makosey. S. “Yield function development for aluminium alloy sheets”. Journal of Mechanics and Physics of Solids, (45):1727–1763, 1997
20) Vegter.H/ Drent.P/ Hu´etink. J.” A planar anisotropic yield criterion based on mechanical testing at multi-axial stress states”. Proceedings of NUMIFORM 1995. Simulation of

Materials Processing: Theory, Methods and Applications, pp 345–350, The Netherlands, 1995
21) Krasovskyy, A/Schmitt, W/Riedel, H, “Material Characterization for Reliable and Efficient Springback Prediction in Sheet Metal Forming”, Steels for Automotive Applications, Steel Research int. 77, No.9-10, 2006
22) Van Riel, M/van den Boogard, A.H, “Stress and strain responses for continuous orthogonal strain path changes with increasing sharpness”, Scripta Materialia, 57, pp-381-384, 2007
23) Haleem, A , “Literature Study on Strain Dependency of the Young’s modulus of HSS”, Reference source no.137502, Project number: 9993.35, Corus
24) Lems, W, “The change of Young’s modulus after deformation at low temperature and its recovery” PhD thesis, Delft University of Technology, 1963
25) Yang M/ Akiyama Y/ Sasaki, T, “Evaluation of change in material properties due to plastic deformation”, Journal of material processing technology 151(2004), pp. 232-236
26) Krempaszky, C/Liedl, U/Werner, E.A, “A note on the diffusion of carbon atoms to dislocations”, Computational Material Science 38 pp.90-97, 2006
27) Read, T.A “Internal Friction Of Single Crystals Of Copper And Zinc”, (1941)
28) Nowick, A.S/Berry, B.S, “Anelastic Relaxation in Crystalline Solids”, Academic Press, New York and London. (1972)
29) Koehler, J.S (1952). In “Imperfections in Nearly Perfect Crystals” By W.Shockley, Chapter 7, Wiley, New York
30) Granato,A/Lücke,K, “Theory of Mechanical Damping Due to Dislocations”, Vol. 27, Number 6, Journal of Applied Physics, (1956)
31) Granato,A/Hikata,A/Lücke,K, “Recovery of damping and modulus changes following plastic deformation”, Acta Metallurgica, Vol.6,1958
32) Wilks, J, “Dislocation Damping in Metals”, British Journal of Applied Physics, Vol.16, 1965
33) Blair, D.G/ Hutchison, T.S/ Rogers, D.H, “Theory of Thermal Breakaway of a Dislocation from a Row of Equally Spaced Pinning Points”, Journal of Applied Physics, Vol. 40, Number 1, 1969
34) Kosugi, T, “Simultaneous Breakaway of a Dislocation from several pinning points”, Material science and engineering A370(2004) 230-233
35) Caswell, H.L, Journal of Applied Physics, 29, 1210, 1958
36) Krempaszky, C/Liedl, U/Werner, E.A, “A note on the diffusion of carbon atoms to dislocations”, Computational Material Science 38 pp.90-97, 2006
37) Elsen, P/ Hougardy, H.P, “On the Mechanism of Bake Hardening”, steel research 64 (1993), no. 8/9
38) Exebio, J.J.M, “Metallurgical Phenomena Governing the Bake Hardening Response of a Bake Hardenable Steels”, M.Sc Thesis, TU Delft, 2002
39) Seal, R.K, “New Ultra low carbon high strength steels with improved bake hardenability for enhanced stretch formability and dent resistance”, M.Sc. thesis, University of Pittsburgh, 2006
40) De, A.K/Vandeputte, S/ De Cooman, B.C, “Static Strain Ageing Behaviour of Ultra Low Carbon Bake Hardening Steel”, Scripta Materialia, Vol. 41, No.8 pp-831-837, 1999
41) De, A.K/De Blauwe, K/Vandeputte, S/ De Cooman, B.C “Effect of dislocation density on the low temperature ageing behaviour of an ultra low carbon bake hardening steel”, Journal of Alloys and Compounds, 310, pp-405-410, 2000
42) De, A.K/Vandeputte, S/ De Cooman, B.C “Kinetics of strain ageing in bake hardening ultra low carbon steel- a comparison with low carbon steel”, Journal of materials engineering and performance, Vol. 10, No.5, pp-567-575, 2001

43) Rosinger, H.E/ Craig, G.B, “The Recovery of Internal Friction in an Iron-Carbon Alloy”, 1971
44) Snoek, J.L, “Effect of Small Quantities of Carbon and Nitrogen On the Elastic and Plastic Properties of Iron”, Physica VIII, no.7, 1941
45) Weller, M, “The Snoek relaxation in bcc metals- From Steel wire to meteorites”, Material Science and Engineering A 442(2006) 21-30
46) Cadel, E/Fraczkiewicz, A/Blavette,D , “Atomic scale observation of Cottrell atmosphere in B-doped FeAl(B2) by 3D atom probe field ion microscopy”, Materials Science and Engineering A309-310, pp-32-37, 2001
47) Cottrell AH, Bilby BA. 1949, Proc. Phys. Soc. London Ser. A 62:49-62
48) Harper,S , Physical Review 83, pp- 709-712, 1951
49) Zhao, J.Z/ De,A.K/De Cooman, B.C, “A model for the cottrell atmosphere formation during ageing of ultra low carbon bake hardening steels”, ISIJ International, Vol. 40, No.7, pp-725-730, 2000
50) Zhao, J.Z/De, A.K/ De Cooman, B.C, “Formation of the Cottrell atmosphere during strain ageing of bake hardenable steel”, Metallurgical and Materials transactions A, Vol. 32A, pp-417-423, 2001
51) Automotive Steel Design Manual (2000), American Iron and Steel Institute, Rev 6.1, Aug 2002
52) Blaimschein, M/Radlmayr, K.M/ Pichler, A/ Stiaszny, E.T.P, “Bake Hardening Effects in Components”, 19th IDDRG Biennial Congress, Eger, 10-14, 1996
53) The US steel Automotive Group: www.ussautomotive.com
54) Dicello, J.A/ George, R.A. , “Design Criteria For the Dent Resistance of Auto Body Panels”, SAE Technical Paper No.740081 ,1974
55) Stephenson, Trans, Met. Soc. A.I.M.E. 233, 1183, 1965
56) Okamoto,A /Takeuchi, K/Takagi,M, “A Mechanism of Paint Bake Hardening”, the Sumitomoe Search No. 39, pp. 183-194, 1989
57) Fine, E,M,”Phase Transformations in Condensed Systems Revisited: Industrial Applications”, Metallurgical and materials transactions A, Vol. 27A, pp-2397-2418, 1996
58) Borsutzki, M/Lempenauer, K/ Hofmann, H/ Friedel, F, “The Influence of deformation and baking on Young’s Modulus of Modern Steels for Automotive Applications”, Internal Report ThyssenKrupp Steel, Germany
59) Baumer,A/ Peter Bork, C/ Emde,T /Evertz,T /Masendorf,R /May,U /Menne,M /Ratte,E/ Steinbeck,G, “Ermittlung des Werkstoffverhaltens und des Beschichtungseinflusses durch rechnerische Methoden zur Verkurzung der Entwicklungszeiten im Fahrzeugbau mit Stahl”, Forschungsvorhaben P 603, 2007
60) Orowan, “Causes and Effect of Internal Stresses”, Internal Stresses and Fatigue in Metals, Elsevier Publishing Company, New York, 1959
61) Hanai,S/Takemoto,N/Tokunaga,Y/Mizuyama, Y, “Effect of Grain Size and Solid Solution Strengthening Elements on the Bake Hardenability of Low Carbon Aluminium-killed Steel”, Transactions ISIJ, Vol.24, pp-17-23, 1989
62) Storojeva,L/Escher,C/Bode,R/Hulka, Burko,D, “Effect of Nb/C ratio and processing conditions on ageing behaviour and BH effect of ULC sheet steels“, 2000
63) Material Science and Engineering- An Introduction by William D. Callister, Jr, ISBN 13: 978-0-471-73696-7
64) Bergstrom, Y, “A Dislocation Model for the Stress-Strain Behaviour of Polycrystalline α-Fe with Special Emphasis on the Variation of the Densities of Mobile and Immobile Dislocations ”, Material Science and Engineering 5, 1969-1970, pp193-200

65) Busche, C. H, “Bestimmung und Beschreibung des Elastizitätsmoduls von Blechwerkstoffen nach dem Umformen”, Ph.D Dissertation, ISBN 978-3-8322-6013-2, RWTH Aachen, 2007
66) K. Tanikawa, Y. Hosoya, T. Koike, "Strain ageing properties of extra low carbon bake hardenable cold rolled steel sheets", NKK Tech. Rev. 72 (1995) 10-19.
67) Vrieze, J, “Ageing Sensitivity of BH260”, Project nr.9984.41, Ref. Source number. 135701,Corus Internal Report, 2007
68) www.polytec.com
69) Hand book on “Laser Technology and Applications” Vol. III, By Colin Webb and Julian Jones
70) ASTM E1876-07, “Standard Test Method for Dynamic Young’s Modulus, Shear Modulus and Poisson’s ratio by Impulse Excitation of Vibration”
71) NEN-EN 843-2, “Advanced Technical Ceramics-Mechanical Properties of Monolithic Ceramics at Room Temperature- Part 2: Determination of Young’s Modulus, Shear Modulus and Poisson’s Ratio”, 2007
72) Kozeschnik, E/Buchmayr,B, “A Contribution to the increase in Yield Strength during bake hardening process”, Steel research 68, No. 5, pp. 224-230, 1997
73) Vasilyev, A.A/ Lee, H.C/ Kuzmin, N.L, “Nature of Strain Ageing Stages in Bake Hardening Steel for Automotive Applications”, Materials Science and Engineering A 485(2008), pp 282-289
74) Abe, H, “Carbide Precipitation During Ageing Treatments”, Scandinavian Journal of Metallurgy 13, pp. 226-239, 1984
75) Schouten, F.J, “Pre Deformation of Bake Hardening Steel”, Automotive Applications Stamping and Hydroforming Technology, Corus Internal Report # 106668
76) ASTM E111 - 04 Standard Test Method for Young's Modulus, Tangent Modulus, and Chord Modulus
77) Horn, Carol Ten, Corus Internal Presentation on Forming